UNIVERSITY OF CALIFORNIA, SAN DIEGO

"Mobile Host" Wireless Sensor Networks - A New Sensor Network Paradigm for Structural Health Monitoring Applications

A dissertation submitted in partial satisfaction of the
requirements for the degree
Doctor of Philosophy

in

Structural Engineering

by

David D.L. Mascareñas

Committee in charge:

Professor Michael Todd, Chair
Charles Farrar
Rajesh Gupta
William Hodgekiss
Gyuhae Park
Yu Qiao
Lanza di Scalea

2008

The dissertation of David D.L. Mascareñas is approved, and it is acceptable in quality and form for publication on microfilm and electronically:

_____

_____

_____

_____

_____

_____

_____

Chair

University of California, San Diego

2008

DEDICATION

To all my assistants: Patrick, Sampson, Jon, Emily, Kyle, Ben and Scott. I really appreciate all your support.

EPIGRAPH

This is a SERIOUS TIME!

— Zhu "Long" Mao

Drop the anvil!

—Ski King

The foreign monk sings better.

—Zhu "Long" Mao

Two tigers cannot live on the same hill.

—Zhu "Long" Mao

When it gets dark the ant will eat the elephant

—Zhu "Long" Mao

The stupid bird should fly first

—Zhu "Long" Mao

TABLE OF CONTENTS

LIST OF FIGURES

LIST OF TABLES

ACKNOWLEDGEMENTS

My thanks go to my advisors Michael Todd, Charles Farrar and Gyuhae Park for the support they have given me throughout my graduate school career at the University of California San Diego. They have always been willing to take chances on my ideas, and they have always been supportive of allowing me to pursue a very diverse range of educational opportunities, without which a multidisciplinary project such as this would not be possible. I would also like to thank Rajesh Gupta from the computer science and engineering department for his support and help easing the transition into the CALIT^2 building.

Pavel Kolinko from the electrical engineering department offered a wide range of helpful advice during the design of the RF energy collection electronics. I would also like to thank Chong Vu from CALIT^2 for his insights into electronics fabrication as well as the many heads ups he gave me concerning projects going on at CALIT^2. Don Kimball provided useful guidance on the design of UAV and sensor node hardware. My friend Daniele Musiani also supplied significant advice on the design of embedded systems and software. I never met anyone who loved electronics as much as Daniele and I hope I get the opportunity to work with him again.

I would like to give Eric Flynn special recognition for his help setting up the Alamosa Canyon Bridge test, as well as his help designing the basestation software, installing strain gages, and calibrating the sensor nodes. Kevin Farinholt also provided very valuable help implementing the Alamosa Canyon Bridge test. The New Mexico Department of Transportation (NMDOT)was also instrumental to the success of the Alamosa Canyon Bridge test. NMDOT built us a road so we could get our equipment to the bottom of the bridge, and they even spent multiple days providing assistance with their dump truck to excite the bridge for our earthquake simulations. The test would not have been achievable without their help. Stan Johnson provided invaluable advice concerning the helicopter throughout the course of the project. I was very impressed with his dedication to helping us make sure the project was

successfull.

Billy Jackson has acted as my "moral officer" since my undergraduate days and I would like to thank him for his musical accompaniment throughout graduate school. Christian Schmidt was my financial advisor/bandsaw operator and I want to thank him for his friendship throughout undergraduate and graduate school. I would like to thank Zhu "Long" Mao for giving me a Chinese name, "Da Niu." I especially want to thank the St Brigid Surf Club for teaching me to surf and their friendship. They made life outside of graduate school significantly more enjoyable.

My work as an undergraduate mechanical engineering student at Colorado State University contributed greatly to the success of my Ph.D and master's degree research. My professors Donald Radford, Patrick Fitzhorn and Steven Schaeffer all played a key role in preparing me for success in graduate school. I really appreciate their help

Lastly I want to thank my family and my parents David and Marie Mascareñas for their support. Both of them had important contributions. My Dad taught me how to use a drill and my Mom taught me how to read.

VITA

2004	B. S. in Mechanical Engineering *cum laude*, Colorado State University
2006	M. S. in Structural Engineering, University of California, San Diego
2008	Ph. D. in Structural Engineering, University of California, San Diego

PUBLICATIONS

Mascarenas, D., Flynn, E., Todd, M.D., Overly, T., Farinholt, K., Park, G., Farrar, C.R. "Development of Capacitance-based and Impedance-based Wireless Sensors and Sensor Nodes for Structural Health Monitoring Applications," *Journal of Sound and Vibration*, submitted.

Mascarenas, D., Flynn, E., Todd, M.D., Overly, T., Farinholt, K., Park, G., Farrar, C.R. "Experimental Studies of using Wireless Energy Transmission for Powering Embedded Sensor Nodes," *Journal of Sound and Vibration*, submitted.

Mascarenas, D.L., Park, G., Farinholt, K.M., Todd, M.D., Farrar, C.R., "A Low-Power Wireless Sensing Device for Remote Inspection of Bolted Joints," Journal of Aerospace Engineering, *Part G of the Proceedings of the Institution of Mechanical Engineers*, accepted for publication.

Mascarenas, D.L., Todd, M.D., Park, G., Farrar, C.R., 2007, "Development of an Impedance-based Wireless Sensor Node for Structural Health Monitoring," *Smart Materials and Structures*, Vol. 16, No. 6, pp. 2137-2145.

Mascarenas, D.M., Flynn, E.B., Todd, M.D., Park, G., Farrar, C.R. 2008, "Wireless Sensor Technologies for Monitoring Civil Structures," *Sound and Vibration Magazine*, April issue, pp. 16-20.

Taylor, S.T., Farinholt, K.M., Flynn, E.B., Figueiredo, E., Mascarenas, D.L., Moro, E.A., Park, G., Todd, M.D. Farrar, C.R. "A Mobile-Agent Based Wireless Sensing Network for Structural Health Monitoring Applications," *Proceedings of 2nd Asia-Pacific Workshop on Structural Health Monitoring*, December 2-4 2008, Melbourne, Australia.

Todd, M.D., Mascarenas, D.L., Flynn, E., Lee, B., Lin, K., Musiani, D., Rosing, T., Gupta, R., Park, G., Farinholt, K., Nothnagel, M., Farrar, C.R., "SHM Sensor Networking with Remote Powering and Interrogation," *Proceedings of 4th International Conference on Bridge Maintenance, Safety, and Management*, July 13-17 2008, Seoul, South Korea.

Mascarenas, D.L., Flynn, E.B., Lin, K., Farinholt, K.M. Park, G., Gupta, R., Todd, M.D., Farrar, C.R., "Demonstration of a Roving-Host Wireless Sensor Network for Rapid Assessment Monitoring of Structural Health," *Proceedings of 15th SPIE Conference on Smart Structures and Nondestructive Evaluation*, March 9-13 2008, San Diego, CA.

Park, G., Overly, T.G., Farinholt, K.M., Farrar, C.R., Mascarenas, D.L., Todd, M.D., "Experimental Investigation of Wireless Active-sensor Nodes using Impedance-based Structural Health Monitoring," *Proceedings of 15th SPIE Conference on Smart Structures and Nondestructive Evaluation*, March 9-13 2008, San Diego, CA.

Farinholt, K.M., Park, G., Farrar, C.R., Mascarenas, D.L., Todd, M.D., "Experimental Studies Using Wireless Energy Transmission for Powering SHM Sensor Nodes," *Proceedings of 15th SPIE Conference on Smart Structures and Nondestructive Evaluation*, March 9-13 2008, San Diego, CA.

Mascarenas, D.L., Todd, M.D., Park, G., Farrar, C.R., "Wireless Sensor Technologies for Rapid Assessment Monitoring of Civil Structures," *Proceedings of IMAC-XXVI A Conference and Exposition on Structural Dynamics*, February 4- 7 2008, Orlando, FL.

Mascarenas, D.L., Todd, M.D., Park, G., Farrar, C.R., "A Low-Power Wireless Sensor Node for Peak Displacement and Bolted Joint Preload Measurements," *Proceedings of 6th International Workshop on Structural Health Monitoring*, September 11-13 2007, Stanford, CA.

Todd, M.D., Mascarenas, D.L., Flynn, E.B., Rosing, T., Lee, B., Musiani, D., Dasgupta, S., Kpotufe, S., Hsu, D., Gupta, R., Park, G., Overly, T., Nothnagel, M., Farrar, C.R.., "A Different Approach to Sensor Networking for SHM: Remote Powering and Interrogation with Unmanned Arial Vehicles," *Proceedings of 6th International Workshop on Structural Health Monitoring*, September 11-13 2007, Stanford, CA.

Farrar, C.R., Park, G., Puckett, A.D., Flynn, E.B., Mascarenas, D.L., Todd, M.D. "Sensing and Optimization Issues for Structural Health Monitoring," *Proceedings of 23rd Aerospace Testing Seminar*, October 10-12, 2006, Manhattan Beach, CA.

Park, G., Overly, T.G., Nothnagel, M.J., Farrar, C.R. Mascarenas, D.L., Todd, M.D., "A Wireless Active-Sensor Node for Impedance-based Structural Health Monitoring," *Proceedings of US-Korea Smart Structures Technology for Steel Structures*, November 16-18 2006, Seoul, Korea.

Mascarenas, D.L., Park, G., Todd, M.D., Farrar, C.R. "Feasibility of X band-based Wireless Energy Delivery Systems for Embedded SHM Sensing Networks," *Proceedings of 4th World Conference on Structural Control and Monitoring*, July 11-13 2006, San Diego, CA.

Mascarenas, D.L., Park, G., Todd, M.D., Farrar, C.R. "X band-based Energy Delivery Systems for Wireless Embedded Sensor Nodes," *Proceedings of 3rd European Structural Health Monitoring Conference*, July 5-7 2006, Granada, Spain.

Park, G., Mascarenas, D.L., Todd, M.D., Farrar, C.R., "Energy Harvesting and Delivery Systems for for Embedded Sensing," *Proceedings of 3rd International Workshop on Advanced Smart materials and Smart Structures Technology*, May 29-30 2006, Lake Tahoe, CA.

Mascarenas, D.L., Todd, M.D., Park, G., Farrar, C.R. "A miniaturized electromechanical impedance based sensor node for the wireless interrogation of structural health," *Proceedings of 13th SPIE Conference on Smart Structures and Nondestructive Evaluation*, February 26-March 2 2006, San Diego, CA.

Mascarenas, D., Todd, M.D., Park, G., Farrar, C.R., "Remote Inspection of Bolted Joints using RFID-Tagged Piezoelectric Sensors," *Proceedings of 24th International Modal Analysis Conference*, January 30- February 2 2006, St. Louis, MO.

Mascarenas, D.D., Park, G., Farrar, C.R., "Monitoring and Control of Bolt Preload using Piezoelectric Active Devices," *Proceedings of 12th SPIE Conference on Smart Structures and Nondestructive Evaluation*, March 7-12 2005, San Diego, CA.

Puckett, A., Mascarenas, D.L, Park, G., Farrar, C.R. "Overview of Sensor Research In Structural Health Monitoring at Los Alamos National Laboratory," *4th annual DOE sensors workshop*, Livermore National laboratory, CA, April 5 2006, Livermore, CA.

ABSTRACT OF THE DISSERTATION

"Mobile Host" Wireless Sensor Networks - A New Sensor Network Paradigm for Structural Health Monitoring Applications

by

David D.L. Mascareñas
Doctor of Philosophy in Structural Engineering

University of California San Diego, 2008

Professor Michael Todd, Chair

Wireless Sensor Networks (WSN) for Structural Health Monitoring (SHM) applications can provide the data collection necessary for rapid structural assesment after an event such as a natural disaster puts the reliability of civil infrastructure in question. Unfortunately, there are many technical challenges associated with employing such a WSN in civil infrastructure for operation over multiple decades with maintenance costs low enough to justify the integration of such a WSN into a given structure. The technical challenges include ensuring power is maintained at the sensor nodes, reducing installation and maintenance costs, and automating the collection and analysis of data provided by a wireless sensor network.

In this work a new WSN paradigm to address these challenges is presented. The new WSN paradigm is called the "mobile host" WSN. In a mobile host WSN, the sensor nodes are placed on the structure with no internal electrical power source. Instead the node is equiped with hardware to collect energy delivered to it wirelessly by a mobile host on an as-needed basis in order to perform its intended data acquisition and interrogation functions. When an event of interest occurs which might compromise the integrity of the structure, the sensor nodes capture relevent data from the

event. In order to collect the data captured by the sensor network, a "mobile host" is sent to each sensor node and wirelessly charges it up. Once the sensor node is fully charged, it turns on and transmits its data wirelessly to the mobile host. The mobile host receives and stores the data and then implements appropriate structural health monitoring (SHM) data interrogation algorithms. If deemed necessary the mobile host then proceeds to interrogate other sensor nodes of interest on the structure. In this way a remote system is presented that can then be used to make a health assesment of the structure.

This dissertation addresses the research challenges encountered when implementing a mobile host WSN. A sensor node (THINNER) capable of collecting data wirelessly in the absence of electrical power was developed. A peak displacement and bolted joint preload sensor capable of interfacing with the THINNER sensor node were designed and implemented. A wireless energy delivery package capable of being carried by an airborne mobile host was developed. Lastly, the system engineering required to implement the overall sensor network was carried out. The culmination of this work resulted in the first field demonstration of a mobile host wireless sensor network. The field demonstration took place on an out-of-service, full-scale bridge near Truth-or-Consequences, New Mexico.

Chapter 1

Overview of the Mobile Host Wireless Sensor Network Paradigm

1.1 The Mobile Host Sensor Network Paradigm

Traditional wireless sensor networks are composed of a number of nodes powered by a conventional battery source. These types of wireless sensor networks have a number of disadvantages especially for structural health monitoring applications. A wireless sensor network for structural health monitoring applications will need to have a maintenance-free lifetime equal to the lifetime of the structure being monitored in order to be cost-effective. For example, it is not economically feasible to place a wireless sensor network on a bridge, and then have to replace batteries as they either run out of power, or they exceed their usable lifetime. Contemporary battery technology has a maximum usable lifetime on the order of a decade, which is only a fraction of the usable lifetime of a civil structure such as a bridge. In some applications (perhaps such as long-span bridges), the sheer number of sensor nodes in place on a structure could potentially create a situation where a technician is constantly replacing inoperative sensor node batteries. Moreover, the sensor nodes

must often be placed in locations that are difficult or dangerous to access, creating life safety issues for these technicians.

A conventional wireless sensor network for structural health monitoring is shown in Fig. 1.1. The conventional wireless sensor network is characterized by a number of sensor nodes creating data streams pertinent to a structural health monitoring analysis. Each sensor node has its own battery power supply capable of supplying power for the sensor node operation. Data acquired by the sensor nodes are passed throughout the sensor network wirelessly. Oftentimes the data is ultimately transmitted back to a base station for a final analysis. The network can be configured in a star topology where every sensor node transmits its data to a local centralized router for final transmission to a base station. In the star configuration, sensor nodes must all remain within the transmit and receive distance of the central router node. An alternative to the star topology is a mesh network where there are no routers, and the sensor nodes determine which other sensor nodes are appropriate to pass the data along to in order to ensure the data arrives at the base station in the most efficient manner. The mesh topology helps solve the distance limitations inherent in the star topology. Oftentimes however, data transfer in the network assumes preferred paths thus causing non-uniform energy depletion throughout the sensor nodes in the network. A major problem with sensor networks regardless of their topology, is that as the energy is depleted from the batteries, there is no way for the sensor nodes to gain more energy. This results in either a down node and/or a replacement cost, and this is not particularly economically beneficial for most applications.

In order to ease some of these concerns, a proposed alternative to the conventional wireless sensor network is the mobile host wireless sensor network shown in Fig. 1.2. In this topology the nodes do not have to have a local energy source. The batteries have been removed from the network entirely. Instead, every node is equipped with a microwave receiver antenna. The sensor nodes are designed in such a way that they are capable of storing peak displacement data without using electrical energy. In the

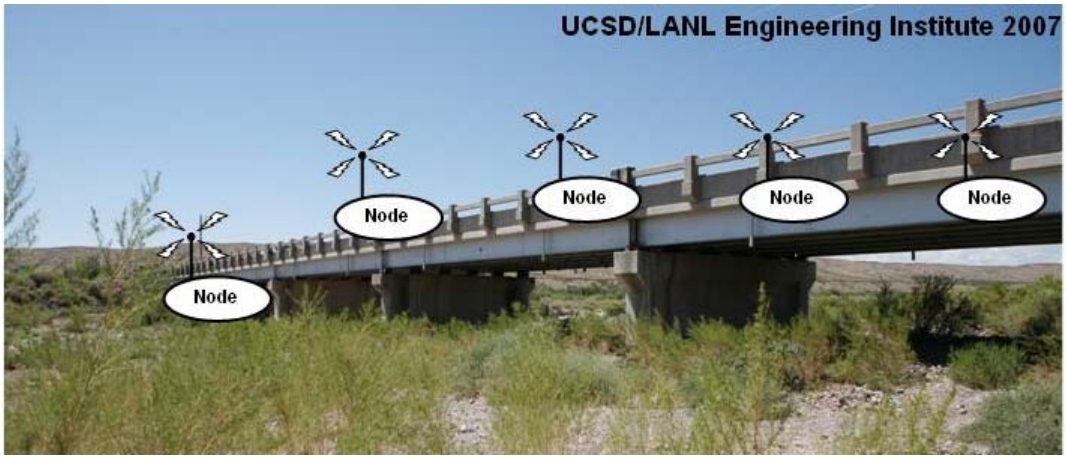

Figure 1.1: Conventional wireless sensor network powered by batteries

event of a potential damage causing event such as an earthquake, it might be desirable to get the data from the sensor nodes, the mobile host is sent to the sensor network to charge a given node using a microwave transmitter antenna. Once the sensor node is charged, the node interrogates its peak displacement sensor and radios the data back to the mobile host. The mobile host receives the data and stores it in its internal memory. The mobile host performs analysis on the data and moves on to other sensor nodes in the network as required. Once all relevant data has been collected, the mobile host returns to its basestation with all the data so a decision concerning the integrity of the structure can be made. With this paradigm maintenance due to the sensor nodes depleting their energy reserve never needs to take place. Energy is simply delivered to the sensor network on an as-needed basis. The ultimate goal is to make the mobile host completely autonomous so no user intervention is required to collect the data from the network. A completely autonomous mobile host could serve to severely cut costs in operating the wireless sensor network.

This work is concerned with the development of the first functioning prototype of a mobile host wireless sensor network. For the first demonstration, it was decided that useful quantities to measure would include peak displacement measurements

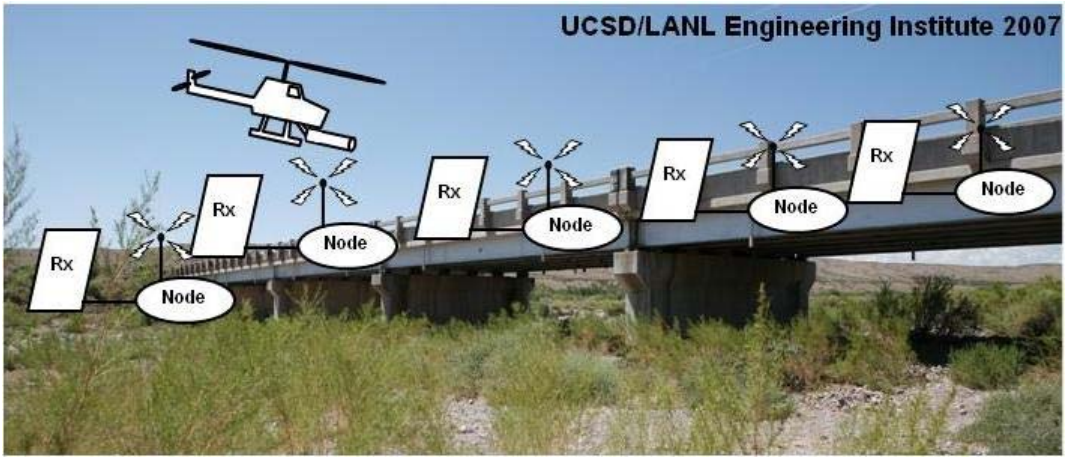

Figure 1.2: Mobile host wireless sensor network

and bolted joint preload measurements. Basically, these are relatively "simple" measurements that can feed “simple” algorithms to yield useful information on the global and local health of the the structure without significant computational and power resources. Furthermore, a peak displacement measurement is very simple metric for decision makers to understand. The mobile host would be implemented using some form of airborne craft in order to demonstrate the concept could be used on a small, low-power, unmanned platform. The implementation of the mobile host wireless sensor network required the integration of a wide range of technologies in order to be successful. Such a mobile host wireless sensor network as envisioned here requires integration of advanced SHM data interrogation algorithms, sensor design, sensor architecture, the sensor node, sensor network, unmanned aerial vehicles (UAV) design, embedded systems, and RF energy delivery. Some specific technologies designed and then integrated include peak displacement sensors, wireless sensor nodes, bolted joint preload sensors, RF power delivery and low-power switching circuits. More over the development of a RF/computational payload for a UAV was required that was light-weight, had low power consumption, and was capable of wirelessly delivering

power to sensor nodes located on a full-scale civil structure in the field. All these technologies then had to be integrated with an Unmanned Aerial Vehicle (UAV) for the final demonstration of the roving host.

1.2 Previous Work in Wireless Sensor Network Development

This section will summarize the most significant relevant work that has led to the proposed mobile host network. Some noteworthy examples will be summarized here. Before the mobile host wireless sensor network, the typical wireless sensor network consisted of a number of wireless sensor nodes each with their own power supply, wireless transceiver, sensors, and computational resources. This form of wireless sensor network is potentially very costly to maintain, because every node has a power supply capable of failing during the lifetime of the sensor network. These power supplies typically consisted of batteries with a shelf life of maximum ten years [1]. In actual use, the power supply would generally drain much faster than ten years, simply because the transceiver built into each wireless sensor node would consume significant resources. Attempts to extend this form of wireless sensor node consisted of measures to turn the radio off when it was not needed [2], [3]. Timing synchronization schemes were implemented to place wireless sensor nodes into low-power sleep modes except at predetermined intervals when all the sensor nodes would wake up and communicate with one another for a short period of time in order to conserve energy resources [4], [5]. Despite these efforts, the battery power supplies still had a shelf life on the order of a single decade, which was not acceptable for civil structural health monitoring applications. The maintenance costs associated with replacing Betties on a periodic basis over the lifetime of the structure are too high to justify the integration of a wireless sensor network into a civil structure for

structural health monitoring. Dove [6] attempted to solve the problems posed by the wireless sensor network by developing a hybrid wired - wireless sensor network. In the hybrid sensor network, subsets of nodes within the sensor network were joined with hard wire connections for data transmission purposes. Each subset of nodes would have one transceiver for wirelessly sending and receiving data to other subsets of sensor nodes in the network. The advantage of the hybrid topology is that it can be configured so there is only one power supply for every subset of sensor nodes, thus the possibility for reducing maintenance expenses at the cost of larger installation expenses.

In addition, various researchers have considered augmenting wireless sensor networks with various robots and mobile agents to enhance the performance of their networks. Tong [7] proposed the Sensor Networks with Mobile Agents (SENMA) concept. In this work, the use of mobile sensor node for performing computationally intense activities was investigated. Tong found that as the deployment density of the sensor network is increased, the energy required by an *ad hoc* wireless sensor network increases exponentially, while the energy required by a SENMA sensor network grew linearly. The SENMA network provided the opportunity for orders of magnitude reduction in wireless sensor network energy consumption by reducing the redundant data processing centers in a network, and shifting computationally complex operations from the sensor nodes to the mobile sensor nodes. Sichitiu [8] considered the localization problem inherent with wireless sensor networks deployed in an uncontrolled manner. Consider the following scenario: a mortar shell is used to disperse wireless sensor nodes across a battle zone. The sensor nodes are not equipped with GPS receivers due to cost, power, and volume constraints. How are the locations of the individual sensor nodes determined? The localization problem is an important concern for wireless sensor networks, because it addresses problem associated with the deployment of the network, as well addressing the need for spatio-temporal tagged data, and the need for sensor location information for routing algorithms.

Sichitiu proposed solving the localization problem using a mobile beacon equipped with a single GPS receiver. The mobile beacon would then travel throughout the sensor network, and help the sensor nodes determine their location using the received signal strength measurements commonly provided by their radios when transmitting to the mobile beacon. The use of mobile agents as data collectors was further advanced by Tirta [9] who proposed having sensor networks with local data collection points. A subset of sensors would transmit its data to a representative node for storage. The mobile agent would then go the the representative node to collect the data for all the nodes within its subset. Tirta used the analogy of the postal system. The representative node is similar to a neighborhood mailbox, and each sensor node is a resident of the neighborhood. Each resident does not need to travel very far to get to the local mail-box, and by congregating all the neighborhood's mail (i.e. data) in one place, the mail carrier (the mobile agent) does not need to travel throughout the entire neighborhood, thus significantly reducing time and energy costs. This concept was somewhat similar to the hybrid sensor network proposed by Dove [6]. In addition to collecting data, mobile agents have also been used to repair "holes" in wireless sensor networks. Corke [10] studied the use of a mobile agent to deploy a sensor network, localize the sensor nodes, drop new sensor nodes when sensor nodes become damaged, and using the mobile agent to move data from one portion of the network to another when connectivity between the nodes is compromised. A demonstration of their study was performed using a radio controlled model helicopter as the mobile host. The ultimate goal of the project was to use the system to deploy and operate wireless sensor networks in remote or dangerous environments.

A few examples of mobile agents being used as structural health monitoring platforms also exist. One structural health monitoring application that can benefit from the use of mobile agent is powerline inspection tasks. It is important for utility companies to ensure the structural integrity of their power line infrastructure in order to avoid costly blackouts or unsafe conditions. Some examples of damage to

powerlines include tree encroachment, sagging lines, leaning poles, damaged/missing safety notices, corrosion, chipped insulators, and signs of arcing. Typical approaches to inspecting power lines consists of manual walk arounds of the lines augmented by sending linemen up utility poles for closer inspections of power transmission equipment [11]. An alternative inspection method involves using a helicopter to fly trained inspectors over the lines to perform a visual assessment of the structural integrity of the lines. Both of these methods are costly and time consuming. Whitworth [12] proposed the use of active video equipment on board the helicopter to record data from the inspection flights in order to improve the quality of information available to the engineers in charge of the powerlines when they needed to plan repair operations. Whitworth began working on addressing the problem of stabilizing the cameras on board the helicopter to improve image quality, as well as developing methods for a camera control system that would automatically lock on and track power lines during inspections in order to reduce camera operator fatigue during rapid flyover operations. Ma [11] suggested the use of an unmanned aerial vehicle to perform power line inspections. The use of unmanned vehicles could potentially significantly reduce the costs of power line inspections, as well as increase the safety of the inspectors responsible for monitoring the power lines. Ma lays out the conceptual design of an unmanned power line inspection system in [11]. Golightly [13] did significant work toward trying to better understand what visual control algorithms would be most successful at controlling a camera onboard an unmanned aerial vehicle in order to perform rapid assesments of the health of power lines.

Another example of a mobile agent being used to inspect structural integrity is presented by Esser [14] and Hurston [15]. In this work, a wireless sensor network using inductively powered sensor nodes was constructed for the purpose of monitoiring strain on an I-beam. An I-beam crawling robot was then built in order to crawl along the beam and delivery inductively coupled energy to each sensor node it came across in its path. A special docking station was also built for the I-beam

crawling robot. In the docking station, the robot could recharge its own batteries via an inductively coupled link. Furthermore, any data collected by the robot could be uploaded to the docking station which was connected to the internet. In this way it would be possible to have the robot collect data from the structure in a completely autonomous manner, as well as perform self maintanance, and make data readily available on the internet.

The "data MULE" paradigm is similar to the mobile host paradigm, except that it does not involve delivering energy to the sensor nodes on an as-needed basis. In the data MULE paradigm a mobile node known as a "MULE" collects data from static sensor nodes and redistributes it throughout the network as the MULE changes its spatial location through time. Signifigant work has gone into the modeling and simulation of the data MULE wireless sensor network. Shah [16] presented and modeled the three-tier data MULE architecture. Kansal [17] considered adaptive algorithms and communications protocols for an "intelligent fluid infrasturcture" which is also very similar to the data MULE wireless sensor network. Jea [18] investigated the case of multiple data MULEs being present in a network in order to improve scalability with spatial size. Sugihara [19] worked on the path selection problem for the data MULE. The data MULE path should be chosen to minimize the latency in the sensor network. Sugihara developed an approximate solution to the path selection problem, and showed a 10% to 50% decrease in latency when compared with other path selection strategies. Many aspects of the data MULE research will be applicable to future versions of the mobile host wireless sensor network. The work in the data MULE field should be monitored so it can be leveraged in future mobile host wireless sensor network research.

1.3 Contribution of the Dissertation

In this work the first field demonstation of a mobile host wireless sensor network for structural health monitoring utilizing wireless energy delivery and an unmanned aerial vehicle is presented. Previous structural health monitoring sensor networks have utilized wireless energy delivery such as that demonstrated by Esser and Hurston [14], [15]. However, the platform delivering the wireless energy was constrained to run either along a magnetic tape, or an I-beam. Furthermore, the inductive wireless energy delivery approach utilized in these works was limited to applications where the mobile agent can get very close to touching the sensor node it is trying to power. For many applications it is not practical for the mobile agent to be so close to the sensor node. In addition, the installation costs for the magnetic tape and the docking station may make the solution less attractive for large scale civil applications. Another drawback to this approach is that the mobile agent is confined to operate along I-beams. Many structures do not make use of exposed I-beams, so this solution would not be suitable in these situations. The main limitations of previous research using wireless power delivery from a mobile host were the lack of range and the highly constrained path along which the mobile host was allowed to travel.

Unmanned aerial vehicles do not suffer from the same shortcomings that plague the typical terrestrial based robot. First off there is no need for a predetermined path or road for the unmanned aerial vehicle to follow. No resources are wasted installing and maintaining the mobile agent path. The aerial vehicle simply flies in the air to the portion of the structure of interest in order to determine whether or not it is structurally sound. Unmanned aerial vehicles are particularly attractive for large structures such as bridges and dams where the majority of the structure is not accessible by a terrestrial vehicle. An aerial vehicle has no problem flying to any portion of such a structure that needs to be inspected assuming it is within range of the vehicle. The concept of using an unmanned aerial vehicle for structural

health monitoring applications was investigated in [11] and [13]. However, to the author's best knowledge, no field demonstration of the power line inspection system has ever been made. Furthermore, the unmanned aerial vehicle used to monitor the power lines only used visual inspection techniques to assess structural health. The mobile agent did not interact with sensor nodes placed on the power lines in any way. Perhaps more fine spatial resolution data could be collected if various sensor nodes could be placed on the power lines, and were interrogated as the mobile agent passed by them. It is also worth pointing out that Golightly's work focused on detecting power lines in order to control the camera used to monitor them. It does not address the problem of pulling relevant structural health monitoring features from the data and automatically searching for potential problems with the lines. It will still be necessary for an engineer to look over all the video to determine whether or not there is a problem with the power lines. Extracting relevant structural health monitoring conditions (such as corrosion or tree obstruction) from the power line video captured by the unmanned aerial vehicle is still a ripe research topic for further investigation.

A number of research challenges needed to be addressed in order to complete the first field demonstration of a mobile host wireless sensor network for peak displacement measurements. The challenges included finding appropriate wireless energy delivery techniques that can be implemented on an unmanned aerial vehicle of a size and cost appropriate for inspecting civil structures. For this investigation the the mobile host should cost on the order of $10,000 and be about 1.5 m in its largest dimension. For the first demonstration of the mobile host wireless sensor network, it was determined that a useful quantity to measure would be peak displacement. Therefore it was necessary to develop a wireless sensor node and sensor capable of being powered by wirelessly delivered energy to properly perform a peak displacement measurement. In addition to the research challenges, there were also significant engineering challenges. All devices used on board the helicopter needed to lie within fixed weight and energy consumption constraints. The development and procurement

of all the hardware and software needed to take place within a one year time frame. Despite the significant challenges posed by the field implementation of a mobile host wireless sensor network for peak displacement measurements, the project succeeded in its goals.

The dissertation will cover three main topics providing a comprehensive picture of the mobile host wireless sensor network research, development and demonstration. After the introductory chapter, the second chapter covers the design, development, and testing of the THINNER sensor node used for performing the peak displacement measurements during the field demonstration of the mobile host wireless sensor network. A detailed overview of the THINNER sensor node is provided in this chapter along with details on the design of the peak displacement sensors built to interface with the THINNER sensor node. A characterization of the energy consumption of the sensor node, and the peak displacement sensor performance is provided. In addition results from the field demonstration of the wireless sensor node are included. The wireless power delivery chapter covers the path toward obtaining a viable means for wirelessly delivering energy to a wireless sensor node located on a civil structure from an unmanned aerial vehicle platform. In addition, the performace of the wireless energy delivery at the Alamosa Canyon Bridge demonstration is presented and thoroughly analysed. The combination of the THINNER sensor node and its sensor package coupled with the wireless power delivery technology are the heart of what made the mobile host wireless sensor network demonstration successful. The final chapter discusses the synthesis of the unmanned aerial vehicle platform used as the mobile host, along with the overarching wireless sensor network the mobile host would act within. The mobile host and its associated payload and software are described in detail, along with a discussion of various design concerns that guided the overall decision making during the fabrication process. A detailed description of the mobile host weight and power trade-offs considered during the design process is presented along with analysis of data from the field demonstration that characterizes

the performance of the unmanned aerial vehicle. The network connectivity between the mobile host, the sensor nodes, and the base station is also described in detail.

The contributions of the dissertation can be listed as the following developments:

- A new capacitance-based sensor node (THINNER) capable of being powered from energy delivered wirelessly by an unmanned aerial vehicle.
- A new capacitance-based peak displacement/strain sensor built to operate with the THINNER sensor node.
- A new capacitance-based bolted joint preload sensor built to operate with the THINNER sensor node.
- A Radio Frequency (RF) to DC converter capable of supplying adequate voltage to the energy storage capacitor for the proper operation of the sensor node was developed and tested.
- A turn-on switch for ensuring power from the storage capacitor only arrives at the THINNER sensor node when the voltage on the capacitor is adequately high.
- An RF/computational payload for wireless energy delivery and SHM algorithm implementation capable of being delivered by a commercially available RC helicopter.
- First demonstration of a mobile host wireless sensor network. In this case it was used for a structural health monitoring application.

The hope is that this work will be able to serve as a guide to future researchers continuing the development of mobile host wireless sensor networks. There are still a multitude of challenges such as machine learning, control, systems integration, thermal management, power management, sensor robustness, autopilots, and machine

visions that need to be addressed before the mobile host wireless will be ready for wide-scale deployment.

1.4 Content of the Dissertation

The dissertation consists of three main chapters. The first chapter covers the THINNER sensor node. The second chapter discusses wireless power delivery, and the third chapter will go over the implementation of the mobile host wireless sensor network.

The THINNER sensor node chapter will discuss the considerations that went into designing a sensor node that collects measurements using a capacitive-to-digital converter instead of the conventional voltage-based analog-to-digital converter. A detailed discussion of the peak displacement and bolted joint preload sensors including their design and modeling will be presented. In addition, the energy requirements and accuracy characteristics of the THINNER sensor node and its associated sensors will be put forth. The THINNER chapter provides an outline of the novel THINNER sensor node and its associated capacitive sensors which proved well-suited for the first field demonstration of a mobile host wireless sensor network for structural health monitoring purposes.

The wireless power delivery chapter will begin by outlining the motivation for using wireless power delivery as an energy source in a wireless sensor network. Next, the characteristics of inductive and microwave wireless power delivery techniques are be presented. Ultimately microwave wireless power delivery techniques were selected as the wireless power delivery technique of choice for this dissertation. The theory behind microwave power delivery is outlined. A detailed discussion of the implementation of the microwave power delivery hardware is presented followed by experiemental test results obtained both in the lab, as well as at the Alamosa Canyon Bridge field demonstration. This chapter gives a thorough overview of the microwave

power delivery technology used in this dissetation and will provide future researchers design information for implementing their own microwave power delivery schemes.

The chapter concerned with the implementation of the mobile host will discuss the various decisions made to ensure a field demonstration could be performed at the Alamosa Canyon Bridge before September of 2007. The helicopter selected to operate as the mobile host will be presented. A detailed discussion of the RF/computational payload carried by the mobile host is given. The communication protocols and topology of the mobile host wireless sensor network are discussed. Lastly, some of the performance characteristics of the helicopter acting as the mobile host are presented. This chapter should give future researchers a good starting point for further developing mobile hosts, as well as mobile host wireless sensor network communication topologies.

Chapter 2

The THINNER Sensor Node

2.1 THINNER Abstract

As mentioned, civil infrastructure health monitoring applications pose several challenges to the development of an appropriate WSN. The WSN must remain in operation over multiple decades, with maintenance costs low enough to justify the integration of such a WSN into a given structure. Battery life should not limit the effective life of the wireless sensor network. One possible solution to these challenges is the use of sensor nodes that collect measurements from a structure in a completely passive manner without any electrical power. When a measurement is needed, as might be the case after an event such as an earthquake, power is wirelessly given to the sensor node by some "mobile host" such as an Unmanned Aerial Vehicle (UAV). The sensor node is charged up and then it wirelessly transmits its data to the UAV. This chapter presents such a node, called THINNER. The THINNER wireless sensor node was specifically built to collect peak displacement and bolted joint preload measurements. To clarify, throughout this dissertation, the term "sensor node" will be used to denote the device which includes a microcontroller, radio, energy storage, and any appropriate interrogation circuitry to collect data from a sensor. The term sensor

will denote the actual transducer that converts one measurable quantity of interest to another form which can more easily be manipulated by the sensor node. The novel aspect of the THINNER sensor node is that the peak displacement sensor and the bolted joint preload sensor are both capacitive-based. Instead of a conventional voltage-based analog-to-digital converter, THINNER is equipped with a capacitance-to-digital converter. Furthermore, the peak displacement sensor used is designed in such a way that it can collect and store data in a mechanical fashion independent of an electrical power source. THINNER was specifically designed to be powered by Radio Frequency (RF) energy on an as- needed basis. THINNER is equipped with a microwave patch antenna and a rectification stage to collect AC microwave energy and covert it to DC power.

In addition, a wireless sensor node designed for collecting electro-mechanical impedance data has also been designed and tested. The Wireless Impedance Device (WID) is designed to collect impedance measurements over the frequency range of 10 kHz to 100 kHz. The WID can be used with piezoelectric bolted joint preload sensors to determine whether or not a bolt has come loose. In addition, versions of the WID have been built with Radio Frequency Identification (RFID) capabilities allowing the WID to be wirelessly triggered to make a measurement. The WID is particularly unique because it offers a low-cost, small size, wireless capabilities, and data processing not seen in any other impedance measurement hardware available today.

In this dissertation the THINNER and WID sensor nodes and their sensors will be described. Energy requirements of the sensor nodes will be outlined. Calibration curves for the peak displacement sensor will be included along with data from the piezoelectric bolt preload sensor. Results from a field test on the Alamosa Canyon Bridge in southern New Mexico will also be presented.

2.2 Introduction

The field of structural health monitoring (SHM) is an integrated paradigm of networked sensing and actuation, data interrogation (signal processing and feature extraction), and statistical assessment (classification of damage existence, location, and/or type) that treats structural health assessments in a systematic way [20].

In the last decade or so, particularly after the 1994 Northridge, California, earthquake, some automated post- event strategies that take advantage of this SHM paradigm and do not rely upon direct human visual inspection have been developed. A recent literature review report considering a number of SHM techniques and applications (not necessarily only applied to civil infrastructure) may be found in [21].

An appropriate sensor network is always required as a first line of attack in observing the structural system behavior in such a way that suitable signal processing and damage-sensitive feature extraction on the measured data may be performed. Sensor nodes for SHM purposes often times have very specialized requirements. In order for these sensor nodes to be successful, they need to perform functions such as active-sensing (ability to excite structure and measure the subsequent response), employ adaptive sampling rate schemes, perform feature extraction on data, operate at very low power levels,and be maintenance-free for multiple decades. In this work sensor nodes capable of interacting wirelessly with a mobile host are developed. In addition to the capabilities mentioned, these sensor nodes must also have capabilities such as the ability to be triggered by a mobile host or even the ability to be powered by energy delivered by a mobile host. These capabilities are not widely used in WSN technology today. Radio Frequency Identification (RFID) tags are the nearest technology employed today with these capabilities. RFID, which is typically used as a substitute for the bar code, can be both transmit data and be powered wirelessly. Some forms of RFID are even capable of transmitting data from measurements such

as temperature, strain, pressure, and velocity. However, the current versions of these sensors do not store data because they are generally operating in the zero-power mode and they typically need electrical energy in order to store data. SHM applications typically require data storage capabilities at all times in order to be effective. In this work a sensor node is explored which relies on a mechanical data storage medium, and thus does not require an electrical energy source. The sensor is designed in such a way that it mechanically deforms to a new state as new peak response occurs. In this way a peak value of the quantity of interest is obtained and stored without a need for electrical energy. When an event of interest such as an earthquake occurs, the reasonable assumption is that the peak excitation occurred during the event. The mobile host can be sent out after the event and charge up and/or trigger the sensor node to make a measurement. The sensor node interrogates the deformed sensor and radios the data back to the sensor node. The mobile host can then travel throughout the sensor network collecting data from other sensors of interest. In order to successfully implement this scheme, it is necessary to develop sensors and sensor nodes capable of storing data mechanically, and then interrogating the sensors and radioing the data back to the mobile host.

2.2.1 Previous Work on Sensor Modalities Suitable for the Mobile Host Wireless Sensor Node.

For the first version of the mobile host wireless sensor network, peak displacement/strain at distributed locations on the structure were the measurments to be obtained. The motivation behind using peak displacement as an indicator of structural damage is that an upper threshold can be placed on the peak displacement measurement to indicate whether or not the structure can be considered fit for use based on exceeding of some limit state. Due to the stringent requirement that the sensor node be powered and interrogated wirelessly, a large variety of sensing modal-

ities to achieve peak displacement/strain measurements were considered. In order to make the mobile host demonstration successful in the time period given it was absolutely necessary to build on previous work. Sensing techniques that had been investigated previously included sensors based on radio frequency resonant cavities, sensors utilising coupling between microwaves and surface acoustic waves in piezoelectric media, low frequency inductively-coupled resonant sensors, and capacitive sensing techniques. An overview of previous work in these sensing modalities will be presented here.

The first form of wireless sensor node considered was the inductively coupled sensor. One particular sensor which seemed promising was the peak displacement sensor developed by Mita [22]. Mita build a peak displacement sensor consisting of a variable capacitor that would change capacitance with peak displacement. The variable capacitor was combined with a coil to produce an inductor-capacitor (LC) resonant circuit. The peak displacement sensor could be interrogated in a non-contact manner by measuring the resonant frequency of the LC circuit with a conventional dip meter. The goal was to be able to integrate this technology into beam-column joints in civil infrastructure that are covered in fire-protection coatings. After an earthquake, it is difficult to visually inspect and quantify the damage experienced by these joints due to the fireproof coating. The major advantages of Mita's sensor is that it is completely passive and requires no power supply whatsoever. In addition it is built from commonly available materials using widely available, inexpensive manufacturing techniques. The concepts presented in Mita's work would later form an integral portion of the mobile host demonstration. Another interesting work utilizing inductive coupled sensing and LC resonant circuits is given by Carlson [23]. Carlson developed a self-healing skin with embedded RC antenna elements. Up to a certain strain level the skin will release an ultraviolet (UV) curable epoxy in order to "heal" the damage. If the skin is stressed to a predetermined higher strain level, the LC resonant circuits will be altered thus allowing a means for wireless determination

of damage in the skin. Another application of the LC resonant circuit concept was employed by Andringa [24]. Andriga used LC resonant circuits to build a wireless corrosion detection sensor. Loh [25] used the LC resonant concept in conjunction with nanocomposite thin films to develop wireless strain and pH sensors. Other examples of LC resonant wireless sensors are given in [26] and [27].

Inductively coupled sensors are generally near-field devices meaning that they are meant to operate within a few wavelengths of the transmitter. The location restriction of these devices make them unsuitable for some applications. An alternative is to build a sensor that is capable of operating in the far field. Thompson [28] developed a far-field resonant-cavity-based strain sensor. Thompson showed that with his system it was theoretically possible to achieve an interrogation distance of 30 to 40 meters using the appropriate antenna combination. Thompson's sensor was completely passive, and required no stored energy source at all. The sensor was interrogated simply by exciting it with the appropriate electromagnetic wave. RF Surface Acoustic Wave (SAW) sensors are another example of passive, far field sensing solutions. Typically in the RF SAW sensing modality, a high frequency RF signal is transmitted from an interrogation antenna. The signal is received at a receiver antenna connected to an interdigitated transducer bonded on piezoelectric material. The piezoelectric material is then, in turn, bonded to a structure of interest. The high frequency RF signal is received by the antenna and then sent to the interdigitated transducer where it is converted to a surface acoustic wave in the piezoelectric material. The acoustic wave is propagated into the structure of interest to act as an interrogation signal. Any cracks in the structure are reflected back to the interdigitated transducer and are radiated back out the antenna to be received by the transmitter. The reflected pulses are then analysed to determine the characteristics of the host structure. A comprehensive overview of these types of sensors and their fabrication is given in [29]. An interesting example of an RF SAW wirelessly readable accelerometer is given in [30]. One example of a far-field powering technique is

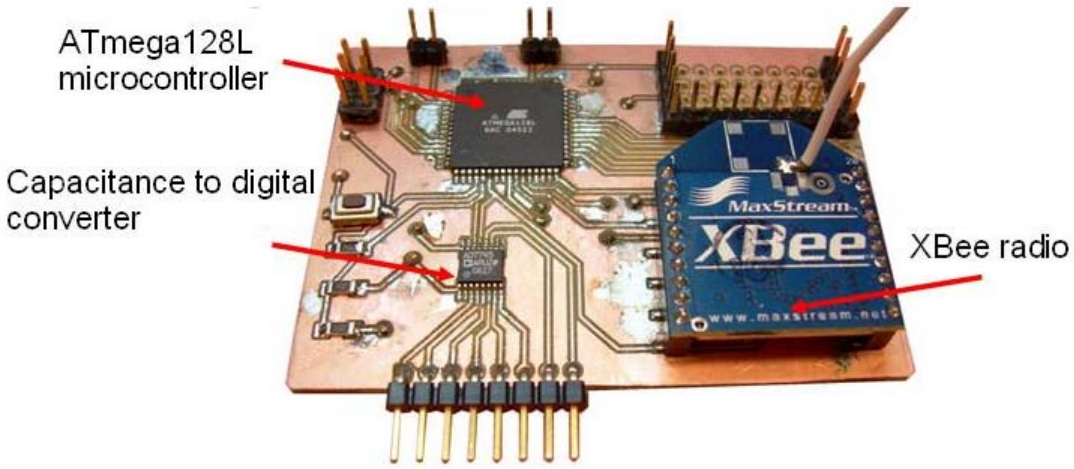

Figure 2.1: THINNER wireless sensor node

given by Zhao [31]. Zhao used X band microwaves to power a device for delivering ultrasonic pulses into a mock airplane wing for structural health monitoring.

The last sensing technology considered was a capacitance based strain gage that could be modified to become a peak displacement sensor. One notable example of a capacitive strain sensor is given by Ko [32]. In this work, a capacitive strain sensor is developed utilizing a novel buckle beam amplification architecture. The sensing package includes charge amplifiers, A/D converters and wireless telemetry circuitry to transmit data to a nearby receiver.

2.3 THINNER Sensor Node

2.3.1 Overview

The wireless sensor node developed in this work is known as "THINNER." THINNER (see Fig. 2.1) is made up of an ATmega128L microcontroller, an AD7745 capac-

itance to digital converter, and an XBee radio. THINNER is unique among wireless sensor nodes in three key ways. First, THINNER was designed to be powered by wirelessly delivered energy supplied from a UAV. In order to operate from such a low energy source, the components were carefully selected in order to ensure that they would perform satisfactorily at low energy levels (< 1J). Second, THINNER employs a capacitance-to-digital converter instead of the conventional voltage-based analog to digital converter used in most wireless sensor nodes. The capacitance-to-digital converter choice was driven by the need to store peak displacement values even in the absence of a power supply. In order to save these data, the sensors that are employed with THINNER are built in such a way that the peak response is stored mechanically as opposed to electronically. Capacitive sensors were best suited to this type of requirement. Finally, THINNER uses an XBee radio to communicate with other sensor nodes, as well as to communicate with the UAV. The XBee radio is a form of Zigbee radio developed by Maxstream. The radio interfaces with the micro-controller via a Universal Asynchronous Receiver Transmitter (UART) connection, employing standard serial port communications protocols.

A block diagram outlines the operation of THINNER can be found in Fig. 2.2. The typical operation of the THINNER sensor node can be described as follows. During normal operation, THINNER sits passively on a structure of interest (here consider a bridge) with no electrical power available. THINNER is thus designed to be connected to a capacitive sensor that resides on the structure (bridge in this case). During an extreme loading event such as an earthquake, the bridge experiences a displacement larger than seen during 'normal' operations.. The peak displacement sensor responds by deforming in a manner proportional to the peak displacement seen by the bridge. The peak displacement sensor then maintains this peak deformation state even after the occurrence of the earthquake (and subsequent deformations, provided those deformations do not exceed the previous maximum; if so, then a new maximum is retained). Subsequently, the THINNER network forms part of a

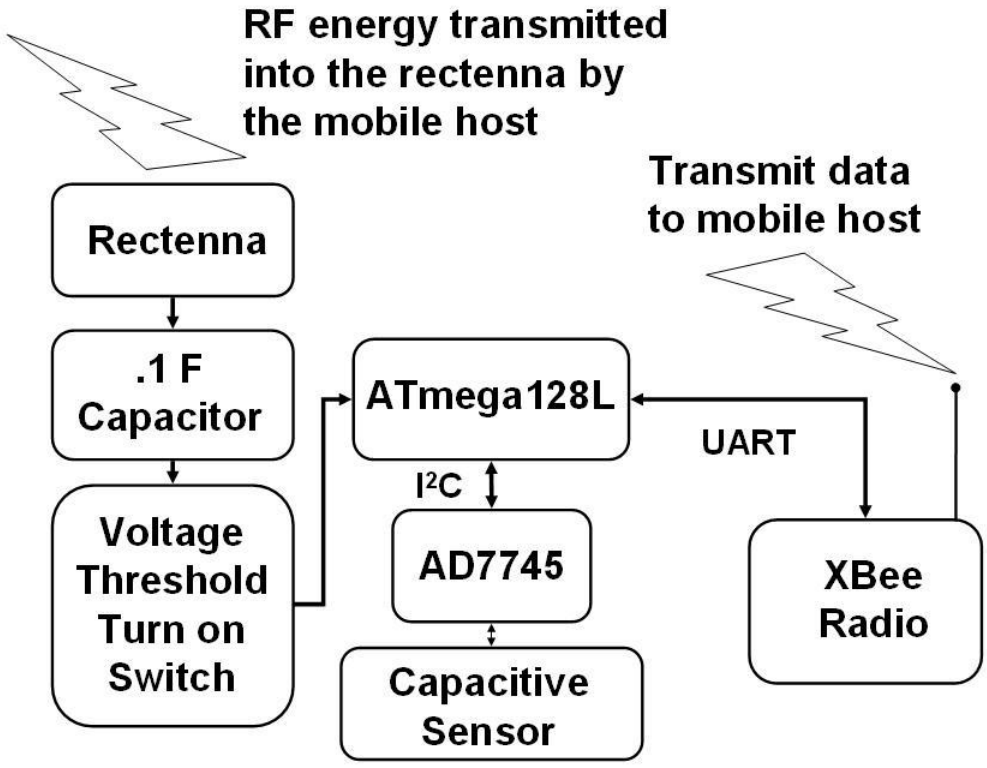

Figure 2.2: THINNER block diagram

response to the event. First, the mobile host flies to the THINNER sensor nodes of interest and wirelessly charges them up. The THINNER sensor nodes collect the transmitted RF energy with their rectennas. The DC energy from the rectenna is then used to charge up a 0.1 F supercapacitor. The supercapacitor stores the energy until the voltage on the capacitor reaches 3.5V. Once the voltage on the capacitor is 3.5 V, the voltage threshold turn-on switch closes and current is allowed to flow from the supercapacitor to the microcontroller, the capacitance-to-digital converter, and the XBee radio. Now that these components have access to energy, they turn on and make measurements of the capacitance in the capacitive-based sensors. In this case the peak displacement sensor is interrogated. The capacitance measurement from the peak displacement measurement is then sent to the XBee radio and transmitted from THINNER back to the mobile host. The roving host stores the data and then continues along to collect more data from the other THINNER sensor nodes on the bridge. A processor on the mobile host can then take the peak displacement data and execute feature extraction and statistical classification algorithms to convert raw data into potentially useful information about the structural integrity of the bridge.

2.3.2 Capacitance to Digital Converter

The THINNER sensor node is very different from other sensor nodes in that it utilizes a capacitance-to-digital converter instead of a conventional voltage-based analog to digital converter. Capacitance-to-digital converters were used because they eased the requirements for the design and fabrication of the sensors for the desired peak displacement and bolted joint preload measurements needed in the first stage of this work. The selected capacitance-to-digital converter was the AD7745 from Analog Devices. The AD7745 is the first commercially available single chip solution for capacitance measurements. The AD7745 has a maximum capacitance input range of ± 4 pF. In addition, the AD7745 also features a digital-to-capacitance converter

that allows up to 17 pF of common-mode capacitance to provide a shift in the range of capacitance values that can be measured. The end result of these two characteristics is that the chip can sense from 0 to 21 pF of capacitance. The chip has 21 effective bits of resolution, and is factory calibrated to ±4 fF of accuracy. In addition, the AD7745 has a temperature sensor with a ±2 °C accuracy and conventional voltage-based analog-to-digital converters. The AD7745 uses a sigma - delta ($\Sigma - \Delta$) converter to obtain the capacitance measurements. An Two Wire Interface (TWI) can be used to interface the AD7745 with a microcontroller for command and data collection purposes. The AD7745 uses a voltage range of 5.25 to 2.7 V and consumes 700 μA of current at 3.3 V. The surface-mount chip measures 5 X 6.4 mm. More information on the AD7745 can be found in [33].

2.3.3 Microcontroller

The microcontroller used in this work is the ATmega128L. This microcontroller was selected because it has the necessary TWI and UART buses needed for communicating with the AD7745 and the XBee radio. Another attractive feature of this microcontroller is the fact that low-cost development tools are readily available. The ATmega128L is the low voltage (3.3 V) version of one of the more large microcontrollers in the AVR family. It features 128 KB of flash memory, and 4 KB of static random access memory (SRAM). In addition the ATmega128L contains dual UARTs and a TWI which are both essential for communicating with the Xbee radio and the AD7745. The UART also allows communication with the RS-232 port on a PC. Another helpful feature of the ATmega128L is that it includes an 8 MHz internal oscillator. The internal oscillator eliminates the need for an external oscillator, which would increase the size of the sensor node printed circuit board (PCB). All measurements performed in this investigation were executed using the internal 8 MHZ oscillator. The 128 KB of flash has so far proven to be more than ample for this sen-

sor node application. The 4 KB of SRAM is sufficient for the applications considered in this dissertation. Most other SHM applications that require the use of memory intensive algorithms would probably call for additional memory. The possibility of adding additional SRAM, or even a USB mass storage device, is currently being explored for more general SHM applications. The ATmega128L sells for around $16.00 U.S. 2007. The microcontroller comes in a 64 pin TQFP surface mount form factor and measures 15.75 X 15.75 mm. More information on the ATmega128L can be found in [34].

2.3.4 Radio

The wireless telemetry selected for the sensor node was the 2.4 GHz Xbee radio from Maxstream. The Xbee radio sells for $19.00 and it comes in a variety of antenna configurations. The radio can operate from a 3.3 V supply, and consumes between 45 and 50 mA for receive and transmit (Rx/Tx) operations. Typical range for the radio is 90 m line-of-sight, and 30 m in a typical office setting. The ease of use of the Xbee radio was the main driver for its integration into the wireless sensor node. The only requirements beside the power and ground lines are the connections to the UART Rx/Tx pins. Furthermore, the radio Rx/Tx lines can be directly connected to CMOS logic levels. No level converter chip is needed as in conventional microcontroller UART-to-PC connections. The microcontroller UART can be directly connected to the radio, and the Xbee can communicate with a base-station enabled PC, in a manner similar to a wired RS-232 serial connection. Transmitted data can be acquired by the PC using serial port emulation software.

2.3.5 Capacitor

The capacitor used on the THINNER sensor node is a 0.1 F supercapacitor manufactured by Cooper Bussmann. The supercapacitor datasheet can be found in [35].

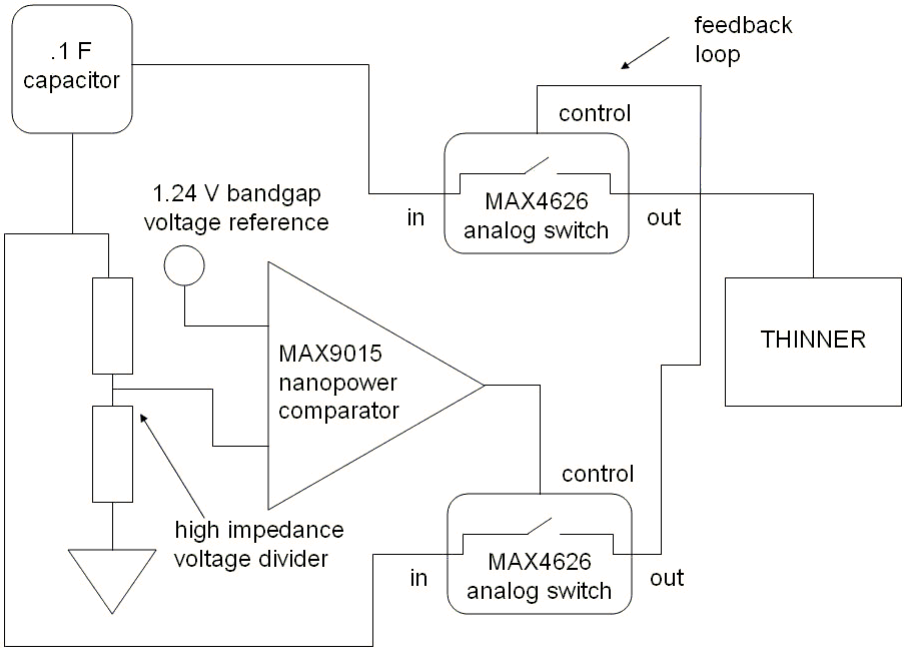

Figure 2.3: THINNER turn-on switch block diagram

The 0.1 F capacitor was selected because it has a maximum voltage of 5 V which exceeds the 3.5 V used to run THINNER. The capacitor measures 5.5 X 10.8 X 12.5 mm which scales nicely with the remainder of the THINNER components. The magnitude of the capacitance is a tradeoff between potential energy storage, and the time required to charge the capacitor to a given voltage. In this work 0.1 F was found to be an appropriate comprimise between the number of measurements that could be completed, and the time required to charge the capacitor to 3.5 V.

2.3.6 Turn-On Switch

Once the energy has been delivered by the mobile host and has been stored in the sensor node's capacitor, energy must be delivered to the electronic components

on the sensor node. One challenge is that if the microcontroller is directly connected to the 0.1 F capacitor, the microcontroller will attempt to turn on before the voltage is high enough for the microcontroller to operate properly. The result is that at a certain voltage, the microcontroller will be in a pseudo-on state that simply drains energy from the capacitor with no useful outcome. Furthermore, the energy drain of the microcontroller on the capacitor is so high that it is impossible for the UAV mobile host to deliver more power than the microcontroller consumes. It is therefore impossible to ever charge the capacitor on the microcontroller to the required voltage for its proper operation.

It is absolutely necessary to develop some form of switch to make sure that the microcontroller does not receive any energy until the capacitor was fully charged to 3.5 V. This switch would have some very stringent requirements. First of all, it would need to have a very high impedance when the switch is in the open position so no energy would reach the microcontroller until the correct time. The switch would have to transition to the closed position when the voltage on the capacitor had reached 3.5 V. The switch would have to consume a very small amount of energy. To make matters more difficult, the switch would have to be capable of operating without any form of stored energy on the bridge because there is no battery at sensor node on the bridge. The switch would have to be capable of running solely form the energy supplied by the helicopter. In addition, the switch should be built from easily-attained, low-cost, small and lightweight components.

The design of such a turn-on switch is not straight forward. First, to the author's best knowledge, a switch fulfilling the requirements is not currently commercially available. Furthermore, techniques such as periodic sampling of the capacitor voltage with an Analog-to-Digital (A-to-D) converter are not practical in this situation because during a large fraction of the charging time, the voltage available from the capacitor is not high enough to run the microcontroller or the A-to-D converter.

The solution to the switching problem was solved by developing a switch made up

of micro-power comparators utilizing voltage-band gap references, low-voltage analog switches and a high impedance voltage divider. The block diagram representation of the switch is shown in Fig. 2.3.

The operation of the voltage threshold turn-on switch can be described as follows. As the 0.1 F capacitor is charged up, a very small fraction of the current is used to excite a high-impedance voltage divider connected to a nanopower comparator. The other pin of the comparator is connected to a 1.24 V band gap voltage reference. Once the voltage on the capacitor reaches a value such that the output of the voltage divider exceeds the 1.24 V supplied by the voltage bandgap reference, the comparator sends a signal to a MAX4626 normally-open analog switch, thus signaling the switch to close. Once the switch closes, current from the capacitor is allowed to flow through the first switch, and then into the control pin of a second normally-open switch. The second normally open switch is connected between the 0.1 F capacitor, and the THINNER sensor node. At this point current begins to flow from the capacitor through the second switch and into the THINNER sensor node. In addition, current also flows from the capacitor through the switch, and through a feedback loop into the control pin of the second switch, thus ensuring that the second switch remains in the closed position throughout the complete discharge of the 0.1 F capacitor. Power for the comparators and switches is supplied by the energy in the 0.1 F capacitor as it is charged. The voltage on the capacitor at which the switch allows current to flow is controlled by the values of the resistors in the high-impedance voltage divider.

2.3.7 Rectenna

The purpose of the rectenna is to receive RF energy from the mobile host, and then convert that energy to DC so it can be used to power the sensor node electronics. A good overview of rectenna research and wireless energy delivery can be found in [36]. The rectenna used in this investigation consisted of two main elements. The

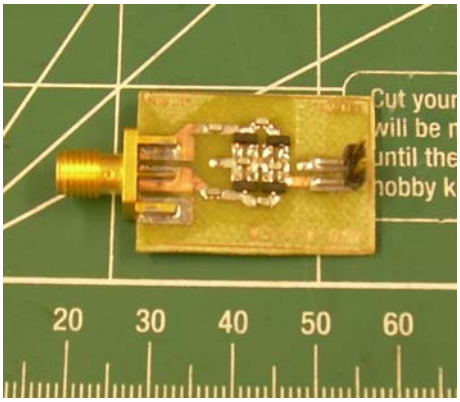

Figure 2.4: RF to DC voltage quadrupler

first element was a 19 dBi patch antenna measuring 387 mm on each side. This patch antenna served the purpose of receiving the RF energy transmitted from the mobile host. The second element of the rectenna was an RF to DC voltage quadrupler. The purpose of the quadrupler was to take the received RF energy and convert it to a DC energy that can be stored in a supercapacitor. The reason a voltage quadrupler was used for this purpose was that it was vital to ensure the voltage output from the RF-to-DC converter was high enough to ensure adequate energy was stored in the supercapacitor. The simplest way to achieve these goals is to use voltage multipliers as found in Ref. [37].

Two factors must be considered when selecting the design of the voltage quadrupler. The first is the factor by which the DC voltage will be multiplied. As more stages are added to the voltage multiplier, the multiplication factor will increase and the voltage used to run the electronics will be higher, and more energy can potentially be stored in the supercapacitor. Unfortunately, as the number of stages in the multiplier increases, more power is lost in the multiplier. This means that it will take a longer time to charge the supercapacitor up to a given voltage. A full-wave series voltage quadrupler was used in this investigation as shown in Fig. 2.4. This architecture was found to be a good trade off between making sure the voltage on the

supercapacitor could be charged to a high enough value, while not overly degrading the efficiency of the wireless power delivery.

2.4 Sensors

In SHM applications data collected from various sensor measurements are analysed in order to make some estimation of a structure's integrity. In order for the analysis to be useful, it is imperative that appropriate sensors are selected for the application. In this work, many competing factors needed to be considered when deciding which sensors will provide useful data for analysis. In this work the goal was to continuously measure the peak displacement response of a structure without having any on board electrical energy source at the sensor. Ultimately the sensor and the THINNER sensor node were designed concurrently in order to ensure this goal could be met. It was also determined that bolted joint preload would also be a useful quantity to measure, so a bolted joint preload sensor was designed to operate with the THINNER sensor node. The peak displacement sensor and the bolted joint preload sensor will be further discussed below.

2.4.1 Peak Displacement Sensors

Design and Operation

In this work a peak displacement sensor capable of storing peak values in the absence of electrical energy was developed. The sensor used in this work is very similar to that developed in Ref. [22]. A photo of the peak displacement sensor can be found in Fig. 2.5. An exploded view of the peak displacement sensor can be found in Fig. 2.6. The peak displacement sensor is essentially a parallel plate capacitor in a cylindrical configuration. The inner and outer aluminum components are the two plates of the capacitor. The capacitance of the sensor changes when the inner

Figure 2.5: Peak displacement sensor

and outer cylinder are moved relative to one another along the axis of the cylinders. The inner Teflon alignment spacer serves the purpose of ensuring that the inner and outer aluminum cylinders remain coaxial. Furthermore, the Teflon alignment spacer also ensures that some level of friction exists to maintain the current axial position of the aluminum cylinders in the face of disturbances. The presence of friction is what distinguishes this particular sensor as a peak displacement sensor.

Fig. 2.7 shows how the peak displacement sensor would typically be interfaced to a structure of interest. The peak displacement sensor is fixed to a point on the structure of interest with a piece of aluminum angle. The gage length of the sensor is determined by placing another piece of aluminum angle equipped with a tension control device a distance away from the peak displacement sensor equal to the desired gage length. Another fixed point is then selected a short distance away from the peak displacement sensor on the side opposite of the tension control device. A wire is then threaded through the tension control device, through the peak displacement sensor, and into a plunger. The plunger is then fixed to the final fixed point with a tension spring. The final adjustment of the sensor is achieved with the tension control

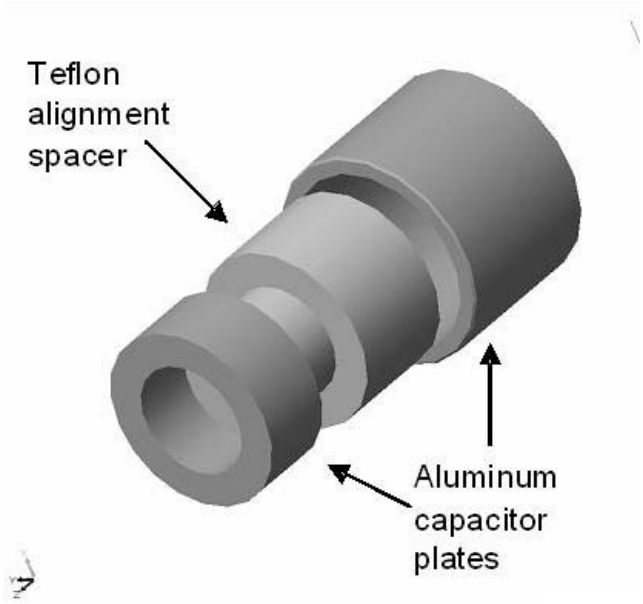

Figure 2.6: Exploded view of the peak displacement sensor

device. The tension in the wire is increased until the plunger is in direct contact with the Teflon alignment spacer on the peak displacement sensor, and the inner aluminum cylinder is in a position possessing a capacitance within the dynamic range of the capacitance-to-digital converter. In the event of a damage scenario such as an earthquake, as the bridge is deflected downward, the lower surfaces of the support beams will be placed in tension. The stiffness of the tension spring connecting the plunger to the fixed point is selected so that it is low compared with the stiffness of the wire. In this way the wire is treated as essentially being rigid, and all the deflection between the two outer fixed points is compensated for by an increase in the length of the spring. As the bridge is deflected, the peak displacement sensor wants to move away from the tension control device. The outer housing of the sensor is free to do so, but the plunger prevents the Teflon alignment spacer and the inner aluminum cylinder from moving away. Thus the two cylinders move relative to one another along their axis, and the capacitance of the peak displacement sensor changes

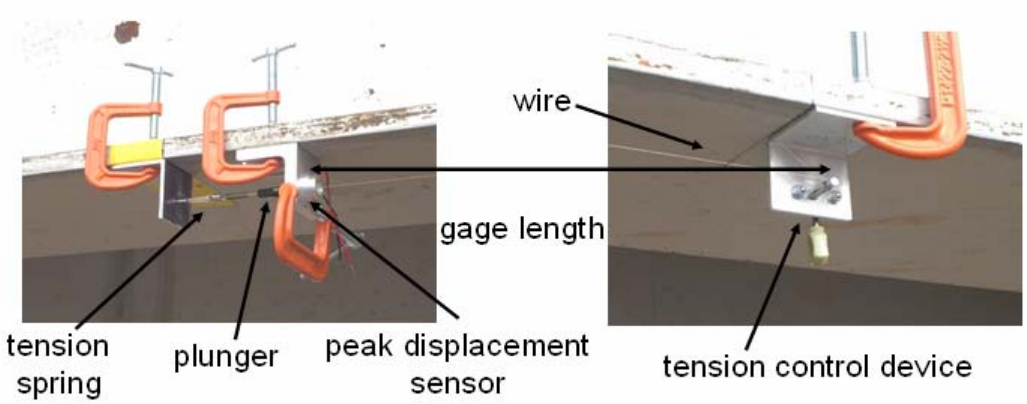

Figure 2.7: Peak displacement sensor as used in the field

until the bridge reaches its peak displacement. When the peak displacement has been reached and the bridge returns to a less deformed shape, the peak displacement sensor is unaware of the return, because the wire does not support compression. The friction of the Teflon alignment spacer causes the inner aluminum cylinder to maintain the peak position relative to the outer cylinder despite the fact that the deformation of the bridge has been reduced. The peak displacement sensor essentially has a mechanical memory of its peak state. It is important to point out that this memory phenomenon is essentially a zero electrical energy data storage scheme. Once the disaster event is over, the data is stored in the sensor, and the mobile host can be sent to the sensor node to charge THINNER up and make a measurement of the peak displacement of the bridge.

Theory of Peak Displacement Sensor

The peak displacement sensor follows very simple physical principles, and is thus its performance is easy to analyze given the physical dimensions of the components. The capacitance of the peak displacement sensor can be described with the parallel plate capacitor:

$$C = \frac{\varepsilon A}{L} \tag{2.1}$$

In this expression, ε is the permittivity of free space, A is the common area of the plates, and L is the distance between the plates. For the case of the concentric cylinder capacitor equation 2.1 can be rewritten as:

$$C = \frac{\varepsilon \pi D x}{L} \tag{2.2}$$

For the case where the gap between the inner and outer cylinders is small, D can be estimated as the mean of the inner diameter of the outer cylinder and the outer diameter of the inner cylinder, and x is the distance over which the two cylinders overlap. If it is assumed that x is the only parameter that can change as a structure deflects, an expression for the sensitivity of the sensor can be obtained by taking the derivative of both sides of equation 2.2. The resulting sensitivity equation is given as:

$$\frac{dC}{dx} = \frac{\varepsilon \pi D}{L} \tag{2.3}$$

Now consider the effect that selection of the gage length has on the sensitivity. It is recognized that $dx = u * Q$ where u is the strain of the lower surface of the bridge where the sensor is mounted, and Q is the chosen gage length. Substituting into equation 2.3:

$$\frac{dC}{u} = \frac{\varepsilon \pi D G}{L} \tag{2.4}$$

Equation 2.4 shows that the sensitivity of the peak displacement sensor can be improved by increasing the diameter of the sensor, increasing the gage length, putting a high dielectric strength material in the gap between the two aluminum cylinders, or decreasing the size of the gap between the inner and outer aluminum cylinders. For the first phase of the sensor, it was decided that putting a dielectric material in

the gap between the cylinders would over-complicate sensor fabrication, so only the D, G and L values were considered variable design parameters.

The design parameters of the sensor should be selected based on the SHM problem of interest. Factors that should be considered include magnitude of displacement, size of the structure, climate, sensor installation, electrical noise, dynamic range of capacitance-to-digital converter, and the common mode capacitance of the sensor due to stray capacitance. The latter two considerations are vital for the success of the peak displacement sensor. The peak displacement sensor should be designed so that the capacitance-to-digital converter has sufficient resolution to detect the displacement changes of interest. Furthermore, it is helpful to design the sensor so that it uses as much of the dynamic range of the capacitance to digital converter as is reasonably possible.

Peak Displacement Sensor Analysis and Characterization

The first peak displacement sensors were designed for monitoring the maximum strain present on the Alamosa Canyon Bridge in southern New Mexico. A disaster event would be simulated on the bridge by driving a 22 ton (20000 kg) dump truck over a wooden board commonly referred to as a 2 X 4 with nominal dimensions of 4 cm X 9 cm placed in the road on the bridge. It was assumed that an estimate of the structural integrity of the bridge could be made by measuring the peak strain experienced by the bridge. Calculations and previous testing experience with the bridge led to peak strain estimates between 10 to 100 $\mu\varepsilon$ depending on the size of the vehicle used to excite the bridge. The peak strain estimate could then be used to guide the design of the peak displacement sensor.

The design of the sensor was an iterative process, but ultimately the following dimensions were selected: inner diameter of outer aluminum cylinder - 20.62 mm ($ID = 20.62\ mm$ (.812 in)), outer diameter of inner aluminum cylinder - 20.29 mm ($OD = 20.29\ mm$ (.799 in)), gap distance - 0.16 mm ($L = 0.16\,mm$ (.0065 in)),

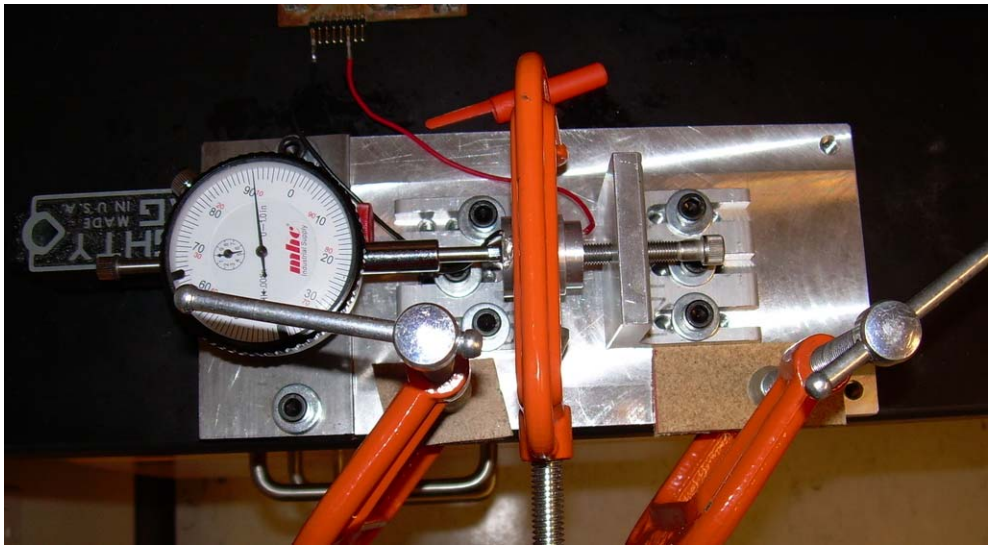

Figure 2.8: Calibration setup for the peak displacement sensor

mean diameter = 20.45 mm ($D = 20.45\ mm$ (.8055 in)). The permittivity of free space is taken as $\varepsilon = 8.85\ pF/m$ These values can be inserted into equation 2.3 to calculate the sensor sensitivity.

$$\frac{dC}{dx} = \frac{\varepsilon\pi D}{L} = \frac{\varepsilon\pi * 20.45\ mm}{0.1651\ mm} = 3.44\ \frac{pF}{mm},\ \left(87.47\ \frac{pF}{in}\right) \tag{2.5}$$

Experimental tests with the THINNER sensor node and the peak displacement sensor showed that a resolution of 1.32 μm (52.3 μin) was feasible. The gage length of the sensor could now be used to determine the final strain sensitivity. A gage length of 889 mm, ($Q = 889\ mm$ (35 in)) was selected to obtain the strain resolution of 1.42 $\mu\varepsilon$, which was determined to be adequate for the range of 10 to 100 $\mu\varepsilon$.

The next step was to determine how the calculated sensitivity compared with the measured sensitivity of the peak displacement sensor. The peak displacement sensor was placed in a measurement fixture as shown in figure 2.8. The peak displacement sensor was then connected to the THINNER sensor node, and three different tests were performed to measure the sensitivity of the sensor. In each test the sensor node

was started at the same point. 20 measurements were performed with the THINNER sensor node. Then the inner aluminum cylinder was advanced into the outer aluminum cylinder by .001" (.0254 mm) and 20 more measurements were obtained. This process would be repeated over the whole range of the THINNER capacitance-to-digital converter. The resulting measurements and the best linear fit approximation to this data are plotted in 2.9. From this chart it is obvious that the peak displacement sensor possesses a linear relationship between capacitance and displacement as predicted. The equation of the best fit line to the data contains two pieces of information. The slope of the line is the sensitivity in points/mm, and the constant value is proportional to the stray common mode capacitance in the sensor and can be ignored because it does not change. The 24-bit capacitance-to-digital converter has an 8 pF range so the sensitivity can be calculated using the slope value as:

$$6.9 * 10^6 \, \frac{points}{mm} * \frac{8 \, pF}{2^{24}} = 3.29 \, \frac{pF}{mm}, \, \left(83.57 \, \frac{pF}{in}\right) \tag{2.6}$$

The measured sensitivity value of 3.29 pF/mm is within 4.3% of the predicted sensitivity value of 3.44 pF/mm. The equations used to design the peak displacement sensor are adequately accurate to predict the peak displacement sensor performance to at least the first order.

Field Demonstration of the Peak Displacement Sensor

The first field test of the peak displacement sensor occurred on the Alamosa Canyon Bridge 17 km north of Truth or Consequences NM. The peak displacement sensor and the THINNER sensor node were placed on the lower surface of the support beams on the under side of the bridge with a gage length of 35 in (889 mm). A 2 X 4 wood board was placed on the bridge roadway, and a 20000 kg (22 ton) dumptruck was driven over the 2 X 4 wooden board to provide structural excitation simulating an earthquake. A conventional electric resistance foil strain gage was also placed on

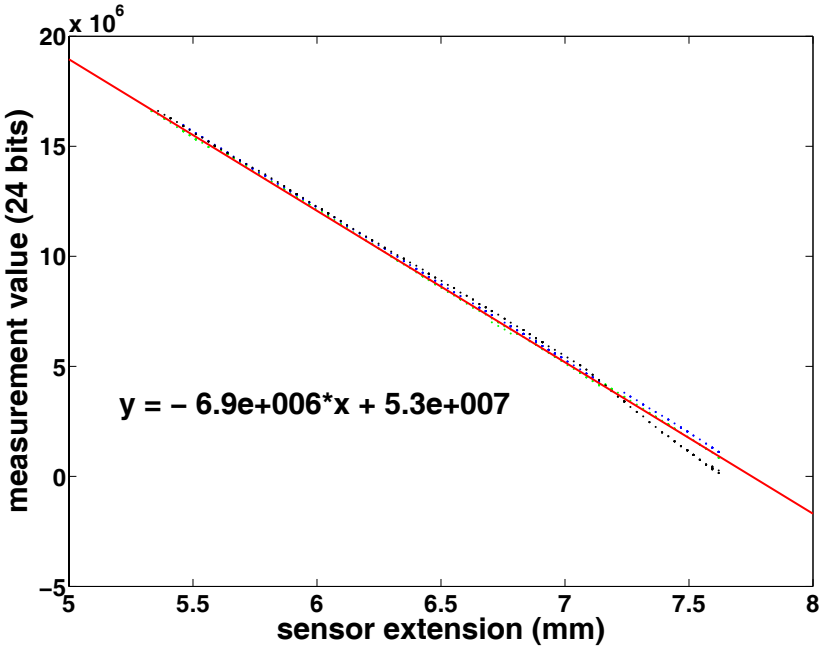

Figure 2.9: Peak displacement sensor linearity and repeatability test

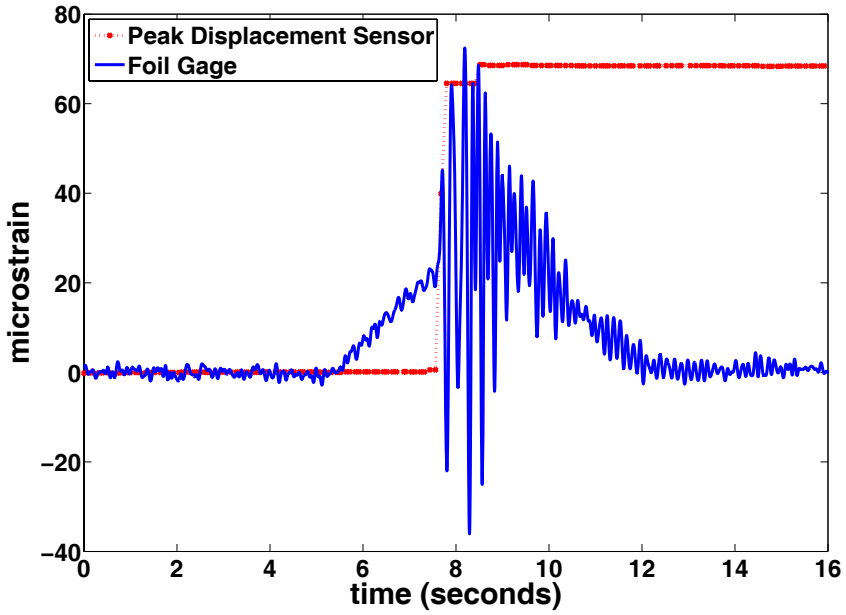

Figure 2.10: Peak displacement sensor vs. strain gage test on Alamosa Canyon Bridge (data acquisition and plot by Eric Flynn)

the bridge to provide a comparison with the peak displacement sensor. A battery was connected to the THINNER sensor node thus allowing it to make continuous measurements. The dumptruck was driven over the bridge and the 2 X 4 wooden board at about 22 mph (35 kph). Data was recorded from both the THINNER sensor node and the foil strain gage simultaneously. The resulting data are plotted in Fig. 2.10. In this plot the displacements calculated by the peak displacement sensor are converted to strain for comparison with the strain gage.

In this plot the strain gage measurement increases in value as the dump truck drives over the bridge until it reaches a peak value. As the truck drives off the bridge the value on the strain gage decreases. The peak displacement sensor on the other hand maintains a low value until a threshold value is reached. When a threshold value of displacement is obtained, the peak displacement sensor goes up to that

value and follows the strain gage up until it reaches the peak value. Once the peak value is obtained and the strain begins to drop off, the peak displacement sensor retains its peak state even though the load has been removed from the bridge. The fact that the peak displacement sensor does not follow the strain gage at low strain levels is due to the fact that the friction between the Teflon alignment spacer and the outer aluminum cylinder has not yet been overcome at these low strain levels. For some applications this characteristics could be considered a helpful feature because it might help eliminate false positives from the system. For example small disturbances caused by normal traffic flow would have a smaller chance of slowly vibrating the cylinders within the sensor apart thus falsely changing the peak displacement For SHM applications such as this, low levels of strain will be unimportant. Designing low cost sensors that perform satisfactorily at higher strain levels will typically be more beneficial. However with additional research, the poor low strain performance of the peak displacement sensor can probably be improved. Overall, the peak displacement sensor performs satisfactorily for demonstrating the viability of the mobile host wireless sensor network.

2.4.2 Bolted Joint Preload Sensor

Design of the Bolted Joint Preload Sensor

In many SHM applications, the structure to be monitored contains many bolted joints. For most applications it is necessary for these bolted joints to maintain some predetermined value of preload. It was decided that attempting to measure this preload value for bolted joints in civil structures would be beneficial for assessing structural integrity. It was determined that, in order to make this measurement with energy supplied by the mobile host and finish all the initial goals on time, it would be necessary to design a bolted joint preload sensor that could be interrogated by the THINNER sensor node. For this reason research began on designing a capacitance-

Figure 2.11: Bolted joint preload sensor

based bolted-joint preload sensor. The implementation of the sensor is shown in Fig 2.11.

An exploded view of the bolted joint preload sensor is shown in Fig. 2.12. The preload sensor is fairly similar to the peak displacement sensor in the sense that both are based on a cylindrical parallel plate capacitor concept. In the case of the bolted joint preload sensor, the outer cylinder is an aluminum cup with two Belleville spring washers placed in a series configuration inside. The inner aluminum cylinder is placed on top of a Delrin alignment spacer, which serves the dual purpose of maintaining the alignment of the inner and outer cylinders, as well as spacing the inner aluminum cylinder so that at the no-load condition the lower face of the inner aluminum cylinder is coplanar with the upper face of the outer aluminum cylinder and the common area between the plates is essentially zero. In addition, the Delrin washer also serves the purpose of electrically isolating the inner aluminum cylinder from the Belleville washers inside the cup. A hole is drilled down the axis of the cylinders thus allowing a bolt to slip through the sensor assembly. When the preload sensor is installed in a bolted joint, it basically resembles a washer. As load is applied to the bolt, the

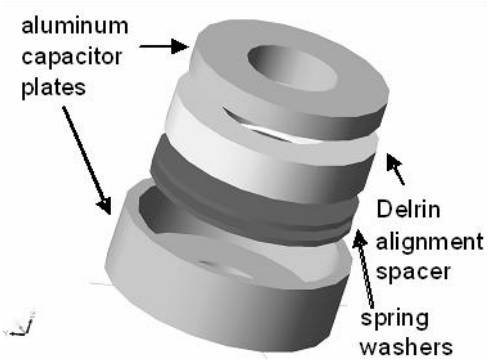

Figure 2.12: Exploded view of the bolted joint preload sensor

bolt exerts force on the inner cylinder, which in tern exerts load on the Belleville washers. The washers respond by deforming the Belleville washers downward. As the washers deform, the inner aluminum cylinder is drawn into the outer aluminum cylinder thus increasing their common area and therefore their capacitance. As the bolt is continuously tightened, the Bellville washers continue to deform until they reach their flat load. Once the washers reach their flat load the stiffness of the washers increases dramatically and the washers cease to act as spring washers. The flat load is essentially the upper load limit of this form of preload sensor.

Theory of the Bolted Joint Preload Sensor

Due to the fact that the bolted joint preload sensor is a cylindrical parallel plate capacitor, its capacitance-deflection properties follow equations 2.2 and 2.3. Basically capacitance and deflection are linearly related. The more interesting relationship in this sensor is the load-deflection characteristics of the preload sensor. The load-deflection characteristics are primarily governed by the series configuration of Belleville washers used in the sensor. The load-deflection characteristics of Belleville washers has been extensively researched, and a good overview of the theory outlining this form of spring is given in [38] and [39]. In this work the closed form solution

for the load deflection characteristics of the spring washer is given as:

$$P = \frac{E\delta}{(1-\nu^2)\,Ma^2}\left[(h-\delta)\left(h-\frac{\delta}{2}\right)t + t^3\right] \tag{2.7}$$

In this expression, P is load, δ is the deflection of the washer, E is the modulus of elasticity, ν is Poisson's ratio, t is the thickness of the washer, a and b are the outer and inner radii respectively, h is the cone height change of either the inner or outer surface, and M is a constant which is a function of a/b whose value is given in a table in [39].

Modeling and Experimental Results from the Bolted Joint Preload Sensor

The design considerations for the bolted joint preload sensor were very similar to those outlined in the peak displacement sensor section. The main factor driving the design was the diameter of the bolt that would be monitored by the sensor. The bolts on the Alamosa Canyon bridge were 3/4" (19 mm) diameter, so the next step was to select Belleville spring washers which would accommodate this bolt. The selected washer was made of steel and had the following parameters: $a = 22.23\ mm$, $b = 11.18\ mm$, $h = 1.45\ mm$ $t = 1.45\ mm$ $M = .7$, $E = 205\ GPa$, $\nu = .3$. The maximum deflection of one washer is $1.45\ mm$. In order to increase the sensitivity of the sensor two Belleville washers were placed in series. This configuration caused the amount of deflection for a given load to double, thus doubling the sensitivity of the sensor. It also caused the maximum deflection of the sensor to double to 2.9 mm. The inside diameter of the outer cylinder was set to the outer diameter of the Belleville washer. The outer diameter of the inner cylinder was set so when the washer was at full deflection the sensor would have increased in capacitance by the 8 pF set by the range of the capacitance-to- digital converter. In this way the full dynamic range of the capacitance to digital converter would be utilized.

Once the peak displacement sensor was designed, it was desired to measure its load-deflection characteristics. The load-deflection characterization work is detailed

Figure 2.13: Bolted joint preload sensor test setup

in [40]. In this work the bolted joint preload sensor was put into a test setup as shown in Fig. 2.13. A dial indicator was placed over the head of the bolt to measure the Belleville washer deflection, and a load cell was placed on the opposite side of the bolted joint to measure the load on the bolt. The resulting measurements, and the simulation predictions given by equation 2.7 are both plotted in Fig. 2.14.

Overall the experimental load vs deflection characteristics match the model predictions fairly well. In some cases the measured force is slightly less than expected for a given deflection. The most probable cause of this discrepancy is the mechanical characteristics of the Delrin washer that is located between the inner aluminum cylinder and the Belleville washers. The Delrin spacer is less stiff than both the aluminum and steel, and it also possesses a nonlinear stress-strain relationship. Most likely, the stiffness characteristics of the solid Delrin washer are approaching those of the Belleville washer, and thus the washer properties are beginning to show up in the measurements. Delrin was selected mainly because of its electrical insulating properties and less so for its mechanical properties (though mechanical properties were a concern during the sensor design). If the performance of the current peak displace-

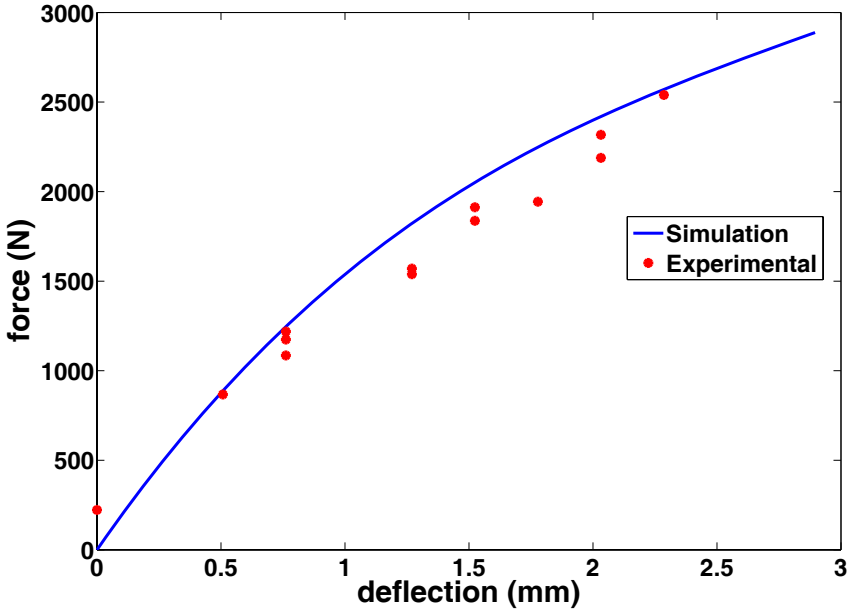

Figure 2.14: Bolted joint preload sensor simulation and experimental results (two bellville washers in series)

ment sensor is not acceptable, the best solution would probably be to redesign the sensor so the properties of the Delrin spacer have a smaller effect on the accuracy of the sensor. Alternatively, a calibration curve can be built for the sensor that simply takes into account the stiffness of the Delrin washer. It is also noteworthy that at the very low deflection end, the force needed to obtain a given deflection is higher than expected. This phenomenon was observed during the tests, and appears to be the result of friction between the Delrin washer and the outer aluminum cylinder. The Delrin spacer is held in the outer aluminum cylinder with a press fit that was meant to allow the Delrin spacer to slide along the axis of the cylinder, while still preventing the sensor from falling apart. The press fit itself will inherently have some amount of friction/stiction that must be initially overcome.

Now that the model and experimental results have been obtained, it is worthwhile to gain some insight into how well the model captures the physical data. For this model, a percentage of absolute error measure will be used to quantify how far the experimental data strays from the model. The percentage of absolute error is defined as:

$$Percentage\ Absolute\ Error = \frac{|X_{data} - X_{model}|}{X_{model}} \times 100\% \tag{2.8}$$

Where X implies a given data point. To gain insight into the error between the model and data, Equation 2.8 is evaluated at each of the displacement values obtained in the experiement. The only exception to this rule, is that the zero deflection value is not evaluated because it evaluates to an infinite error case. The average percentage absolute error over all the data points is 8.2 %. The maximum absolute error is 15.5 % which occurs at 1.27 mm, and the minimum absolute error is 1.2 % which occurs at 2.28 mm. Despite the fact that multiple, complicated, nonlinear phenomena are occurring in the sensor, the Belleville washer load-displacement model does a very good job of capturing the behavior of the bolted joint preload sensor. The Belleville load-displacement model is completely satisfactory for sensor

design purposes since the error between the model and the experiment are within 20 %.

2.5 THINNER Energy Usage Behavior

2.5.1 Estimated Energy Usage

The energy consumption of wireless sensor nodes is always a top priority becuase it determines the usable life of the sensor network. Wireless sensor nodes are typically powered by batteries. If the nodes consumes too much power, the batteries may need to be changed so often that the sensor network loses cost effectiveness due to maintenance costs. In the case of the THINNER sensor node, power requirements are even more demanding than the typical sensor node because the node is meant to operate from power delivered to it wirelessly. Energy delivered to the sensor node in a wireless fashion is inevitably going to be low primarily because of free space losses and the efficiency of the RF-to-DC rectification stage. Typical power received at the storage capacitor in the sensor node ranged from 2 - 8 mW. The 0.1 F capacitor on THINNER needs to be charged to 3.5 V in order for THINNER to operate properly, so it will take roughly 76 to 306 seconds to charge the sensor node wirelessly. This time is the duration the mobile host must remain at any one sensor node. It is very attractive to reduce this latency time as much as possible, so any reduction in THINNER power consumption is worth pursuing. Table 2.1 outlines the power requirements of the components on the THINNER sensor node based on the data sheet estimates. From this table it is clear that the main power consumer in the sensor node is the radio. It would be desirable to measure the energy consumption of the radio alone, as well as the consumption of the THINNER sensor node without the radio.

Table 2.1: Thinner Power Requirements

Sensor Node Component	voltage (V)	current (mA)	power (mW)
ATmega128L	3.3	12.1	39.93
AD7745	3.3	.7	2.31
XBee Radio	3.3	45	148.5
	total	57.8	190.74

2.5.2 Effects of Changing Power Supply Voltage on Accuracy

Before beginning the power consumption analysis of the THINNER sensor node, it was deemed important to first determine how a changing power supply voltage would affect the accuracy of the node's measurements. In this work, the sensor node is essentially connected directly to the 0.1F energy storage capacitor. As THINNER draws energy from the capacitor the voltage on the capacitor drops. The first step in the energy analysis would be to see how this changing power supply voltage would affect the accuracy of the measurements. In order to make this determination, the 0.1 F capacitor was charged up to 3.6 V (3.6 V was chosen to ensure the voltage threshold turn on switch would close). The capacitor was then connected to the THINNER sensor node. The XBee radio was disconnected from the sensor node and the data was sent by a wired serial connection to a PC. The capacitance-to-digital converter on the node was connected to a 19.4 pF "nominal" capacitor. Measurements of the capacitor voltage and the UART voltage during the sensor node operation are shown in Fig. 2.15. The UART measurement indicates roughly when data is being transmitted to the PC. The sampling rate is not high enough to accurately capture these data, but it does serve the purpose of visualizing what is occurring with the sensor node data transmission. Each spike in the UART voltage measurement roughly corresponds to a measurement being transmitted to the sensor node. From this plot, the sensor node appears to be successfully transmitting data until the voltage on the capacitor reaches 2.15 V.

The next step is to determine how the accuracy of the data transmitted by

THINNER changed throughout the measurement regime. The capacitance values measured by THINNER throughout this test are plotted in Fig. 2.16. It can be observed from this plot that initially THINNER measures the capacitance of the nominal 19.4 pF capacitor to be 19.76 pF. After the 27th measurement however, the measured value drops significantly down to 17.76 pF. Then at the 34th measurement the value raises up to 18.76 pF where it is basically consistent until the 0.1 F capacitor is no longer able to support data transmission. It is clear, that the measurement of the sensor node is fairly stable until a certain low voltage threshold on the 0.1 F capacitor has been reached. Once the low voltage threshold has been passed, the measurements supplied by THINNER are no longer reliable. The low voltage threshold was estimated from these plots as 2.6 V based on the time duration of discharge, data transmission, and the number of measurements. 2.6 V is fairly close to the 2.7 V lower operating voltage specified for the AD7745. Most likely, when the 0.1 F capacitor voltage drops below 2.7 V, the AD7745 no longer operates properly and cannot supply reliable values to the microcontroller for transmission. For the remainder of this work, it will be assumed that the sensor node is capable of supplying measurements until the 0.1 F capacitor voltage drops below 2.6 V. In this way, the energy consumption calculations will be more conservative.

2.5.3 THINNER Energy Consumption

The first measurement of interest is the power consumption of the microcontroller and the AD7745 over the useful measurement range of 0.1F capacitor voltage. The energy stored in a capacitor can be calculated from:

$$e = \frac{1}{2}CV^2 \tag{2.9}$$

Here e is energy, C is capacitance and V is capacitor voltage. The calculated energy stored in the 0.1 F capacitor over the useful voltage range is shown in Fig.

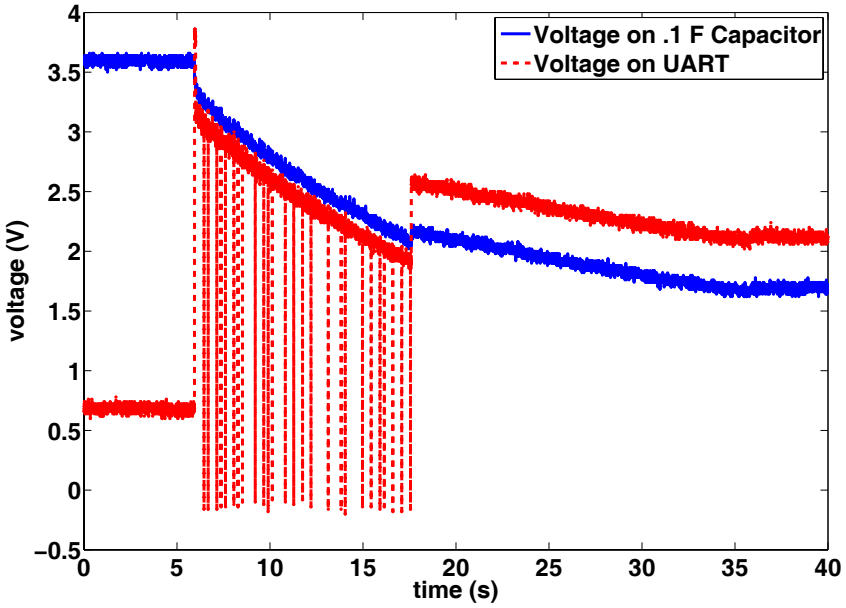

Figure 2.15: Voltage on the 0.1 F capacitor and the UART while THINNER discharges the capacitor. The Xbee radio is not connected

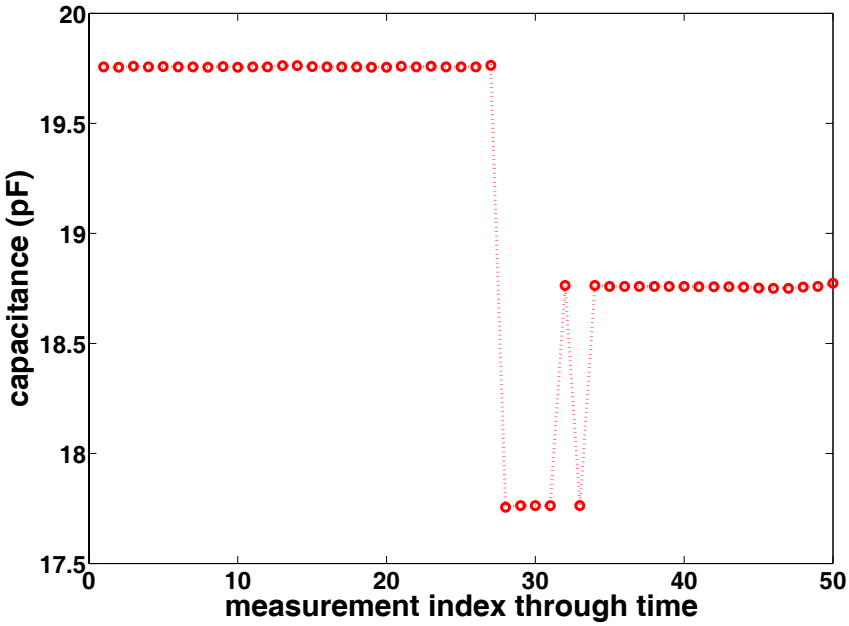

Figure 2.16: Change in measurement accuracy throughout the discharge of the capacitor. THINNER connected to a capacitor with nominal 19.4 pF capacitance

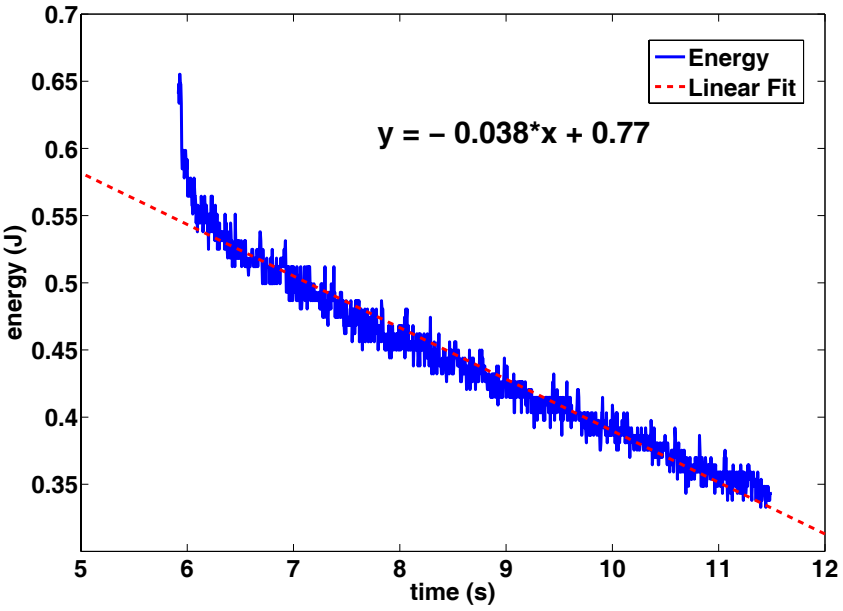

Figure 2.17: Energy in 0.1 F capacitor as it is discharged by THINNER through its usable range. The XBee radio is not connected

2.17. A linear fit to the data is also shown to make an estimate of the power consumption of the microcontroller and the AD7745 while there are actively making measurements. The best fit line shows the power consumption for the AD7745 and the ATmega128L is 38 mW which is only slightly lower than the 42.4 mW estimated from the data sheets. Over the usable voltage range, twenty-seven, 3 byte measurements were successfully completed. The result is that each measurement requires about 11.5 mJ or about 3.8 mJ/Byte. Five of these tests were completed, and the average energy consumption was 12.17 mJ/measurement or 4 mJ/Byte.

The next measurement of interest was the energy consumption of the Xbee radio on its own sitting in its power-on state. In this test the XBee radio was not transmitting data. It was simply connected to the 0.1 F capacitor. The reason was that the transmission of data drains the capacitor very quickly, almost in an impulsive man-

ner, and the actually power usage during these spikes is really not very important. What is more important is a measure of the energy usage for every measurement transmitted. This value can be calculated quite easily using the voltage on the capacitor, and the number of successful measurements transmitted. It was however interesting to find out how much power the radio is consuming while it is simply sitting on the board not transmitting data. If the amount of energy consumed by the radio was high enough, there might be justification to increase the sensor node complexity to try and turn the radio on and off on an as-needed basis. The resulting voltage on the 0.1 F capacitor is shown in Fig. 2.18, and the energy stored in the capacitor over the useful voltage range is shown in Fig. 2.19. The slope of the best-fit line to the energy measurements shows that the power usage of the radio in the power-on state is 130 mW, which is 18.5 mW lower than the value predicted by the data sheet. It is important to note however that the radio will consume more power when it is actively transmitting data from the sensor node. The 130 mW consumed by the radio in its idle state is significantly higher than the 38 mW required to run the remainder of the sensor node. In future work it would be advisable to address this situation. Possible solutions include putting the radio into sleep mode when the rest of the sensor node is making measurements. It might also be beneficial to have the AD7745 make multiple measurements, and then average them in the ATmega128L. Once the average has been made, the radio could turn on and the single average measurement would be transmitted to the mobile host. Another possibility might be to place switching circuitry in series with the radio power supply to ensure the radio is not draining energy until the measurements are ready for transmission. It is worth pointing out that these schemes imply that the THINNER sensor node is not concerned with receiving data. If a future wireless sensor network concept requires the THINNER sensor node to receive data, it may be unavoidable to maintain the radio in the power-on state.

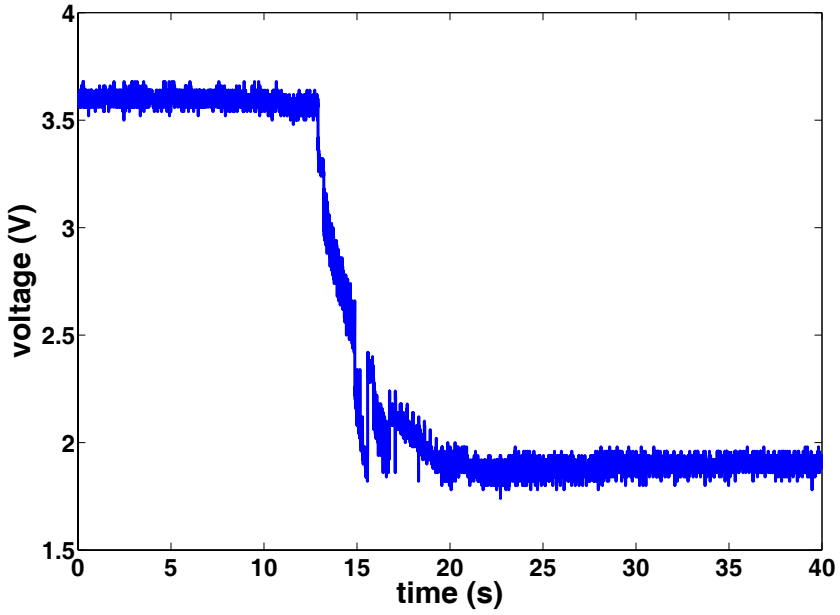

Figure 2.18: Voltage vs. time on the 0.1 F capacitor as it runs the XBee radio

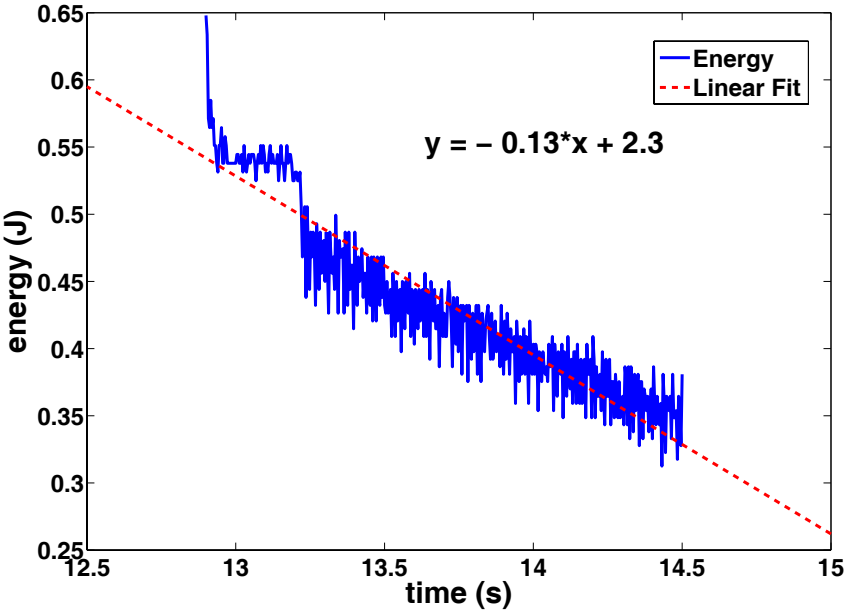

Figure 2.19: Energy vs. time on the 0.1 F capacitor as it runs the XBee radio

2.5.4 Measured Energy of the Complete THINNER Sensor Node

The final determination of the energy usage of the THINNER sensor node, was to measure the energy needed to perform measurements and data transmission with the XBee radio installed in the node. In these tests, the 0.1 F capacitor was charged to 3.6 V. It was then connected to the THINNER sensor node and THINNER was allowed to make measurements continuously. The resulting measurements of voltage on the capacitor are shown in Fig. 2.20. The result was that THINNER successfully output either 2 or 3 measurements consisting of 3 bytes each. It is important to note that all of the measurements transmitted by THINNER were high quality in the sense that none of the measurements seemed to exhibit the sub 2.6 capacitor voltage phenomenon seen in Fig. 2.16. Now making the conservative estimate that 2 measurements were completed over the 3.6 to 2.6 V usable range, and using equation 3.5, the energy required to complete a single measurement is 155 mJ or 52 mJ/Byte. These values are 13 times larger than the measurements that were completed without the radio. The radio is clearly the largest power consumer in the system, and in future work, effort should be aimed at lowering the energy required to transmit a measurement. It is worth noting however, that the THINNER sensor node is capable of making the required measurements solely using the energy stored in a 0.1F capacitor charged to 3.6 V. Experiments have shown that the "mobile host" wireless sensor node is capable of delivering this amount of energy to the sensor node in the field conditions. The current THINNER sensor node is suitable for inclusion in the first version of the "mobile host" wireless sensor network. It utilizes capacitance-to-digital technology to interrogate peak displacement and the bolted joint preload sensor. Furthermore, it is also capable of being operated soley on energy provided by energy wirelessly delivered by microwaves.

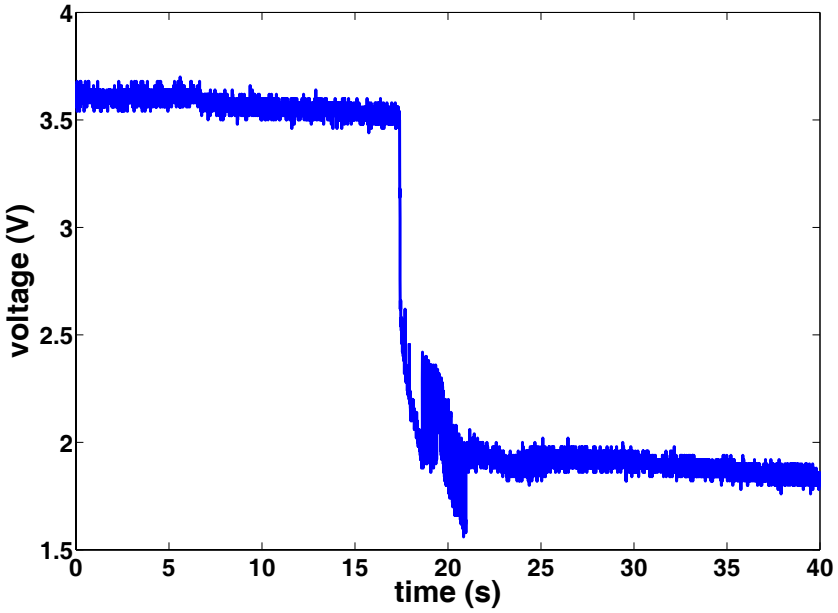

Figure 2.20: Voltage on 0.1 F capacitor as the THINNER sensor node with the XBee radio is operated

2.6 Conclusions

In this work, the wireless sensor nodes designed for inclusion in the "mobile host" wireless sensor network have been described. The sensors designed to operate with the sensor nodes where described and characterized. Simulations of the sensor behaviour were outlined, and compared with experimental data. Lastly, a thorough investigation of the energy consumption of the THINNER sensor node has been carried out. The THINNER sensor node has been deemed adequate for operation in a "mobile host" wireless sensor network.

Chapter 3

Wireless Power Delivery

3.1 Abstract

A major challenge impeding the deployment of wireless sensor networks for structural health monitoring (SHM) is developing means to supply power to the sensor nodes in a cost-effective manner. In this work an initial test of a roving-host wireless sensor network was performed on a bridge near Truth or Consequences, NM in August of 2007. The roving-host wireless sensor network features a radio controlled helicopter responsible for wirelessly delivering energy to sensor nodes on an "as-needed basis". In addition, the helicopter also serves as a central data repository and processing center for the information collected by the sensor network. The sensor nodes used on the bridge were developed for measuring the peak displacement of the bridge, as well as measuring the preload of some of the bolted joints in the bridge. These sensors and sensor nodes described in chapter 2 were specifically designed to be able to operate from energy supplied wirelessly from the helicopter. The ultimate goal of this research is to ease the requirement for battery power supplies in wireless sensor networks for some applications.

3.2 Introduction

One of the main limiting factors for wireless sensor networks today is maintaining the required energy level at the sensor node for extended periods of time at an acceptable cost. Contemporary wireless sensor nodes almost exclusively use conventional energy sources such as batteries. However, battery powered sensor nodes will only have a lifetime on the order of a decade due to the shelf-life of the battery. Generally the useful maintenance-free life of the sensor node is significantly shorter because the sensor node is operating at a higher duty-cycle than it would simply sitting on the shelf. Other options for powering wireless sensor nodes include the use of solar cells and various vibration-based and thermo-electric based energy harvesting schemes [41]. Unfortunately the energy harvesting approaches are generally not dependable enough for continuous monitoring in structural health monitoring applications. In this work, another avenue of providing energy to the sensor node is explored. Instead of maintaining a power source at the sensor node, power is delivered to the sensor node wirelessly on an as-needed basis. The proposed model is similar to that used in passive Radio Frequency Identification Tag (RFID) applications. The following discussion will cover the theory behind wireless energy transmission, the hardware developed to implement wireless energy transmission, as well as experimental results in the lab and from a field test at the Alamosa Canyon Bridge in August 2007. In this test the RF energy delivery equipment was attached to a Radio Control (RC) helicopter and used to supply power to a sensor node.

3.3 Literature Review of Wireless Power Delivery

A number of different methodologies exist for performing wireless power delivery including lasers, Tesla coils, microwaves, and inductive coupling. Of these technologies, lasers and Tesla coils were eliminated as possible contenders for this work

because of safety, size, and power constraints. Inductive coupling and microwave power delivery were deemed to be the best possible candidates for a wireless power delivery system mounted on the mobile host (the RC helicopter here).

3.3.1 Inductive Coupling

Inductive coupling has been utilized as a means for RF power delivery for a number of different applications. A common example of the use of inductive coupling for wireless power delivery is passive Radio Frequency Identification Tags (RFID). RFID tags are a potential replacement for optical bar codes. When the identification information from a tag is desired, a reader device is used to direct RF energy to the tag. The tag collects energy from the RF signal and uses it to power its own operation. The RF signal is reflected back to the reader in a modulated fashion in order to transmit tag identification information wirelessly with low energy consumption. Research efforts are currently underway to reduce the cost of these tags in order to make their use more widespread. Research has also gone into building sensor nodes capable of being powered from inductive power supplies. Townsend [42] developed a strain sensing node to be integrated into a knee implant. The knee implant could not be powered from a battery source because of its long service life, so instead a coil and rectification circuitry was included inside the knee in order to wirelessly deliver power for its operation. By using the inductive link, it is possible to provide power to the implant when data are desired, without the need for engaging in invasive surgery to periodically replace batteries. A wireless strain sensor was developed by Chaimanonart [43] for industrial strain sensing applications. Chaimanonart's strain sensor was a custom integrated circuit that could be powered by inductively delivered wireless energy. Strain was measured using a capacitive MEMs wireless strain sensor. Ryan [44] proposed a universal inductive charging system for delivering power to multiple robots. The goal of this work was to allow autonomous robots the option of

recharging their batteries at a wireless charging station on an as-needed basis, as opposed to forcing the robots to charge themselves up at a hard wired connection. The universal inductive charging station could potentially make swarms of autonomous robots more feasible. Another interesting example of a sensor node/UAV which receives power wirelessly from an inductive source is the Power Line Urban Sentry (PLUS) UAV discussed in [45]. The PLUS UAV attempts to solve the problem of supplying power to UAVs for persistant surveillance by equiping the UAV with a special hook which can be used to inductivly draw energy from a power line. The PLUS concept is that when a persistence surveillance UAV is low on power, it can fly down to a power line and land on it using its hook. The UAV then perches on the power line until its battery is adequately recharged. Once the battery is charged the UAV takes off from the power line and continues on its data gathering mission.

The main disadvantage of inductive coupling methods is that in order for them to be effective, the receiver and transmitter must be very close to one another in order to work properly. For example inductively coupled RFID tags typically need to be within one meter of the reader in order to operate.

3.3.2 Microwaves

Wirelessly transmitting power from farther distances (>10 m), requires far-field techniques as opposed to the near-field inductive coupling techniques. The first major pioneer of far-field microwave power delivery was W.C. Brown. Brown developed some of the first major attempts at large scale RF power delivery. He would use large parabolic reflectors to transmit kilowatts of power over a 1 mile (1.6 km) distance. Brown [36] contains a comprehensive overview of the history of wireless power transmission from the work of Hertz to microwave powered aircraft in the late 1970's. Some examples of more recent work in the field of microwave energy delivery include Shams [46]. Shams investigated the use of microwave energy delivery at 5.7 GHz

to power a sensor node embedded in concrete. Sensors embedded in concrete could potentially be commonplace in structural health monitoring systems, so Sham's work focuses on the same application space as this dissertation. Avramov [47] developed a wirelessly powered sensor based on a Surface Acoustic Wave (SAW) oscillator which would change resonant frequency with the quantity being measured. The interrogation signal incident on the device would provide power to operate a frequency modulated (FM) transmitter that would change frequency based on the resonant frequency of the SAW device. The importance of this work is that the FM signal is very appropriate for commonly encountered bandwidth-limited applications. One noteworthy attempt at commercializing wireless power delivery is being undertaken by Powercast. Powercast builds integrated circuits for converting RF energy to DC power. They demonstrated the ability of their technology to continuously provide power to wireless sensor nodes monitoring the temperature of the penguin exhibit at the Pittsburgh zoo [48]. Powercast demonstrated that by using their technology it was possible to significantly improve the useful lifetime of battery powered sensor nodes.

3.4 Theoretical Overview of Wireless Energy Delivery

An outline of the theory used to describe wireless energy transmission by electromagnetic waves is given in [36]. A short description will be given here. In this work Radio Frequency (RF) energy was typically transmitted at 2.5 GHz for a variety of reasons including the ease of obtaining inexpensive hardware at this frequency, and the ability to buy high gain antennas with a weight and volume appropriate for the Radio Control (RC) helicopter. The Friis formula, 3.1, found in [49], can be used to describe the RF energy transmission:

$$P_R = \frac{G_T G_R \lambda^2}{(4\pi R)^2} P_T \tag{3.1}$$

In this equation P_R is the power received, G_T is the gain of the transmitter antenna, G_R is the gain of the receiver antenna, λ is the wavelength of the radiation, R is the distance between the antennas, and P_T is the power transmitted. The wavelength is given by:

$$\lambda = \frac{c}{f} \tag{3.2}$$

In this expression c is the speed of light, and f is the frequency of the single-tone signal. The typical Friis-link parameters used in this investigation are shown in 3.1.

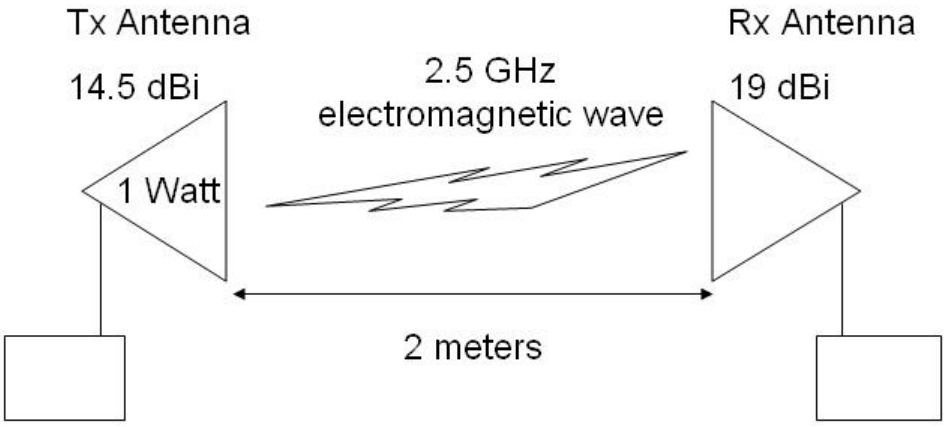

Figure 3.1: Typical wireless energy transmission parameters and test setup used in this investigation.

The Tx antenna is a 14.5 dBi Yagi antenna, and the Rx antenna is a 19 dBi patch antenna. The two meter spacing was selected as an estimated powering distance because it appeared to be the reasonable limit of proximity the helicopter would be able to approach the bridge for the field demonstration at Alamosa Canyon Bridge based on a 1.8 m rotor diameter. The values in Fig. 3.1. can be used with equation

1 and 2 to estimate the theoretical power delivery to the sensor node assuming 100% efficiency.

$$\lambda = \frac{c}{f} = \frac{3 * 10^8\ m/s}{2.5 * 10^9\ Hz} = 0.12\ m \tag{3.3}$$

$$P_R = \frac{(28.18)(79.43)(.12\ m)^2}{(4\pi(2\ m))^2} 1\ W = 0.051\ W \tag{3.4}$$

Equation 3.5 gives the expression for calculating the energy in a capacitor:

$$e = \frac{1}{2}CV^2 \tag{3.5}$$

e is the energy, C is the capacitance, and V is the voltage. Inserting the relevant information yields:

$$e = \frac{1}{2}(0.1F)(3.5\ V)^2 = .6125\ Joules \tag{3.6}$$

$$time = \frac{e}{P_R} = \frac{.6125\ Joules}{.051\ W} = 12.0\ seconds \tag{3.7}$$

So for the assumed 2 m distance, the capacitor can be charged up in no less than 12 seconds assuming there are no losses from the rectifier, antennas, destructive interference, misalignment errors and positioning errors.

3.5 RF Energy Transmission Implementation

3.5.1 Implementation Overview

An overview of the implementation of the wireless energy delivery system is shown in 3.2. The scenario is envisioned as follows. The structure is assumed to be instrumented with sensors/nodes as described above where information such as peak strain or load is mechanically (or otherwise non-electrically) recorded. These sensor nodes

are designed to accept wireless energy transfer via a form of mobile host (such as the RC helicopter in this work). The mobile-host transmits a 2.5 GHz signal through the 14.5 dBi Yagi antenna. The energy is received at the sensor node using the 19 dBi patch antenna. The RF signal then goes to an RF to DC voltage-quadrupler. The function of voltage quadrupler is to convert the RF signal into a DC signal, and to then multiply the DC signal by roughly a factor of 4. The DC signal is then fed to a 0.1 F supercapacitor for storage purposes. The 0.1 F supercapacitor is isolated from the THINNER sensor node by a voltage threshold turn-on switch. The purpose of this switch is to ensure that the sensor node does not unnecessarily attempt to turn-on and waste energy until the voltage on the capacitor is high enough to ensure correct operation of the sensor node. Once the voltage on the capacitor has reached 3.5 V, the turn-on switch closes, and the THINNER sensor node turns on. THINNER uses a capacitance-to-digital converter to interrogate the capacitive sensors discussed in Ch 2. Once the data from the sensors has been collected, THINNER uses its onboard Zigbee radio to transmit the data back to the RF/computational payload on the mobile host. The interrogation process for this sensor node is now complete, and the mobile host can store the data and perform any relevant feature extraction and classification procedures on it. The helicopter can then proceed to any other sensor nodes for interrogation.

3.5.2 RF/Computational Payload

The RF/computational payload is shown in 3.3. Computing on the helicopter is provided by an AMD Geode LX 800 CPU running Unbuntu Linux. The computer boots from a compact flash card for weight savings as well as the elimination of moving parts within the helicopter payload that might compromise reliability. The CPU controls a NovaSource RF signal generator via an RS-232 connection. The RF source sends signals into the RF amplifier so the power level is suitably high for

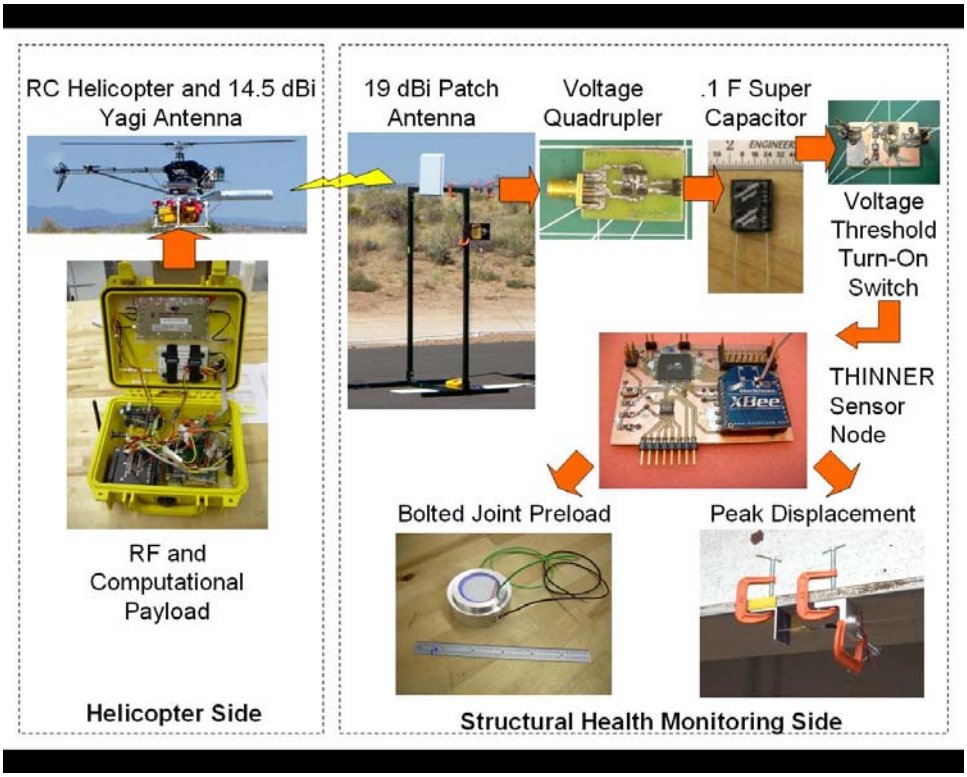

Figure 3.2: Overview of wireless energy delivery implementation scheme.

wireless power delivery ($\sim$ 1 Watt). The computer is running Apache Web Server thus allowing command and control of the computer and RF source from the base station via an 802.11g link. Data is received from the sensor node via an RS-232 enabled XBee modem. The data is stored in the helicopter memory until requested by the base station. The helicopter is also carrying an Axis 207W wireless webcam for recording events as seen by the helicopter. The payload is carried inside a rugged Pelican 1200 case. The helicopter was designed so Pelican 1200 cases with different sensor network payloads could be swapped out quickly. The RF/Computational Payload is powered by two separate 4s 14.8 V nominal, 1500-2200 mAh, Lithium-Polymer (LiPo) batteries. One of the batteries is used to power the computer, Xbee radio, and Nova Source. The other LiPo battery is used to power the RF amplifier. A

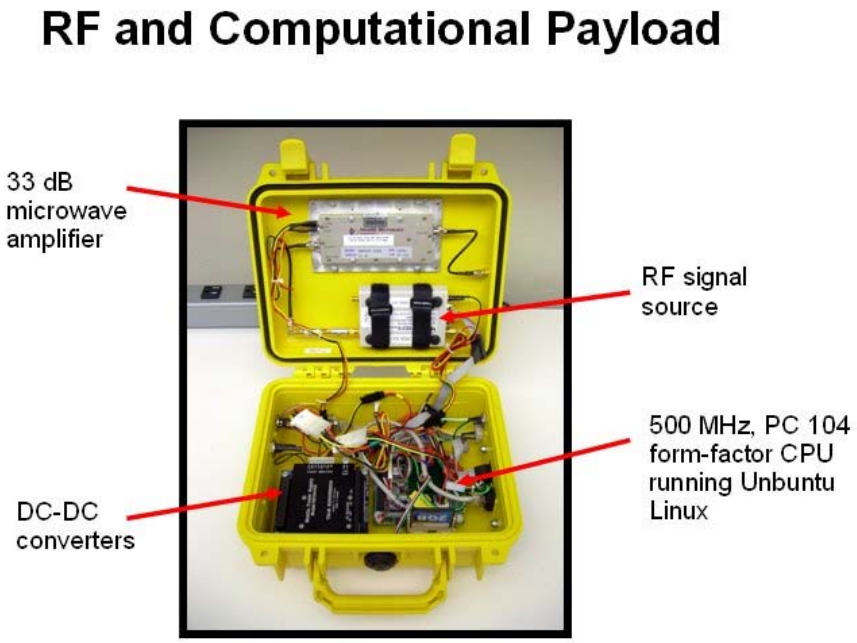

Figure 3.3: RF and computational payload carried by the mobile host

separate 2s, 7.4 V nominal, 800 mAh LiPo battery is used to power the Axis webcam. The helicopter servos, gyro, governor and receiver are powered by an additional 4.8 V, 4 cell, 1.5 Ah, nickel-cadmium (NiCad) battery.

3.5.3 Transmitting Antenna

The transmitting antenna used on the helicopter is a 14.5 dBi Yagi antenna, as shown in Fig. 3.4. The antenna is basically cylindrical in shape due to the radome covering the actual Yagi antenna itself. The overall dimensions of the antenna are 476 mm long X 76.2 mm diameter (18.75 in. long X 3 in. diameter).

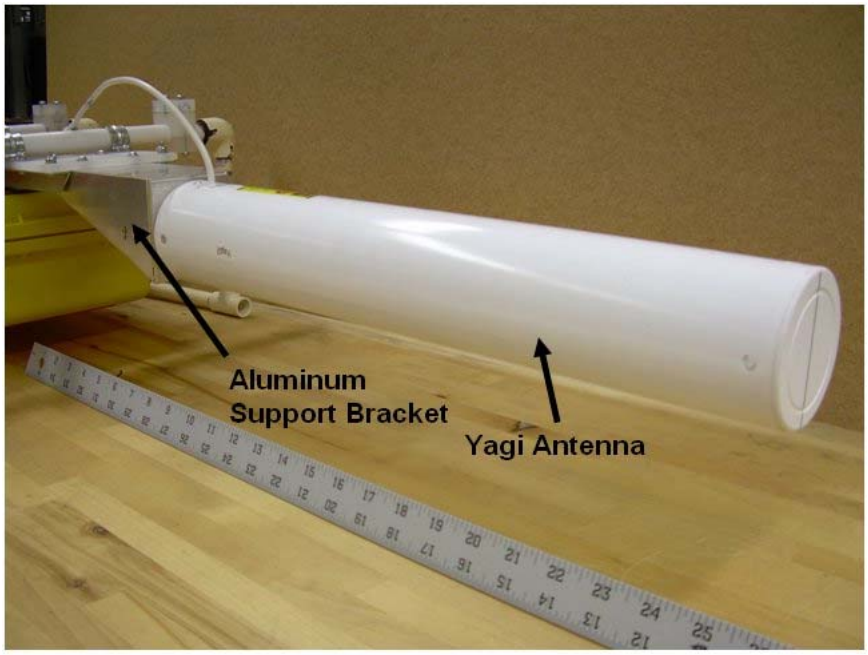

Figure 3.4: Yagi antenna used to transmit RF energy.

The selection of the antenna for the helicopter was not trivial. In order to improve the performance of the RF energy transmission, it would be necessary to place the antenna as far toward the front of the helicopter as possible. Unfortunately the farther forward the antenna is on the helicopter, the larger the risk that the helicopter center-of- gravity would be shifted forward of the main shaft, thus upsetting the aerodynamic balance of the helicopter. Furthermore, any bracket that put the antenna toward the front of the helicopter would have to be long, lightweight, and stiff enough to support the weight of the antenna. If the bracket stiffness were too low, there was concern that the antenna might vibrate wildly and break off, or be incapable of maintaining adequate pointing accuracy with the receiving antenna. Furthermore, it was decided that the antenna should be relatively high gain for a higher power transfer, but not so high gain that the pointing accuracy of the helicopter would have

to be so precise that the helicopter may end up only being aligned with the receiver antenna on a sporadic basis. As can be seen from Equation 3.1, the higher the gain of the antennas, the higher the energy transmission to the receiver. However, as gain increases, the main lobe of the antenna decreases in size, thus requiring more precise alignment between the receiving and transmitting antenna. Another concern with high-gain antennas is that as antennas increase in gain, they also increase in size and weight. The characteristic size of the antenna depends on the wavelength of the radiation being transmitted from it. This is a major reason why a 2.5 GHz frequency with a wavelength of 0.120 meters was chosen as the RF signal frequency over other widely used frequencies such as 900 MHz with a wavelength of 0.333 meters. 900 MHz antennas with comparable gain were deemed too large for the initial test of the mobile host wireless sensor network. A number of different types of antennas were considered for placement on the helicopter. The antennas included patch antennas, Luneburg lenses, microwave horns, waveguide antennas (a.k.a. cantennas), parabolic reflectors, and Yagi antennas. Given the constraints discussed, the main contenders were the parabolic reflector and the Yagi antenna. Both were high-gain, acceptable cost, and readily available, but the parabolic reflector did not have a shape conducive to being mounted in a structurally sound manner to the airframe. Furthermore, it was deemed to be difficult to mount the parabolic reflector adequately toward the front of the helicopter without both increasing the rotational inertia of the airframe unacceptably and needing an overly heavy bracket to maintain the required stiffness. The parabolic reflector was also relatively heavy. On the other hand, the Yagi antenna was fairly lightweight. The shape and size of the Yagi made it conducive to be placed in the front of the helicopter. In addition, the weight of the Yagi antenna was distributed fairly uniformly throughout the length, so a large amount of mass was not located at a far distance from the current center of gravity thus increasing the rotational inertia. Furthermore the Yagi antenna was relatively easy to mount in a stiff manner. Because the Yagi antenna has a high aspect ratio as shown in

Fig. 3.4, the antenna did not need a long mounting bracket to place it properly at the front of the helicopter. Instead a short aluminum sheet fabrication was used to mount the Yagi to the airframe. This mount was very stiff because of its short length and high moment of inertia. The mount was then attached to a polypropylene sheet with two longitudinal aluminum angle stringers. The polypropylene sheet was then attached to the airframe completed the load path from the end of the Yagi antenna to the airframe center of gravity. Simple static tests on the lab table showed that the mount was very capable of transferring forces from the far end of the antenna to the center of gravity of the helicopter without unacceptable deflections.

3.5.4 Receiving Antenna

The receiving antenna selected for this investigation is shown in Fig. 3.5. The antenna shown is a 19 dBi patch antenna with overall dimensions of 387 mm X 387 mm X 25.4 mm (15.25 in X 15.25 in X 1 in). The main driving factors for the selection of the receiving antenna were overall size and gain. Another important consideration would be wind loading. The chosen antenna could not be permitted to have a size and shape that would facilitate high wind loading, snow loading, etc. For these reasons, the receiver antenna should have a low profile. Weight was not as large a factor because the antenna is placed on a civil structure. The aesthetic nature of the antenna was also of some concern because, in some applications, it may be mounted within view of the public. The nature of the antenna should also be such that it would facilitate alignment with the transmitting antenna on the helicopter.

Once again a wide range of antennas were considered for the receiver. Ultimately however, a patch antenna was selected for use because of its low profile on the bridge and the ease of mounting and alignment with the helicopter. Furthermore, of all the antennas considered, the patch antenna had the highest gain for the allowable volume on the bridge. Concern also has to be taken when mounting the antenna on

Figure 3.5: 19 dBi Yagi patch antenna used for receiving wireless energy transmissions from the helicopter.

the structure. Civil structures such as buildings and bridges often contain structural elements which can facilitate multi-path distortion. Multi-path distortion is caused when signals take more than a single path to travel between two locations. In general, the time the signal takes to travel along different paths is different from path to path. The effective result is that multiple identical signals arrive at the final location out-of-phase. The effect on RF energy transmission applications of the out of phase arrivals is that nulls and peaks are created in the spatial electromagnetic field. There may be some locations where the efficiency of RF energy transmission is either greatly reduced or improved, although in general multi-path distortion is an undesirable phenomenon. Structural elements which can give rise to multi-path distortion include steel girders, metal siding, metal-coated glass, ground vehicles and metal guard rails. Multi-path distortion effects should be considered when selecting a mounting location for the receiver antenna. The reader is referred to Ref. [50] for more discussion of the multi-path distortion phenomenon.

3.5.5 RF to DC Converter

A vital portion of the RF energy delivery process is taking the RF energy, and converting it to DC energy that can be used to power a sensor node. The combination of a receiver antenna and an RF-to-DC converter is commonly referred to in the literature as a "rectenna". The reader is referred to Ref. [36] for a thorough discussion on the history of rectenna research. It is desirable that the RF-to-DC converter be relatively low-cost, small size, and high efficiency. Furthermore, it is vitally important that the RF-to-DC converter be able to supply the DC output at a high enough voltage to run the desired electronics. In this work, the sensor node was designed to operate from a voltage of 3.3 V. Given the resources of the investigators, the easiest way to supply this voltage using RF energy transmission techniques has been to build multiple-stage RF voltage multipliers that effectively rectify the RF-to-DC, and also multiply the DC output voltage. A detailed discussion on voltage multipliers operations and design considerations is given in [37]. In this work, two types of voltage multipliers were primarily considered. The first type was the half-wave series voltage multiplier, and the second was the full-wave series voltage multiplier. The diodes used in both applications were HSMS 8202 surface mount microwave Schottky mixer diodes available from Avago technologies. These microwave diodes are designed to have a bandwidth up to 14 GHz in frequency and they can dissipate up to 75 mW of power. Equation 3.4 showed 51 mW of theoretical maximum power received so these diodes should be able the handle this RF energy delivery application. The schematic for the half-wave series multiplier is shown in Fig. 3.6. An image of the hardware implementation of the half-wave voltage quadrupler is shown in Fig. 3.7. This particular voltage multiplier was tested in the lab using the parameters described in the theoretical section.

The results of the test can be seen in Figs. 3.8 and 3.9. Figure 3.8 shows the voltage on the 0.1 F capacitor during the charging process, and Fig. 3.9 shows the calculated energy in the capacitor as time proceeds. In addition, Fig. 3.9 shows a

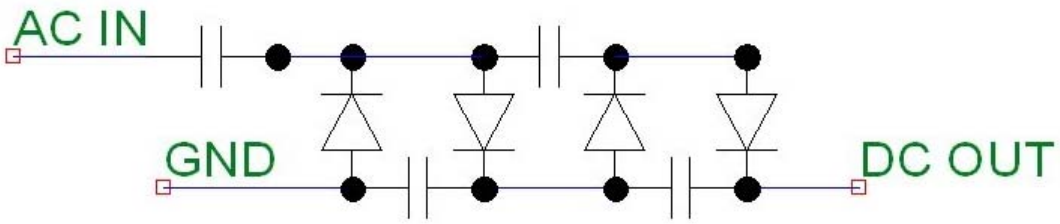

Figure 3.6: Schematic of half-wave voltage quadrupler circuit.

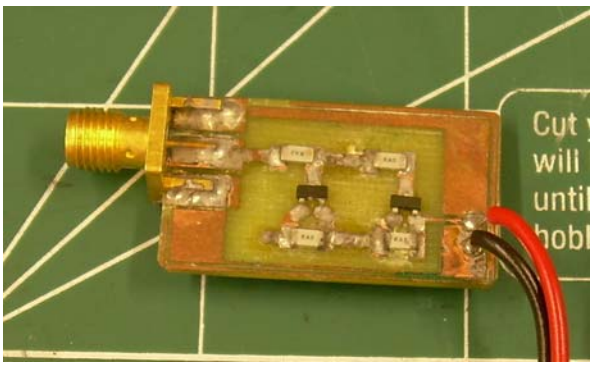

Figure 3.7: Half-wave voltage quadrupler.

least squares linear fit in order to estimate the power being delivered to the capacitor. The result is that about 5.1 mW of power is actually being delivered to the capacitor. Based on the result of equation 3.4, only 10% of the theoretical amount of power is actually being delivered to the capacitor and it will take 2 minutes to charge the 0.1 F capacitor to 3.5 volts. It was not clear at this time if the current rectenna performance would be acceptable for charging a sensor node with a moving helicopter. It was ultimately decided that the performance of the rectenna should be improved.

The most logical next step appeared to require a change the multiplier architecture from a half-wave configuration to a full-wave configuration. The hope was that changing to the full wave configuration would double the power output of the

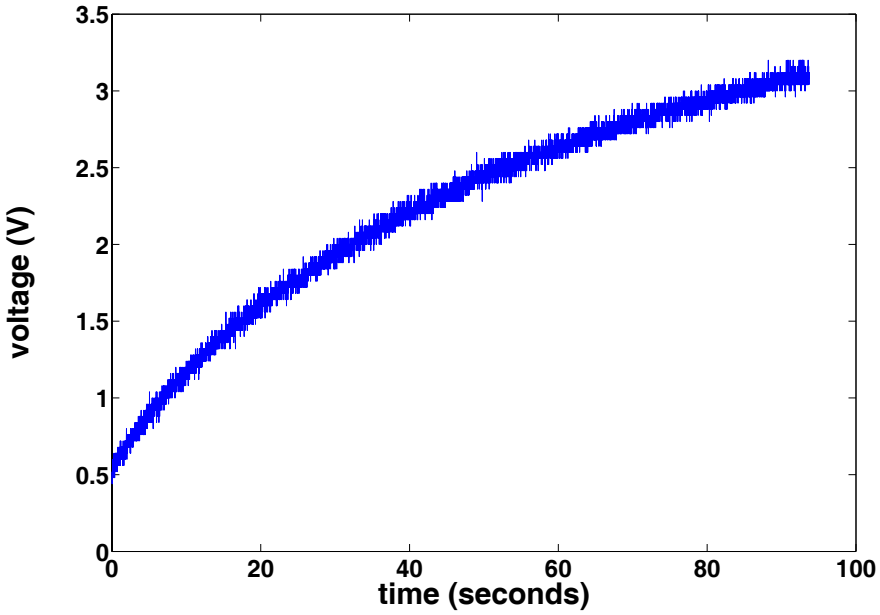

Figure 3.8: Voltage present on 0.1 F capacitor when connected to half-wave voltage quadrupler. 2 meters transmission distance, 1 watt of transmit power.

rectenna. The schematic for the full-wave configuration is shown in Fig. 3.10. The hardware implementation of the full-wave voltage quadrupler is shown in Fig. 3.11 The full-wave rectifier was then placed through the same testing as the half-wave rectifier. The resulting voltage vs time curve is shown in Fig. 3.12. The calculated energy in the capacitor is shown in Fig. 3.13.

The most important features of these plots is the fact that the average power delivered to the capacitor is 8.1 mW. These full-wave power value is significantly larger than the power value obtained with the half-wave rectifier. The power has increased by 58%. The added complexity of the full-wave voltage quadrupler is more than offset by the increased power received by the capacitor. It was decided that the full-wave voltage quadrupler would have adequate performance to meet the objectives of the first phase of the "mobile-host" structural health monitoring wireless

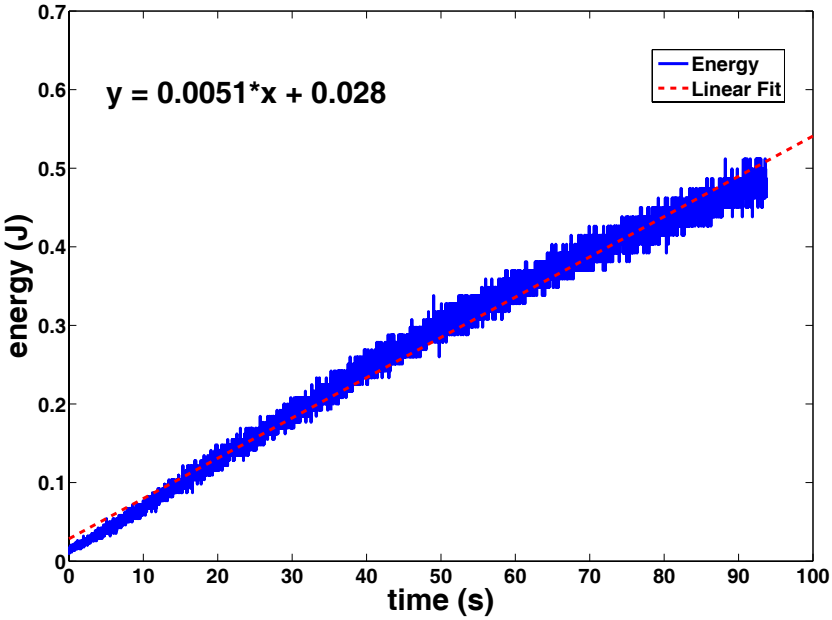

Figure 3.9: Energy in the 0.1 F capacitor when connected to the half-wave voltage quadrupler. Note the power on the capacitor is on average 5 mW.

senor network.

3.5.6 0.1 F Supercapacitor

The selection of the energy storage medium for an RF energy delivery application is vitally important. The energy storage medium that seemed to be most appropriate for this application was the super capacitor. To be specific, PowerStor PB series super capacitors as shown in Fig. 3.14 were chosen for their many attractive characteristics. These super capacitors are built based on a Aerogel carbon foam. The super capacitor is small 12 mm X 11 mm X 5 mm (.472 in X .433 in X 0.196 in), lightweight, and very simple to use. There is no need for power conditioning electronics as might be needed with some batteries. Furthermore, the super capacitors have a low Equivalent Series Resistance (ESR), 10 Ohms nominal at 1000 kHz. The chosen supercapacitor

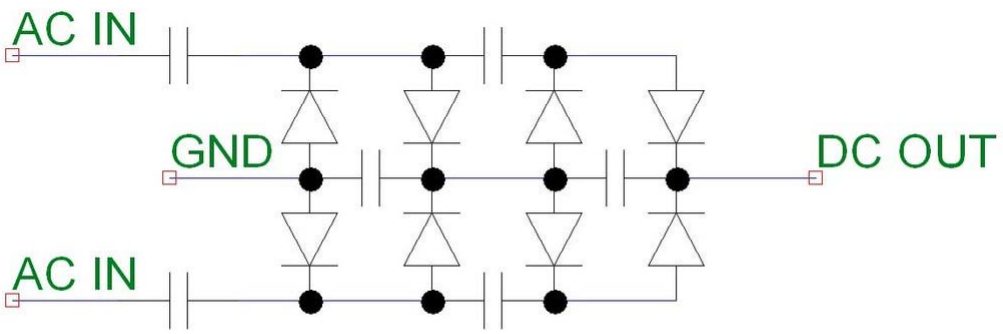

Figure 3.10: Schematic of the full-wave voltage quadrupler.

has a value of 0.1 F. This value was chosen based on previous wireless sensor network research using 0.1 F capacitors to charge Zigbee radios [51]. A number of different capacitors were considered including 0.47 F, and 1 F, but the time-to-charge, and energy storage capacity of the 0.1 F capacitor seemed the most appropriate for an RF energy delivery application. The super capacitors were also relatively low-cost at $3.93 each and very easy to obtain from commercial vendors.

3.5.7 Voltage Threshhold Turn-on Switch

Once the energy has been delivered by the mobile host and has been stored in the sensor node's capacitor, the next step is to deliver the energy to the electronic components on the sensor node. If the microcontroller is directly connected to the 0.1 F capacitor, the microcontroller will attempt to turn on before the voltage is high enough for the microcontroller to operate properly. The result is that at a certain voltage, the microcontroller will be in a pseudo-on state that promotes heavy, wastefull charge leakage from the supercapacitor. Furthermore, the energy drain of the microcontroller on the capacitor is so high that it is impossible for the helicopter

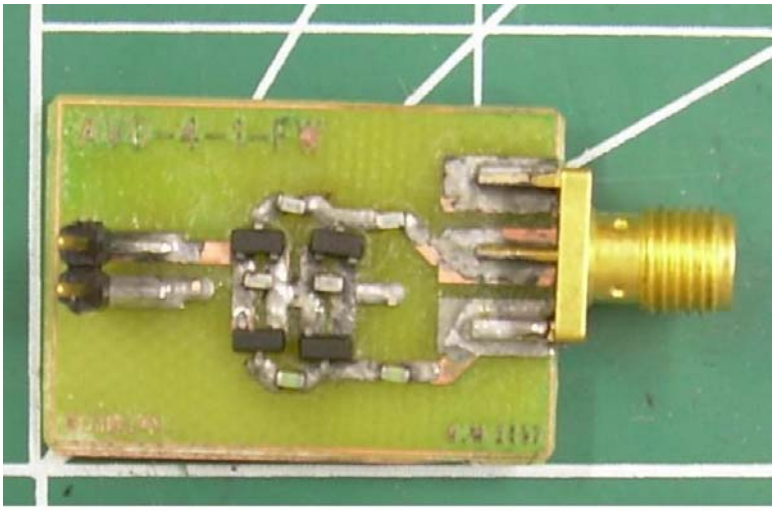

Figure 3.11: Full-wave voltage quadrupler RF to DC converter.

to deliver more power than the microcontroller consumes. It is therefore impossible to ever charge the capacitor on the microcontroller to the required voltage for its proper operation. It would be absolutely necessary to develop some form of "switch" to make sure that the microcontroller did not receive any energy until the capacitor was fully charged to 3.5 V. This switch would have some very stringent requirements. First of all, it would need a very high impedance when the switch is in the open position so no energy would reach the microcontroller until the correct time. The switch would have to transition to the closed position when the voltage on the capacitor had reached 3.5 V. The switch would have to consume a very small amount of energy. To make matters more difficult, the switch would have to be capable of operating without any form of stored energy because there is no battery at the sensor node. The switch would have to be capable of running solely from the energy supplied by the helicopter. The acquisition of such a turn-on switch was not simple. First off, to the author's best knowledge, a switch fulfilling the requirements is not currently commercially available. Furthermore, techniques such as periodic sampling of

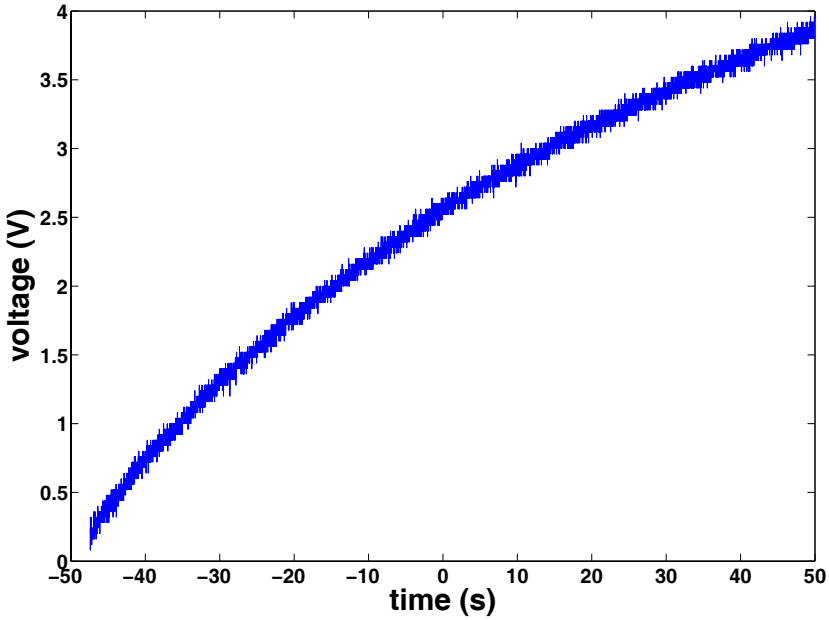

Figure 3.12: Voltage on 0.1 F capacitor when connected to full-wave voltage quadrupler

the capacitor voltage with an Analog-to-Digital (A-to-D) converter are not practical in this situation because during a large fraction of the charging time, the voltage available from the capacitor is not high enough to run the microcontroller or the A-to-D converter. The solution to the switching problem was solved using input from the author (structural engineering), Daniele Musiani (electrical engineering), Donald Kimbal and Cuong Vu (electrical engineering CALIT^2), and Eric Flynn (structural engineering). The resulting switch was made up of micro-power comparators utilizing voltage-band gap references, low-voltage analog switches and a high impedance voltage divider. The block diagram representation of the switch is shown in 3.15.

The operation of the voltage threshold turn-on switch can be described as follows. As the 0.1 F capacitor is charged up, a very small fraction of the current is used to excite a high-impedance voltage divider connected to a nanopower comparator. The

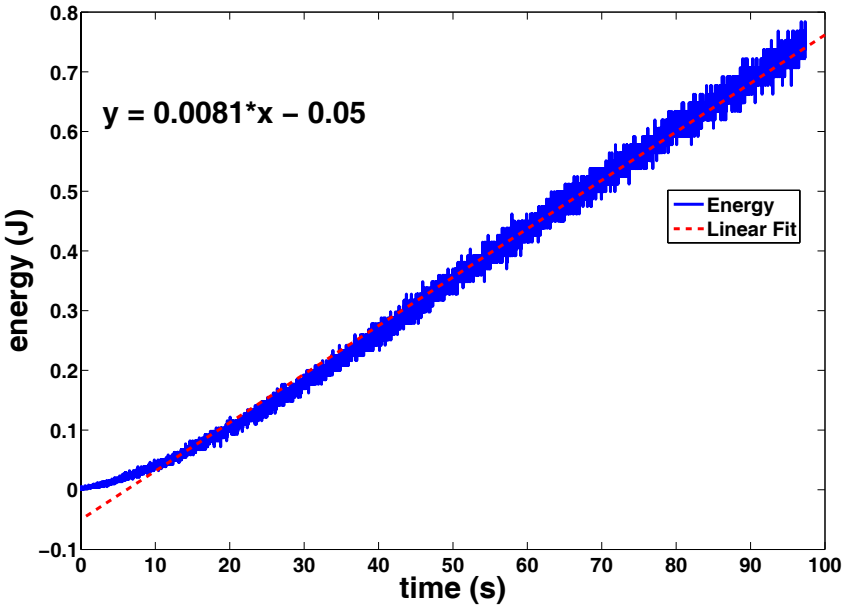

Figure 3.13: Energy on 0.1 F capacitor connected to full-wave voltage quadrupler. Note the power is 8.1 mW.

other pin of the comparator is connected to a 1.24 V band gap voltage reference. Once the voltage on the capacitor reaches a value such that the output of the voltage divider exceeds the 1.24 V supplied by the voltage bandgap reference, the comparator sends a signal to a MAX4626, normally-open, analog switch, thus signaling the switch to close. Once the switch closes, current from the capacitor is allowed to flow through the first switch, and then into the control pin of a second normally-open switch. The second normally open switch connects the 0.1 F capacitor, and the THINNER sensor node. At this point current begins to flow from the capacitor through the second switch and into the THINNER sensor node. In addition, current also flows from the capacitor through the switch, and through a feedback loop into the control pin of the second switch, thus ensuring that the second switch remains in the closed position throughout the complete discharge of the 0.1 F capacitor. Power for the comparators

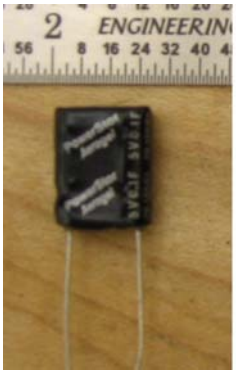

Figure 3.14: PowerStor PB series Aerogel super capacitor.

and switches is supplied by the energy in the 0.1 F capacitor as it is charged. The voltage on the capacitor at which the switch allows current to flow is controlled by the values of the resistors in the high-impedance voltage divider. The resistor values used in the high-impedance voltage divider are selected as follows. The switches will go from their open position to the closed position when the voltage in the middle of the voltage divider is greater than the 1.24 V bandgap reference. The relationship can be written in terms of the voltage on the capacitor as follows:

$$\frac{R_1}{R_1 + R_2} V_{cap} > 1.24\ V \tag{3.8}$$

In this expression R_1 is the resistor in the voltage divider closest to ground, and R_2 is the resistor in the voltage divider connected to the 0.1 F capacitor. In order to measure the characteristics of the turn on switch, a test was conducted using Agilent 33220A function generator. The switch was excited with two periods of a ramp function. The ramp function had a low value of 0 V and a high value of 4 V with a period of 20 seconds Fig. 3.16 shows the input and output voltages of the switch during the test.

The voltage divider is using values of $R_1 = 56$ kOhms, and $R_2 = 100$ kOhms. Using these values and Equation 3.8, the estimated voltage at which the switch closes

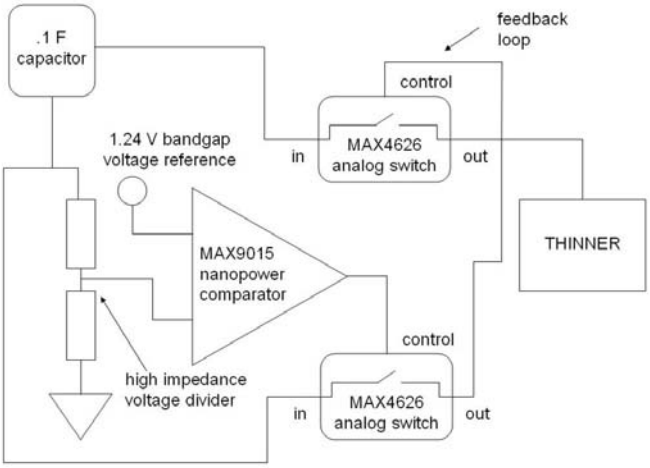

Figure 3.15: Block diagram of voltage threshold turn-on switch.

is 3.45 V. This value corresponds very closely with results of the test in Fig. 3.16. at about 10 seconds the switch closes and the output voltage matches the input voltage. Then as the voltage drops the input and output voltage follow from that point on. This dropping voltage following characteristic has good and bad effects. The positive outcome of the voltage following is that the capacitor will continue supplying energy as the voltage drops, which is absolutely necessary for the proper operation of the switch. On the negative side, if the capacitor is recharged after it begins to discharge, the output of the switch will follow the input and the switch will allow the sensor node to attempt to turn on before the voltage on the capacitor is high enough to allow the sensor node to operate properly. It would be preferable if the switches closed when the voltage on the capacitor dropped below 2.7 V. This voltage is the threshold at which the capacitance to digital converter stops working properly. If the switches reopened at 2.7 V, the RF energy delivery could be used to recharge the capacitor from 2.7 volts back up to 3.5 V. This recharging should take half the time as the time required to go from 0 to 3.5 V because about half the energy is stored

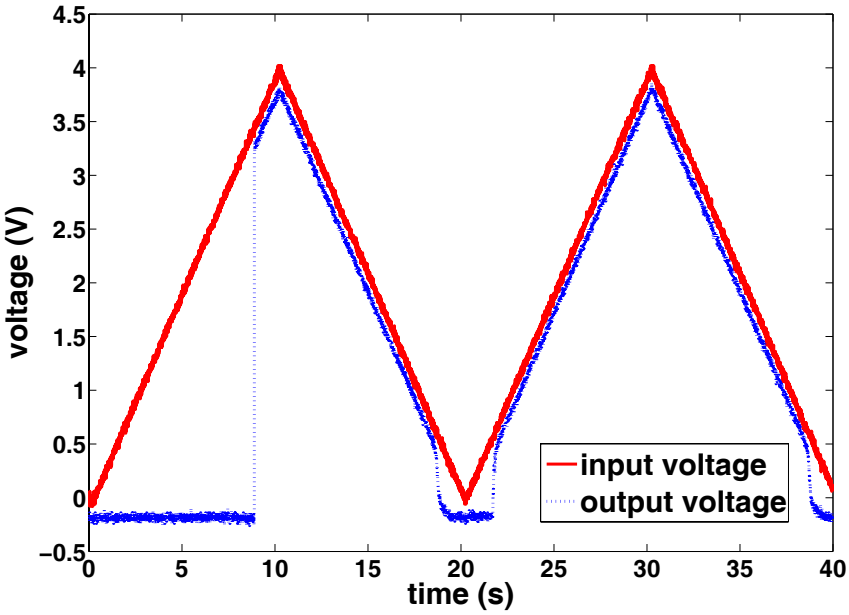

Figure 3.16: Characteristics of voltage-threshold turn-on switch.

in the first 2.7 V. At this time the switches do not reopen unless the capacitor is completely discharged. Future work will consider a slightly modified design of the switch to obtain more favorable on-off characteristics.

Since one of the main concerns of the present wireless sensor node applications is power consumption, it was desirable to measure the effect the switch had on the net power consumption of the sensor node. Initial calculations of the power consumption of the various components suggested the use of the circuit model shown in Fig. 3.17. Basically the switch is modeled as the 0.1 F super capacitor in parallel with the voltage divider made up of the 100 k Ohm and 56 k Ohm resistors in series. Two 100 k Ohm resistors are also in parallel with the capacitor and voltage divider. These two resistors were used to lower the effective impedance of the circuit board to minimize voltage divider effects which were manifesting themselves between the input and output signals. By using this circuit model basically it is assumed that if

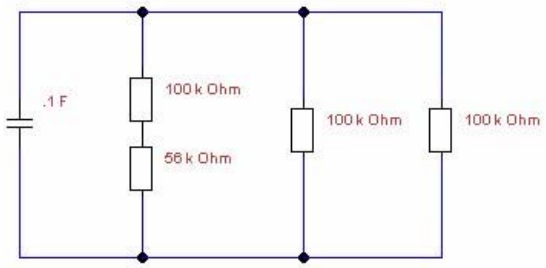

Figure 3.17: Discrete circuit model of turn-on switch for energy dissipation modeling.

the capacitor is initially charged, the charge on the capacitor will discharge through the resistors, and the voltage vs. time relation can be described with the expression:

$$V = V_o e^{\frac{-t}{RC}} \tag{3.9}$$

Where V is the voltage on the capacitor, V_o is the initial voltage on the capacitor, R is the net resistance, t is time, and C is the 0.1 F value of the capacitor. Using the circuit model of Equation 3.9, the expected value of R is 37.86 k Ohms. In order to verify the model, measurements were taken with an Agilent 34410A 6 1/2 digit multimeter. Measurements were made over approximately two hour period with a 1 Hz sampling rate. The 0.1 F capacitor was initially charged to 4V and then attached to the remainder of the switch to begin the switch energy consumption process. The resulting data is shown in equation 3.18, along with a plot of the modeled voltage using equation 3.9 with parameters $R = 37.86$ k Ohms, $C = 0.1$ F and $V_o = 4$ V.

The plot in Fig. 3.18 shows a very close agreement between the measured and modeled voltages, thus suggesting that the model in Fig. 3.17 does a good job of describing the dynamics of the voltage-threshold turn on switch. Using equation 2.8 to calculate the percentage absolute error, the data deviates from the model a

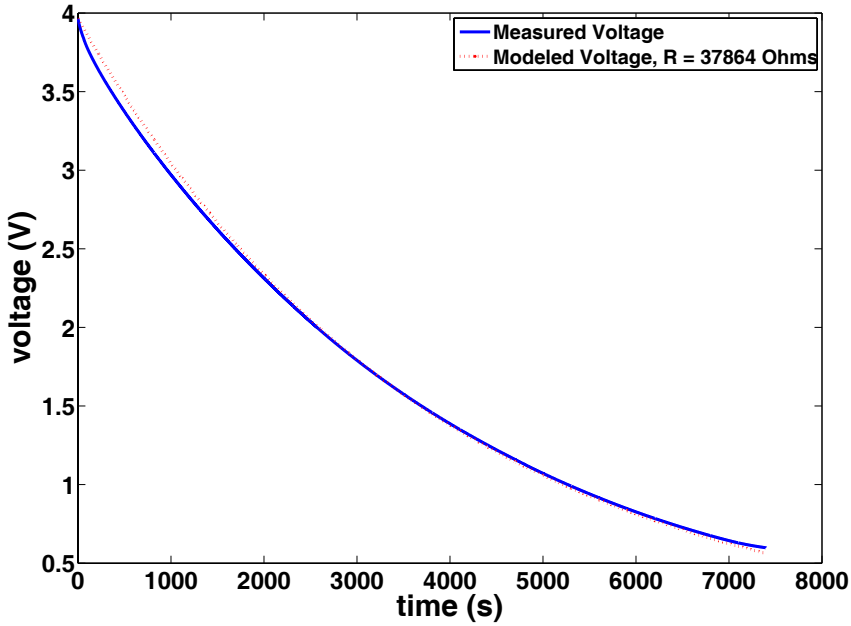

Figure 3.18: Measured and modeled voltage characteristics of the voltage threshold turn-on switch.

maximum of 6.4% and on average the data is different from the data by 1.57 %. In order to gain further improvement, it is desirable to find the effective R value assuming the model in equation 3.9. An exponential curve was fit to the data shown in Fig. 3.18. The effective R value was calculated to be 39 kOhms. A plot comparing the measurement with the exponential model with the two R values is shown in Fig. 3.19.

The two models both compare very well with the measured voltage data. Equation 2.8 is used to calculate the percentage absolute error. When R is set to 39 kOhms the maximum absolute divergence of the data from the model is 3.35% and the mean absolute difference is 2.77 %. These results suggest the following conclusions. First the exponential model describing the voltage on the capacitor as it self-discharges is at least correct to first order. Second, because the exponential

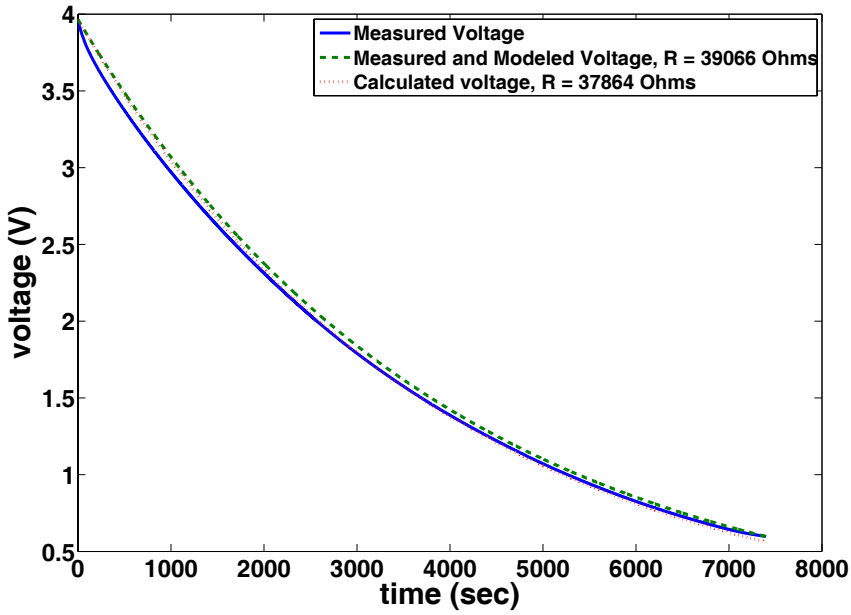

Figure 3.19: Comparison of the measured voltage vs. the two models with different resistor parameters.

model is primarily correct, the majority of the energy lost in the circuit is lost when the capacitor discharges through the resistors. The most obvious way to reduce the power consumption of the switch is to increase the effective R value used in Equation 3.9. The R value can be increased in two ways. First, the values of all the resistors can be increased. Increasing the resistor values increases the impedance, but it is important to note that the net impedance will always be less than or equal to the impedance of the lowest resistance parallel current path. The second way to increase the effective R value is to put fewer resistors in parallel. Further investigation may show that this approach is, or is not, possible.

Next it was found desirable to estimate the power usage of the switch. Since the voltage on the capacitor is governed by an exponential law, the energy on the capacitor will also be governed by an exponential law. For quick power usage estimates

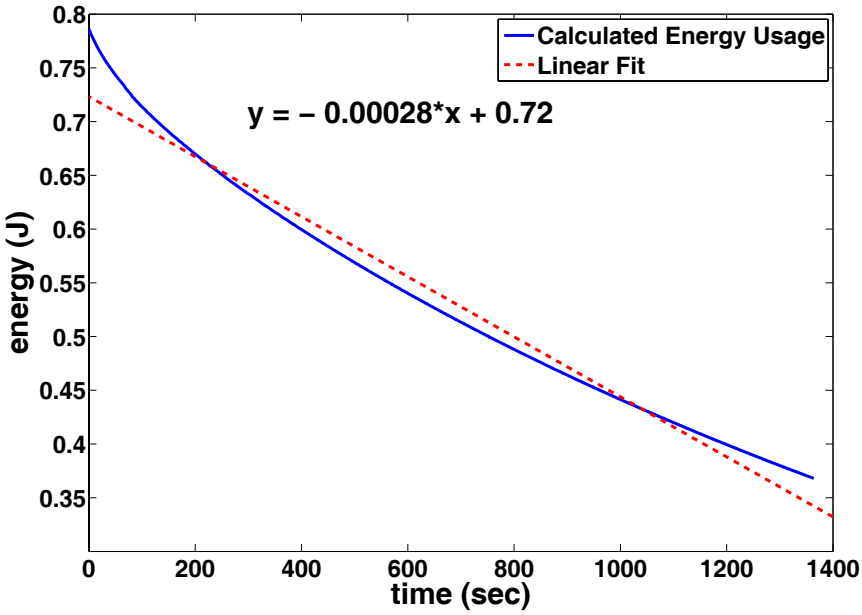

Figure 3.20: Calculated energy stored in 0.1 F capacitor as energy is drained from 4 V to 2.7 V by the turn-on switch.

the exponential law is cumbersome, so the decision was made to make a linear approximation to the exponential law. It was determined the most useful time period on which to base the linear approximation would be to start when the voltage on the capacitor is 4 V, and continue to the point where the voltage on the capacitor is 2.7 V. A plot showing the calculated energy in the 0.1 F capacitor and the linear approximation to these data is shown in Fig. 3.20. This plot shows that the linear fit is a reasonable average fit to the energy in the capacitor. The slope of the linear fit indicates that the switch is consuming 279 μW, rounded to 280 μW on the plot. Going back to the model shown in Fig. 3.17, and using the relation:

$$Power = \frac{V^2}{R} \tag{3.10}$$

An average voltage V of 3.35 V, and a resistance R of 39 kOhms can be used

based on the linear fit from the measured data to calculate power. The resulting power consumption is 287 μW, which is within 2.9% of the 279 μW derived from the linear fit to the exponential energy data shown in Fig. 3.20. The power consumption is acceptable for the first phase of the mobile host wireless sensor network project, but there is much room for improvement. Further research should be focused on both improving the power consumption of the switch as well as improving the overall on-off behavior of the switch for further energy conservation and robust operation.

3.6 Experimental Test Results

Experimental evaluation of the RF energy delivery circuit consisted of three different test. The first experiment involved using the RF energy delivery setup in the laboratory environment. The second test involved the use of the RF energy delivery to charge up a THINNER sensor node on the Alamosa Canyon Bridge in southern New Mexico. The final test was also conducted at Alamosa Canyon Bridge, but instead of THINNER being placed on the bridge, THINNER was placed on a step ladder in order to mitigate some aerodynamic effects on the helicopter. A summary of the results from the three tests is given below.

3.6.1 RF Energy Delivery in the Lab

The first tests conducted using the RF energy delivery were done at CALIT^2 in San Diego, as well as the Engineering Institute in Los Alamos, NM. The RF energy delivery hardware was set up in exactly the same way as is mentioned in the theoretical Section 3.5. The full-wave voltage quadrupler was used as the RF to DC converter. The results of these tests have already been presented in Fig. 3.12, and Fig. 3.13. The tests showed that the typical time for the 0.1 F capacitor to charge to 3.5 V was 95 seconds. If the average power is defined as the slope of a least squares fit to the calculated energy on the 0.1 F capacitor, the average power delivered is

8.1 mW. This value was deemed acceptable for the first version of the "mobile-host" wireless sensor node. Next the RF energy delivery was tested at Alamosa Canyon Bridge in Southern New Mexico.

3.6.2 RF Energy Delivery to the THINNER Sensor Node Located on Alamosa Canyon Bridge, Using Helicopter

The first full-scale test of the "mobile-host" wireless sensor node was at the Alamosa Canyon Bridge in southern New Mexico. The THINNER sensor node was placed on the understructure of the bridge. A capacitive peak displacement sensor was connected to THINNER. The 19 dBi antenna was hung slightly below the longitudinal steel bridge supports. The RF energy delivery equipment was placed on an radio control (RC) Spectra G helicopter, which was manually flown up to the 19 dBi patch antenna on the bridge to charge up the thinner sensor node. An image of the Alamosa Canyon Bridge test setup is shown in Fig. 3.21. A schematic of the test is shown in Fig. 3.22.

A plot showing the charging characteristics of the THINNER sensor node as it receives the the RF energy delivery from the helicopter is shown in Fig. 3.23. Figure 3.24 shows the calculated energy on the 0.1 F capacitor as it is charged. These plots show that to reach 3.5 volts took more than 270 seconds, which is significantly larger than the 95 seconds needed in the laboratory experiment. The reason for this discrepancy can be attributed to a few different factors. First, the pilot reported that the helicopter was very difficult to align with the patch antenna on the bridge. The first issue was that he was on the ground level, and he did not have a good view of the alignment between the patch antenna and the Yagi antenna and thus had no direct feedback as to the quality of RF link he was maintaining. The second reason was that the pilot reported that wind blowing on the underside of the bridge was making helicopter control difficult in a hover mode. Furthermore, the pilot also

Figure 3.21: Alamosa Canyon Bridge test setup.

reported a tendency for the helicopter to want to travel into the bridge, so he would need to periodically draw back from the bridge structure to avoid damage to the helicopter. Video footage of the tests show that the helicopter is constantly traveling in a loop in an effort to maintain the proper distance and orientation of the bridge. This behavior is also observed in the voltage vs. time plot (Fig. 3.23).

The plot exhibits characteristics in common with a stair step. The flat portions of the "stairs" correspond to times when the helicopter was either too far away from the antenna, or was misaligned with the patch antenna. The vertical portions of the "stairs" correspond to the periods where the helicopter was tending to move toward the bridge and/or had the best alignment with the patch antenna. Once again take an average of the power delivery in a least squares sense as is calculated in Fig. 3.24, there is an estimated average power delivery of 2.5 mW. The value of the

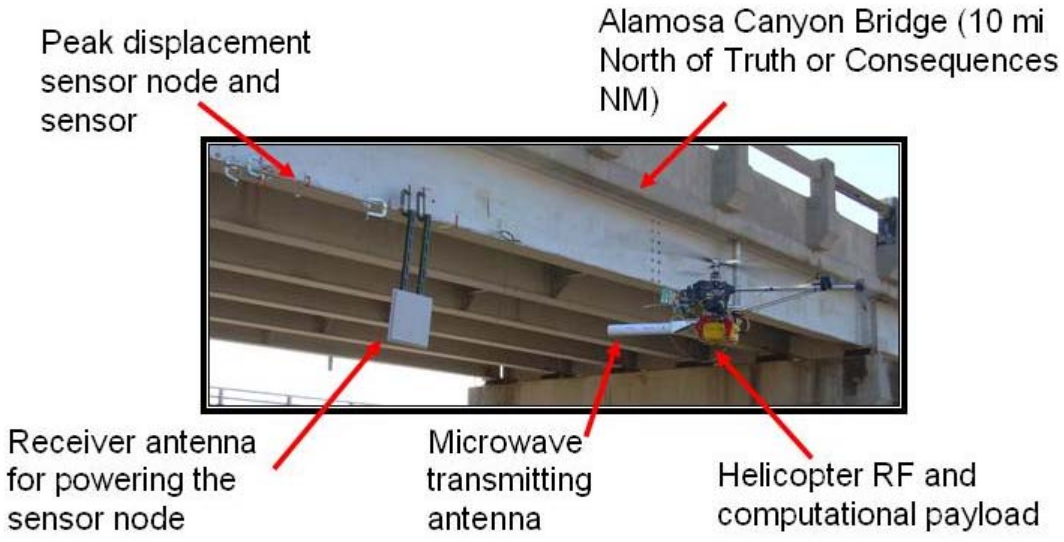

Figure 3.22: Bridge test schematic.

power delivered in the field is significantly lower than the power delivered in the lab. The discrepancy is mainly caused by errors associated with the misalignment of the antennas. On interesting feature of Fig. 3.24 is that there is a portion between 166 and 180 seconds that has a higher power delivery over a characteristically significant time than most of the rest of the plot. The high power portions of Fig. 3.24 will be discussed further in a later section. Despite the low-power RF energy delivery, the THINNER sensor node was successfully charged to 3.5 V, and the sensor node completed 3 peak displacement sensor measurements with the energy stored in the 0.1 F capacitor.

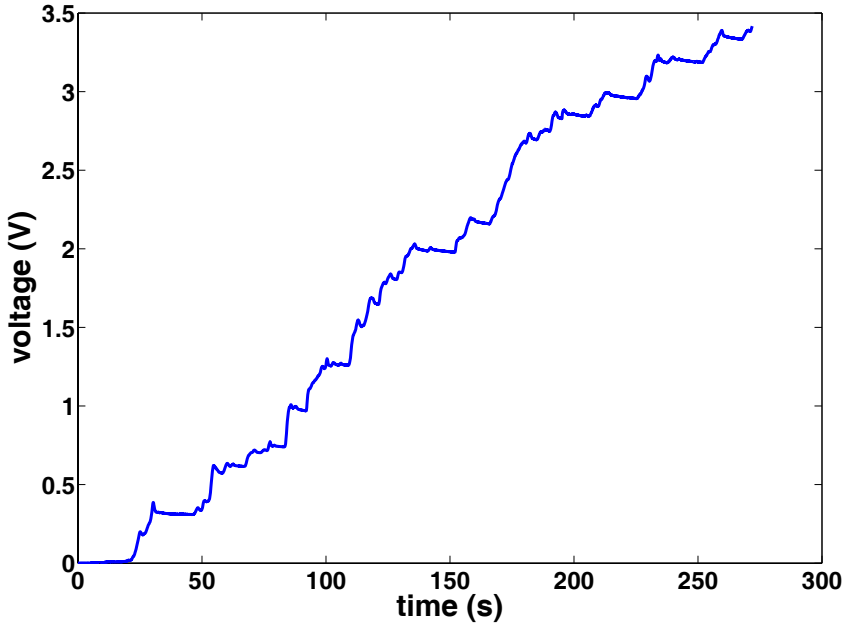

Figure 3.23: Voltage on 0.1 F capacitor as the helicopter charges THINNER for peak displacement sensor test demonstration

3.6.3 RF Energy Delivery to the THINNER Sensor Node Located on Ladder, Using Helicopter

The results of the first field experiment suggested that perhaps the RF energy delivery efficiency could be increased by improving the accuracy of the alignment between the Yagi antenna on the helicopter and the patch antenna on the bridge. In order to test this hypothesis, the patch antenna and THINNER sensor node was moved closer to ground level by mounting it on a step ladder as shown in Fig. 3.25. In addition, a wireless camera was also placed on the helicopter in order to better record the helicopter position relative to the patch antenna. In this experiment, the bolted joint preload sensor was connected to THINNER. Mounting the patch antenna on the step ladder allowed the pilot a better view for aligning the antennas.

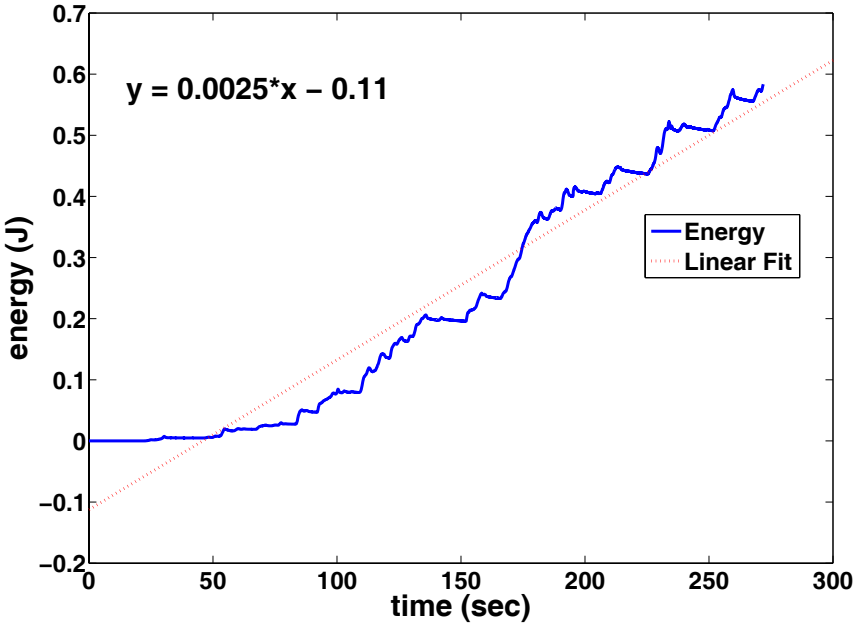

Figure 3.24: Calculated energy on 0.1 F capacitor as the helicopter charges THINNER.

Furthermore, aerodynamic forces caused by the wind blowing off the bottom of the bridge were reduced. Once again the helicopter was used to charge up the THINNER sensor node. The resulting plot of voltage vs. time and energy vs. time are shown in Fig. 3.26 and Fig. 3.27, respectively. In these plots the "stair step" phenomenon is not present to the same degree as in the previous test. The "stair step" effect is gone is because the pilot was able to maintain a more constant hover position with the helicopter. The pilot reported that it was easier to visually maintain alignment of the antennas at the lower height. He also reported that the aerodynamic forces acting on the helicopter in the previous test were significantly reduced when the sensor node was located at ground level further facilitating a constant hover position. The linear fit to the energy curve in Fig. 3.27 shows that the average power delivered to the capacitor had increased to 4.8 mW. Furthermore, the time to charge to 3.5 volts was

approximately 100 seconds, which is much closer to the 95 seconds reported in the lab experiments. These results show that maintaining the proper alignment of the antennas has a very significant impact on the performance of the RF wireless energy delivery. In this test, four measurements were successfully completed by THINNER. In addition it is also worth noting that Fig. 3.27 also shows a period between 75 and 79 seconds where the power is significantly higher than the other portions of the curve. The higher power phenomenon will now be explored further.

Figure 3.25: THINNER sensor node moved closer to ground level.

3.6.4 RF Energy Delivery Best-Achieved Performance Calculations

In both of the experimental field tests of the RF energy delivery certain portions of the energy vs. time graphs exhibited higher slopes for sustained periods of time

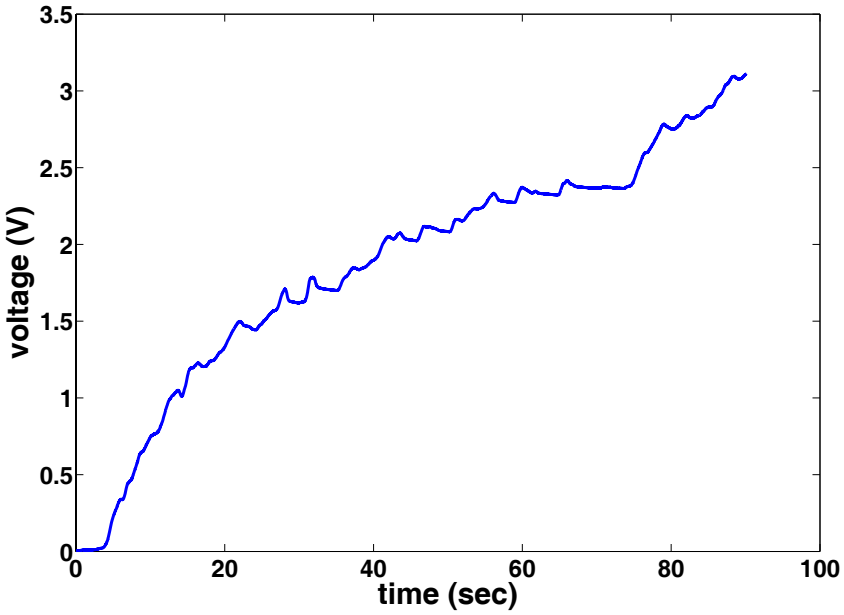

Figure 3.26: Voltage vs. time for the RF energy delivery test to THINNER mounted on a ladder.

resulting in a large amount of energy transfer. In the case where THINNER was mounted on the bridge, the period of time where this occurred was between 166 and 188 seconds, and in the case of THINNER being mounted to the ladder, peak energy transfer occurred between 74 and 79 seconds. Fig. 3.28 and Fig. 3.29 show expanded plots of the energy vs. time curves corresponding to the high energy transfer periods for the bridge test and ladder test, respectively. A line was fit to each curve to estimate the average power delivery over these periods. From the plots it is seen that the peak power delivered with THINNER is 10 mW. This value is 4 times higher than the average power value for the whole test. Furthermore, it is higher than the average value for the tests conducted in the lab. In the case of THINNER mounted on the ladder, the peak power delivery is 23 mW. Fig. 3.30 shows an image taken from the control graphical user interface (GUI) during the period of peak

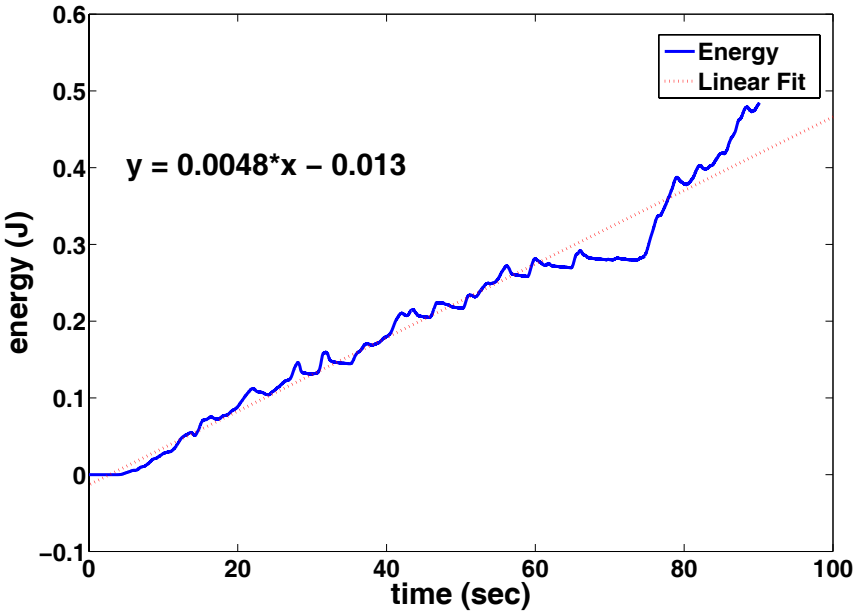

Figure 3.27: Energy vs. time for the RF energy delivery test to THINNER mounted on a ladder.

energy transfer in the ladder test. This image shows the camera views form both the helicopter as well as the ladder. The data in this photo can be used to determine the best helicopter location and orientation for peak energy transfer. Further tests should include multiple angle photos for better determination of the optimal antenna alignment.

The peak power values are low compared to the theoretically available 51 mW, so there is still room for improvement and increased performance of the mobile host wireless sensor network. The next question is, if the peak power delivery can be maintained throughout the energy transmission, what time would be required to maintain the hover position to fully charge THINNER? The answer to this question is summarized in Table. 3.1.

Table 3.1 shows that if the peak power locations and orientations can be main-

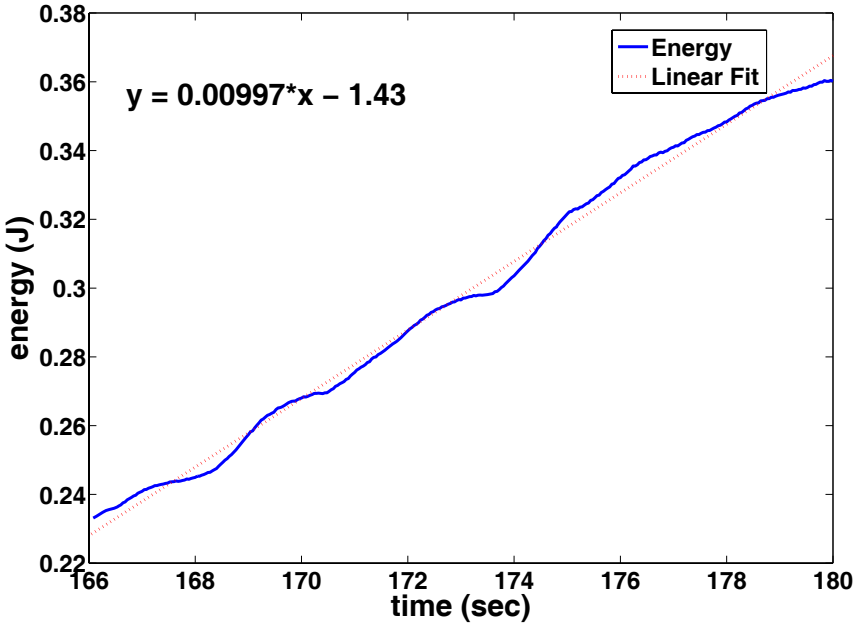

Figure 3.28: Peak energy transfer for test with THINNER mounted to bridge.

tained, the time to charge THINNER will be significantly reduced. The time could be as low as 26.6 seconds, which is fairly reasonable for the mobile host wireless sensor network application based on the ability of the pilot to maintain a given helicopter location and orientation.

3.7 Conclusions and Future Work

The first phase goals to use the mobile host to wirelessly charge up structural health monitoring sensor nodes were successful. The nodes were fully charged, and the data were successfully received at the helicopter. Future work on wireless energy delivery for mobile host should primarily focus on improving the techniques used to align the receiver and transmitter antennas. Perhaps some form of active control

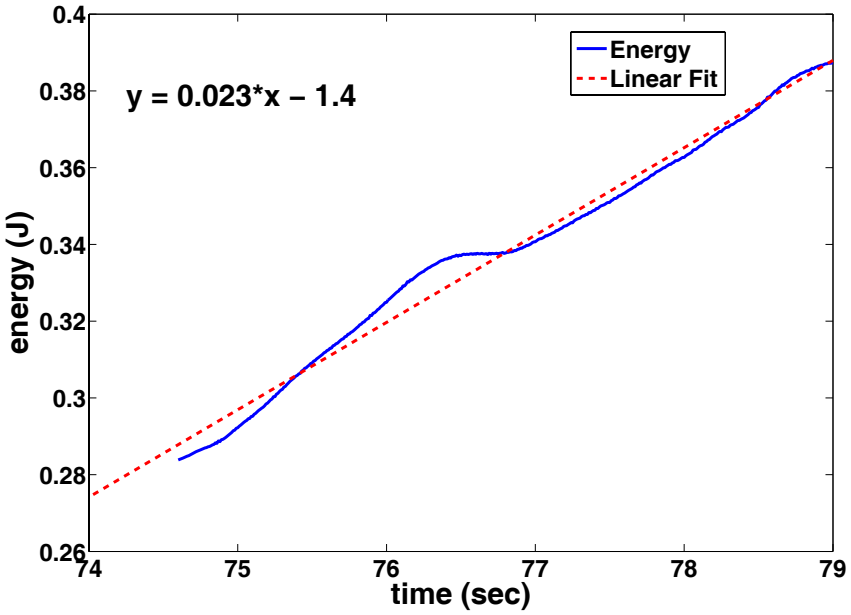

Figure 3.29: Peak energy transfer for test with THINNER mounted to ladder.

could be used for this purpose. Work on optimizing alignment would probably result in the most improved performance. In addition work should be concentrated on improving the on-off characteristics of the voltage-threshold turn-on switch.

Figure 3.30: Image showing helicopter position obtaining highest energy transfer efficiency.

Table 3.1: Summary of the average and peak power delivery during the lab, bridge, and ladder tests.

Test	**Average power (mW)**	**Peak power (mW)**	**Estimated charge time to 3.5 V at average power (s)**	**Estimated charge time to 3.5 V at peak power (s)**
Lab	8.1	8.1	75.6	75.6
Bridge	2.5	10	245	61.4
Ladder	4.8	23	127.6	26.6

Chapter 4

Mobile Host Wireless Sensor Network Implementation

The design of the "mobile host" wireless sensor network required a multi-disciplinary effort. A holistic approach was required to design and select every portion of the network. Important considerations included weight, size, commercial availability, manufacturability, power consumption, time-to-implementation, ease of use, and cost. In this chapter, the design of the mobile host wireless sensor network will be outlined. The design considerations for the various components will be described and the final design decisions will be presented.

4.1 Overview

The roving host wireless sensor network essentially contains three major subcomponents. These components are the mobile host itself, the sensor nodes on the bridge, and the basestation used to monitor the test. In this chapter the mobile host, and the basestation will be expanded upon.

In this work, the mobile host was implemented using a commercially available

Radio Control (RC) helicopter. A flying mobile host was selected for multiple reasons. First, this platform can fly to areas on tall structures that would otherwise be unaccessible to ground based mobile hosts. Furthermore, the use of a flying mobile host would force the design of the RF/Computational payload to be light in weight and low in power consumption. The requirements for a flying mobile host would be significantly more stringent than the requirements for a ground based mobile host. In some applications however, a ground-based mobile host will be more appropriate. In these situations, it is trivial to take the RF/Computational payload developed for the flying host and modify it for use on a ground based vehicle. A helicopter was selected as the mobile host because of its ability to hover in a single location. This capability would be vital for charging up sensor nodes located on the bridge. Furthermore, in future work a helicopter will facilitate the ability to perform other forms of monitoring on a bridge in question. For example, in corrosion detection applications it may be wise to take pictures from a bridge in question in order to determine if corrosion damage is present.

4.2 Literature Review of Unmanned Aerial Vehicles and Autonomous Operations

Interest in unmanned aerial vehicles has exploded in recent years because of the commercial availability of low-cost hardware and software needed to build and fly such devices. Small scale radio controlled helicopters and airplanes are available for a little as a few hundred dollars. Furthermore microcontrollers and radio telemetry is easily obtained for tens of dollars. Small, lightweight, low power Inertial Measurement Units (IMU) capable of providing acceleration and tilt data for autopilot operations are available from a number of sources. In addition camera technology continues to shrink thus enabling the addition of machine vision capabilities to un-

manned vehicles.

The history of unmanned aerial vehicles stretches back farther than the development of manned flight. Models built by aviation's early pioneers such as Cayley were used to perform some of the earliest flight experiments. Attempts to use gyroscopes to provide control to unmanned vehicles stretch as far back as Elmer Sperry's work with the US Navy in 1911 [52]. Unmanned aerial assault drones were used by America to destroy Japanese artillery, tunnels, munitions, and a lighthouse. Unmanned drones were used in a reconnaissance role for the first time during the conflict in Vietnam [52]. More recently unmanned aerial vehicles such as the Global Hawk have been used extensively in the current conflicts in Iraq and Afghanistan [53]. Unmanned aerial vehicles are beginning to make headway into civilian applications as well. In August of 2003 Global Hawk was the first unmanned aerial vehicle to recieve a Certificate of Airworthiness (COA) from the Federal Aviation Association (FAA) [54]. The Global Hawk can now operate in U.S. national airspace, and the aircraft is even capable of filing its own Instrument Flight Rules (IFR) flight plans. It has also been used to support civil disaster response as well, for example Global Hawk was used to aid in civil emergency operations during the California wildfires of October 2007 [55].

The success of military UAVs has lead researchers to look for possible opportunities using UAVs for civilian purposes. Golightly studied the use of unmanned aerial vehicles for the autonomous inspection of powerlines [13]. He was especially interested in investigating how to train the unmanned aerial vehicle to follow power lines using visual approaches.

4.3 Helicopter Airframe

In this work the selected airframe was the commerically available X-Cell Spectra G radio controlled (RC) helicopter produced by Miniature Aircraft. Fig. 4.1 shows

the final mobile host implementation. The helicopter airframe used in this test is the X-Cell Spectra G. The helicopter power plant is the 23 cc two-cycle Zenoah G231 gas engine. The overall length of the helicopter is 2 m. The helicopter is using 810 mm anti-symmetrical, high-lift blades to carry the RF/computational payload. In addition, the stock exhaust has been exchanged with a Hatori muffler for a broadened power curve. The helicopter also features a Tempest FAI rotorhead for improved hovering stability during the sensor node charging phase. The helicopter weighs approximately 5.5 kg (12 lb) ready to fly in the stock condition. When loaded with the sensor network payload, the all up weight of the helicopter rose to 10 kg (22 lb). In the fully loaded condition, the .23 l (8 oz) fuel tank provided approximately 5-6 min of run time at 1615 m (5300 ft), 32.2^oC (90^oF) on a calm day. Flight duration was generally hampered by either the engine overheating and losing power, or the helicopter running out of fuel. Fig. 4.2 shows the mobile host with many of its additional components.

4.4 RC Reciever/Transmitter

The ultimate goal of the mobile host wireless sensor network paradigm is to fully automate the operation of the mobile host so it can collect data from the network autonomously. For the first phase of the mobile host wireless sensor network it was decided that the mobile host would be flown manually. This decision was based mainly on the time constraints of the project. Because the mobile host would be flown manually, it would be necessary to obtain an RC transmitter for piloting purposes. The transmitter would have to be capable of supplying suitable range for the mobile host to fly across its sensor field. It would need to demonstrate immunity to interference produced by the RF power delivery as well as the wireless sensor network communications and stray RF transmissions. At this time, the main choice in selecting a radio controller is deciding on a transmitter frequency of 72 MHz or

Figure 4.1: Mobile host airframe

2.4 GHz. A detailed description on the advantages and disadvantages of these two transmitter frequencies can be found in [56]. Ultimately, the decision was made to use the 72 MHz transmitter. The primary reason for this choice was the fact that the wireless sensor network already had Zigbee, 802.11g, and RF power delivery all occurring near 2.4 GHz. The communications using 2.4 GHz were already experiencing interference and slower performance. In the case of the helicopter controls however, interference that could slow down reaction times was completely unacceptable. Any loss of control to the helicopter could quickly result in a crash. The 72 MHz transmitter/receiver combination would be robust in the face of 2.4 GHz interference.

The transmitter selected was the 9 Channel Super RC controller as shown in Fig.

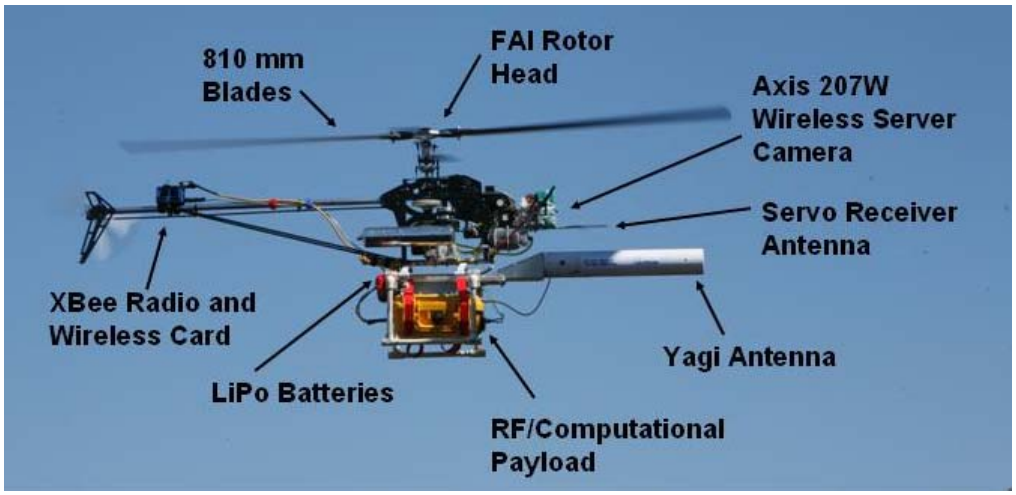

Figure 4.2: Helicopter components

4.3. Fig. 4.4 shows the receiver and helicopter control servos as they were mounted on the mobile host. The antenna was wrapped around a small piece of wood and mounted in the front of the helicopter as shown in Fig. 4.4. With the receiver antenna in this configuration, the receiver typically got a minimum of a few hundred yards of range in open areas during the range tests. The receiver works with the servos and a Futaba GY401 rate gyro to manage the control surfaces on the mobile host. A Futaba GV-1 Engine governor and Stator Gator provide constant engine speed control.

4.5 RF/Computational Payload

The RF/computational payload carried by the helicopter was designed to turn a commercially available RC helicopter into a mobile host wireless sensor node. When designing the RF/computational payload, it requires a variety of attributes such as low power consumption, lightweight, sufficient computational capability, efficient RF energy and data transmission as well as the ability to control the RF package and

Figure 4.3: 9 channel radio control system

execute SHM analysis. It also had to be rugged enough to fly on a model helicopter and survive rough landings on uneven surfaces. The package would need to be able to dissipate heat produced by the electronics. In addition, the package would need to be powered by lithium polymer battery backs. It was decided that the total payload of the helicopter should not be greater than 4.54 kg (10 lb).

It was desired that the RF/computational package should also be capable of transmitting video in real time. Furthermore, the RF computational package should be capable of communicating with, and be controlled by, a remote base station.

4.5.1 RF Package

The RF package was responsible for generating the RF energy used to charge up the sensor nodes located on the bridge. An image of the RF package is shown in Fig. 4.6. The main components of the helicopter include the RF signal source, the attenuators, the RF power amplifier, and the Yagi transmission antenna.

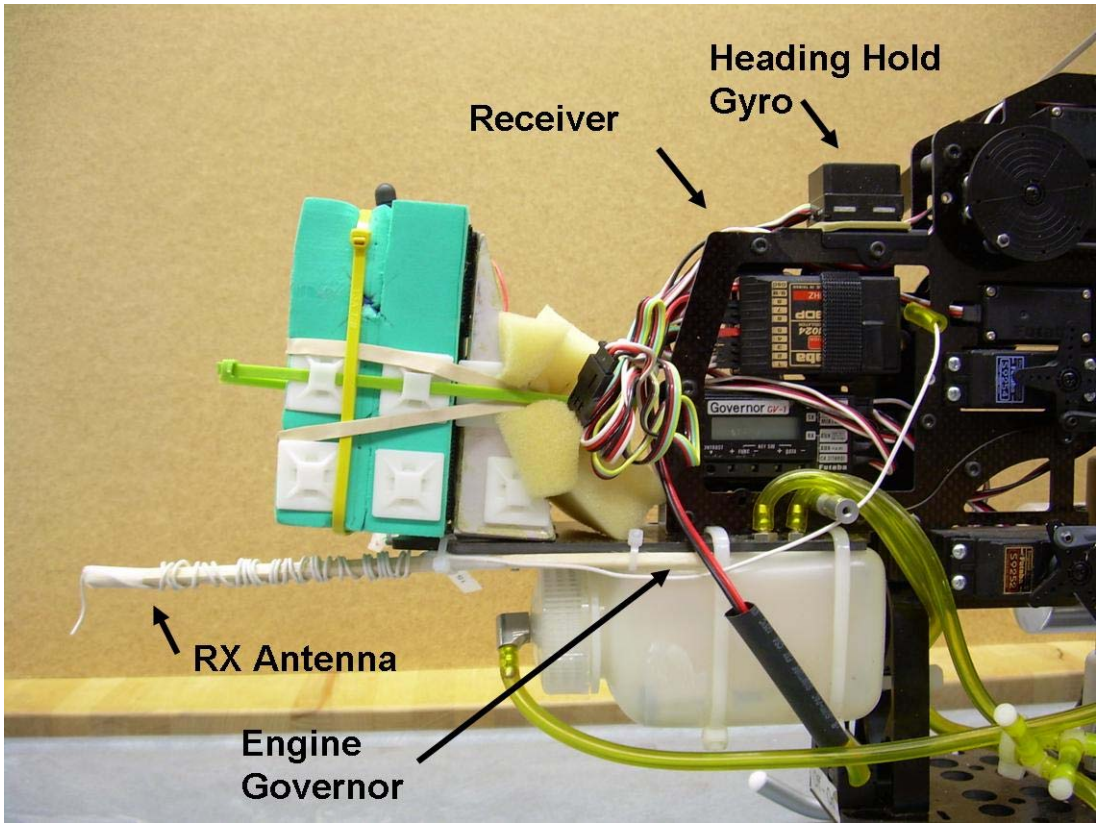

Figure 4.4: Receiver on the helicopter

RF Signal Source

The RF signal source is the first part of the RF power chain in the mobile host. The source determines what RF frequency is transmitted to the sensor nodes. The selection of the frequency is one of the most important decisions in the overall design of the mobile host. This parameter has a very large impact on the size of the antennas used in the mobile host, the cost of the components, and the availability of the components. In this work, 2.5 GHz was selected as the mobile host power transmission frequency. 2.5 GHz will have a wavelength of 12 cm in free space. This characteristic length leads to antennas sizes appropriate for high-end, commercially

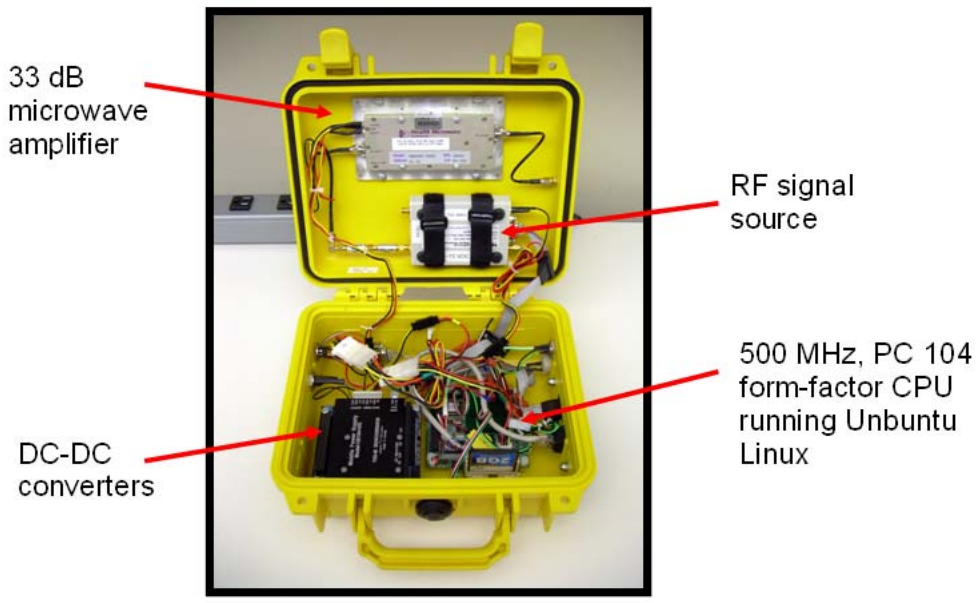

Figure 4.5: RF/computational payload

available RC helicopters, as discussed in detail in Chapter 3. Furthermore, components at this frequency are readily available commercially. The RF signal source chosen for the mobile host was the Nova Source NS3-2401102. This signal source was chosen because of its size, low cost, low power consumption, and ease of programmability. The NovaSource can generate signals between 2.4 and 3.4 GHz at 8 dBm. It can be controlled through an RS-232 serial interface, and consumes 175 mA at 9 V DC. The source measures 95 X 70 mm and it weighs .2 kg (0.42 lb). The NovaSource costs roughly $700.

Attenuators

The attenuators are the next link in the RF power chain. In this particular system, the power amplifier has 33 dB of gain and the Nova Source outputs 8 dBm

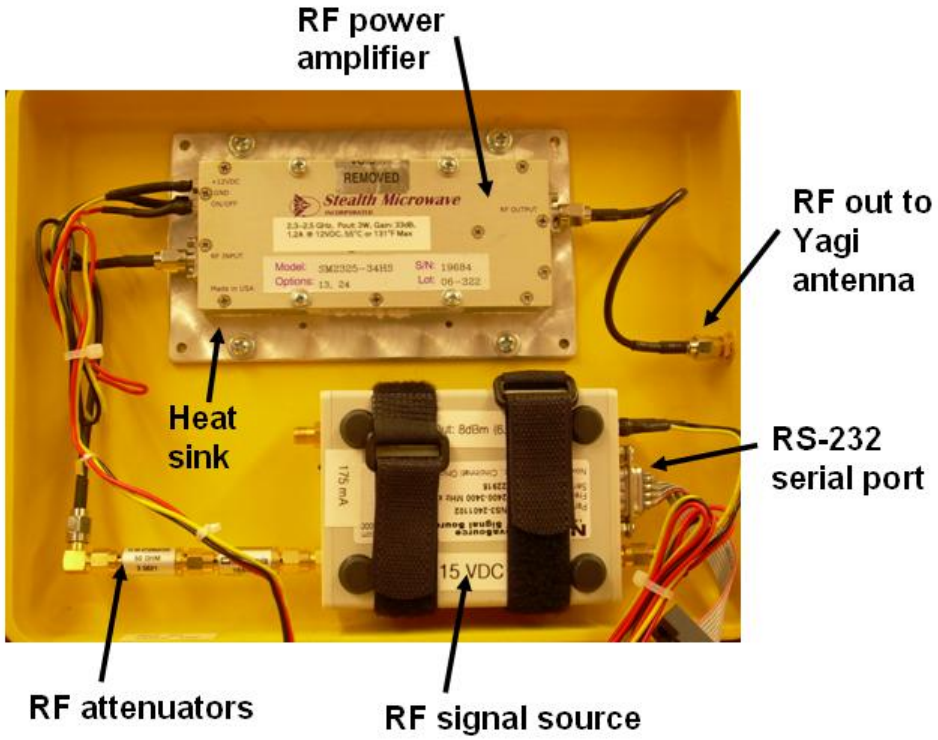

Figure 4.6: RF package

of power. It is desired to limit the output power to 30 dBm (1 W) for safety reasons. Furthermore, the power amplifier can only output 3W max. If the RF source is fed directly to the amplifier it will output 11 dBm of excess power or 41 dBm of total power. If too much power is presented to the amplifier, it is in danger of being damaged. In order to avoid this situation, the attenuators were placed after the signal source and before the power amplifier. This arrangement ensures the power output from the amplifier is at the appropriate level and the amplifier does not sustain damage. Furthermore less energy is dissipated if the attenuators are placed before the amplifier than after the amplifier. Each attenuator weighs 8.5 g (0.3 oz) and is 3.5 cm long and 1 cm in diameter. The chosen attenuators can dissipate 1 W

of power. It is possible to program the Nova Source to output a lower power level, but experience showed that if there was a problem with the computer booting up, the possibility existed for the Nova Source to automatically output the higher power level possibly damaging the amplifier. The attenuators were placed in the RF power chain as a failsafe measure.

RF Power Amplifier

The purpose of the power amplifier is to increase the RF signal source powers to levels appropriate for RF power delivery. The most important considerations when selecting the amplifier are its bandwidth, maximum power out, weight, size, remote control capability, and power requirements. The selected amplifier is the SM2325-34HS. It has a bandwidth of 2.3 - 2.5 GHz, a maximum output power of 3W and supplies 33 dB of Gain. The amplifier runs from a 12V DC power supply and consumes 1.2 Amps. The amplifier can also be toggled on and off using a TTL logic line, thus facilitating computer control. The amplifier is attached to an aluminum plate acting as a heat sink. The amplifier measures 119 X 51 X 13 mm and weighs 180 g (6.2 oz). The aluminum heat sink measures 135 X 80 X 3 mm and weighs 100 g (3.5 oz). The selected amplifier was deemed suitable for the first version of the mobile host because it had appropriate weight, size and power characteristics, as well as the ability to be toggled on and off by the computer.

4.5.2 Computational Package

The computational package selected for this project had to be capable of facilitating communications with the base station as well as with the wireless sensor nodes. Furthermore, it would have to be capable of controlling the RF package. These requirements lead to both hardware and software specifications. Figure 4.7 shows a block diagram of the RF/Computational payload. This diagram outlines the power

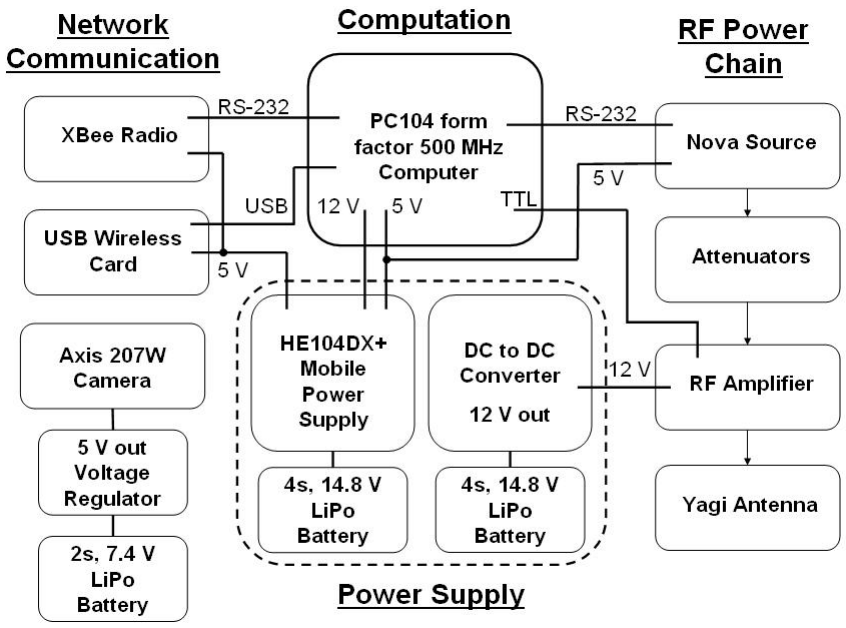

Figure 4.7: RF/computational payload block diagram

connections and the data flow throughout the payload.

Computational Hardware

The computer carried by the mobile host has a wide variety of responsibilities. It must be capable of controlling the RF package, receiving data collected by the sensor nodes, and eventually it would have to take the data and perform structural health monitoring analysis to determine whether the structure is damaged, or whether the helicopter needs to collect measurements from other sensor nodes in the network. The package selected for this work would also have to be capable of operating on power supplied by commercially available batteries. It would also need to have a weight and size suitable for mounting to the helicopter.

The main computational block onboard the helicopter is the AR-B1622 from Acrosser. The AR-B1622 comes in the PC 104 form factor, and has a 500 MHz AMD

Processor. The processor utilizes a heat sink for passive cooling thus elimintating moving parts. The AR-B1622 has two RS-232 ports, an ethernet port, 8 general purpose input/ouput (GPIO) pins, and four USB ports for communicating with auxiliary devices. It was decided that the AR-B1622 would boot from a compact flash disk. The reason for using the compact flash card was that a compact flash disk is significantly lighter than a laptop hard drive, and it contains fewer parts. It also has a lower power consumption.

It was deemed desirable to have an image of the helicopter view in real time. In order to acquire these data, an Axis 207W Wireless network camera was mounted on the front of the helicopter. The 207W contains a webserver so it can wirelessly transmit images to any computer connected to the same local area network. This camera provides a real time image of the view observed by the helicopter. This information is important because it helps determine how well the antennas on the helicopter are aligned.

Computational Software

The software on the mobile host was co-developed by members of the structural engineering department and the computer science department. The structural engineering department was responsible for laying out the requirements of the software, and the computer science department was responsible for writing, installing, and configuring the software for proper operation. Important considerations when designing the software included cost, speed and ease of development, customizability, availability, reliability, speed, and ease of use. The development of the software onboard the helicopter is not a significant portion of this dissertation, but a summary is given here for completeness.

The operating system used on the AR-B1622 was Ubuntu Linux. Linux was chosen over Windows for a variety of reasons. Firstly, it was deemed simpler to configure a Linux computer to perform the low level processes such as using the

GPIO. Furthermore, Linux more easily lends itself to implementing fine control over processes such as assigning privileges to programs and files. The open source nature of linux also lends it to modification, which can be important when designing custom embedded systems. Lastly, Ubuntu is free software, and thus would substantially reduce costs in future work involving multiple roving hosts.

The software used to control the 802.11g network communications is Apache 1.3 HTTP server. Apache is the most popular web server in use today, and it is freely available. When the remote basestation sends commands over the local area network, they are received at the helicopter by the Apache web server. The web server then executes the appropriate applications to perform the desired functions.

The software used to control the RF computational payload was written primarily in Python. Python was selected because it supports rapid development of software, is freely available, and is easy to learn. Also, the RF computational payload is controlled primarily by serial port. The Python libraries that deal with the serial port are very simple to use. Another reason for using Python on the mobile host is that the NumPy package could easily be used for complex structural health monitoring algorithms. NumPy is an open source alternative to programs such as Matlab. NumPy's strengths lie in its ability to use object oriented code. In the event that multiple roving hosts were developed, programs written in Matlab would need to be installed on every machine, thus significantly increasing costs.

Another feature of Python is that the license agreement binding Python allows for the distribution of binary-only versions. It is not necessary to release source code. The advantage here is that structural health monitoring algorithms can be developed using Python with NumPy without the need to lose control of your intellectual property when it is released to the public. Typical open-source software is bound by the General Public License (GPL). The "copyleft" portion of the GPL license requires a user to provide source code when they distribute a copy of a program based on software covered by the GPL. In the case of this particular project, there are reasons

why releasing the source code related to experimental structural health monitoring algorithms may not be appropriate.

A more detailed description of the software used to control the RF/computational payload as well as the manner in which it was installed can be found in [57].

4.5.3 Wireless Networking Hardware

The mobile host wireless sensor network consisted of two main wireless systems. The sensor node to mobile host communications were provided by a Zigbee wireless sensor network, and the basestation to mobile host communications were provided by and 802.11g wireless network. Fig. 4.8 shows the Wireless network communications hardware as mounted on the helicopter. The hardware was mounted at the rear of the helicopter as shown in Fig. 4.2 in order to minimize interference caused by the RF power transmitted from the Yagi antenna. The selected hardware for the Zigbee communications was an XBee serial modem. The serial modem weighs 23 g (0.8 oz) and connects to the PC104 computer via an RS-232 connection. The Xbee serial modem measures 74 X 64 X 15 mm. The 802.11g wireless network was implemented using a Netgear wireless ethernet USB adaptor. This particular adaptor was selected because the operating system on the PC104 is Unbuntu Linux which supports this particular card [57]. The USB adaptor weighs 34 g (1.2 oz) and measures 85 X 25 X 13 mm. The wireless USB adaptor connects to the PC104 through the USB port on the PC104. The 802.11g RF/Computational payload to basestation communication is facilitated through a Wireless-G broadband router built by Linksys. The router creates a Wireless Local Area Network (WLAN) within which data can be passed between members. A laptop computer connected to the WLAN functions as the basestation for command and control of the RF/computational payload.

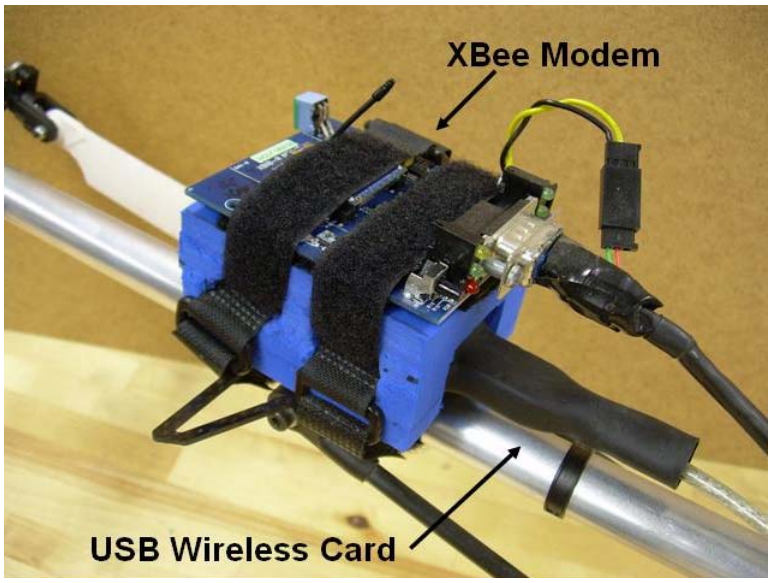

Figure 4.8: Wireless network communications equipment on-board the helicopter

4.5.4 Power Supply and Energy Requirements

The design of the power supply for the RF/computational payload is critical to the success of the mobile host wireless sensor network. The power supply must be able to provide adequate voltage and current for the components of the mobile host during operation. Furthermore, the power supply must be lightweight, and it must be easily and quickly replenished. The energy level in the power supply should also be very easy to monitor. Another very important consideration is that should an element of the power supply fail, it should fail in as graceful a manner as possible. Given the nature of RC helicopters, even a momentary loss of power to the helicopter control servos could lead to very disastrous consequences.

The first step in designing the power supply for the mobile host was to consider the power requirements of the components making up the RF/computational payload. Table 4.1 shows the voltage and current requirements of all the components onboard the mobile host. These numbers were obtained from the component data sheets, and

represent the worst case power consumption.

Table 4.1: Power requirements of mobile host payload.

Component	Current (mA)	Voltage (V)	Power (mW)
AR-B1622	600	5 and 12	3000
Xbee Modem	300	5 to 14	4200
Nova Source	175	9 to 15	2625
RF Amplifier	2000	12	2400
Ethernet Card	500	5	2500
Axis 207W Camera	700	5	3500

With the identified power requirements of the system, it was now possible to make decisions regarding the power supply. The first decision was to make the battery powering the helicopter control servos completely independent of the RF/computational power supply. The reason for this decision was that the RF/computational power supply was still experimental, and had relatively large power requirements. The concern was that some operation may cause the voltage on the servos to drop so low that the helicopter could lose control and crash. For this reason all electronics related to the control of the helicopter were powered by their own 4.8 V, 1.5 Ah Nickel Cadmium battery. The components powered by this battery include the servos, heading hold gyro, engine governor, and the receiver. This battery was supplied with the servos and thus should be well suited to the unique demands placed on the battery from the control of the helicopter.

After reviewing all the voltage requirements in Table 4.1, both a 5 V and 12 V supply were deemed required. This decision was primarily driven by the fact that the PC 104 computer needed 5 and 12 V to operate, and all the remaining components could be powered by one of these voltages. In order to supply the required power the HE104 DX mobile power supply was selected for providing the proper voltages from a battery power supply. It was decided that because the RF amplifier and the AR-B1622 were the main power consumers in the system, they

should be supplied by separate power supplies. The reason for this decision was that the load imposed by the amplifier was so large at startup that the AR-B1622 would have to reboot. To solve this problem, the amplifier was given its own battery and its own DC to DC converter. This setup provided a number of advantages. Not only was the computer able to run uninterrupted in the face of the high current draw caused by the amplifier initialization, it also provided a simple way to safely run the RF/computational payload without the fear of accidentally turning on the amplifier. By simply disconnecting the amplifier battery, the risk of operating the Yagi antenna in an unsafe manner near people, or in such a way that the amplifier might be damaged is eliminated. Also, the amplifier consumes on the order of 100 mA even in the idle state, so significant power savings can be achieved during debugging if the battery supplying the amplifier is removed from the system. Not only is energy saved, but there is less heat that needs to be dissipated from the payload package. Because of the spatial location of the camera, it was deemed impractical to power it from the same power supply as the rest of the RF/computational payload. Instead, it was decided to use a separate local battery to power the camera. The power requirements of the battery were low enough that a simple voltage regulator could be used to provide the proper voltage to the camera from a battery. Fig. 4.7 shows the final setup of electrical power supply for the RF/computational payload.

The next step was selecting the batteries to use for the power supply. The maximum flight time of the helicopter was estimated to be 30 minutes based on the fuel tank size. For this reason it was decided that the batteries on board the helicopter should be able to power the electronics for 30 minutes to an hour to allow for debugging time. The batteries should be lightweight, and be of an appropriate size and shape for the helicopter. The battery should also be able to supply the needed current to run the RF/computational payload in all of its operating regimes. There is a wide variety of battery technology available today. Possible battery chemistries include alkaline, nickel metal hydride, lithium polymer, and nickel cadmium. All these

batteries fulfill specific purposes. A good overview of contemporary battery technology suitable for unmanned vehicle operations can be found in [58]. Ultimately the batteries selected for the payload were two 4s, 14.8 V, lithium polymer batteries with capacities ranging from 1000 mAh to 2170 mAh. Lithium polymer batteries were selected primarily because of their low weight. They also are commercially available at any hobby store. Downsides with these types of batteries include dangers associated with fires and explosions if they are not charged properly. In addition these types of batteries cannot be carried on board an airplane, which may cause problems with shipping the mobile host. It was determined that the weight saving achieved with lithium polymer batteries far outweighed any disadvantages inherent in this type of battery chemistry. The battery selected to operate the camera was an 800 mAh, 2s, 7.4 V lithium polymer battery. This battery had ample voltage to run the camera and had no problem supplying the required current for half an hour to an hour. It was also the lightest battery technology available.

4.5.5 RF/Computational Payload Packaging

The packaging of the RF/computational payload required a great deal of consideration. The selected packaging would have to be lightweight, yet large enough to house all the necessary electronics. It would need to be sufficiently stiff to support loads imparted to it, keep dust and debris out out the electronics, and be durable enough to survive rough landings in the desert and possibly even a crash landing. It should be easy to access the keyboard and VGA ports on the PC104 in the even that trouble shooting needs to take place, and the package should also be capable of dissipating the required amount of heat to protect the electronics inside. The package should also facilitate the mounting of the electronics.

After considering a wide range of possibilities, the final decision for the helicopter electronics package was a Pelican 1200 case as shown in Fig. 4.9.

Figure 4.9: Pelican 1200 Case

The case is built from ultra high impact structural copolymer which makes the case very durable, yet simple to drill into for mounting purposes. The case was fairly heavy at 1.15 kg (2.54 lb), but the double throw latches used to keep the case closed left little doubt that the case would remain sealed in the event of a helicopter crash. The case also gave a standard package, so other payloads could be developed which fit in the same case and would be very simple to mount to the helicopter. The case allowed for easy modification so access to the VGA port, PS/2 keyboard, mouse connectors and an ethernet connector was easily achieved. These connectors were protected from dust by a spring loaded cover plate as shown in Fig. 4.10. Pass through connections for the batteries, XBee radio modem, and wireless card were achieved using multi-pin, mobile connectors with a screw-on retaining ring and built in strain relief. These connectors are typically used for microphone connections. These connectors proved to be both durable to the vibration environment produced

by the helicopter, as well as robust to the dust environment presented by the desert during initial field testing. These connectors were also relatively low-cost.

Figure 4.10: Spring Loaded Cover to Protect Connectors From Dust and Debris

One concern with this form of case was the buildup of heat from the electronics operating within it. The case did not have any vent because of the fear that dust from the desert might enter the case. Active cooling solutions were avoided because of their weight and power consumption penalty. Despite concerns however, preliminary tests in the lab showed that the computers remained within their operating ranges during the normal duration of a test.

Major factors leading to the selection of the Pelican 1200 case being used as the electronics package were time and cost. The Pelican 1200 case could readily be purchased for around $45.00. However, the case is relatively heavy and its heat dissipation characteristics are not ideally suited for this application. In future work, it is suggested that some form of sheet aluminum case be used. Sheet aluminum

construction similar to that used in experimental homebuilt aircraft, such as the RV-7, can be used to build lightweight, high- stiffness, structures with relatively good heat dissipation characteristics. An example of this form of construction is shown in Fig. 4.11. The control surface shown here measures 330 X 285 X 51 mm (13 in X 11.25 in X 2 in) and weights only 420 g (14.8 oz). The size of the control surface is roughly similar to the pelican 1200 case, yet it has about 40 % the weight, and the high conductivity aluminum provides improved heat dissipation performance. Such a structure can be built by relatively unskilled labor using low-cost tools. Alternatively, similar lightweight mil-spec electronic enclosures are manufactured, but it is not unusual to pay between $30k to $100k for such an enclosure. The high cost of these items are due to the fact that these forms of case are very high performance and practically custom made. In the event that the mobile host wireless sensor network is involved in a larger scale test, it will be absolutely necessary to spend significant time ensuring that the packaging protects the electronics from the environment they will be subjected to at a low weight while still providing adequate heat dissipation. Furthermore, if a test is ever conducted over a body of water, the requirements will very quickly become much more stringent and expensive. For example, it is not unusual for waterproof pass through connectors to cost on the order of $100.00 each. These considerations must be made for future tests involving the mobile host wireless sensor network for more general applicability.

4.6 Weight Breakdown

Clearly, overall, weight was a primary factor governing the payload being designed for the mobile host. The helicopter has a limited load carrying capability, and as weight increases, the helicopters performance decreases in terms of maneuverability and endurance. Furthermore, as weight increases, the inertial loads encountered by the helicopter also increase. As inertial loads increase, the possibility of damage

Figure 4.11: Sheetmetal construction typical of experimental homebuilt aircraft.

occurring to the helicopter also increase, especially in the event of a hard landing. It is best to design components with as little weight as possible. The problem is then that the inertial forces increase, and the component needs to be even stronger to resist the higher loads. At this point a dangerous spiral of increasing weight and inertial forces has been initiated. It is generally better to simply design components to be as light as possible with low inertial forces.

The breakdown of the weights of the various components can be found in Table. 4.2. The first set of measurements in Table 4.2 correspond to the components in the RF computational payload. According to these numbers, the RF/computational payload should weigh 2.37 kg (5.21 lb). The actual weight of the RF/computational payload is 2.44 kg (5.36 lb). The discrepancy of .07 kg (0.15 lb) can be attributed to all the wire, connectors, hardware, glue and miscellaneous components that make the payload functional. The next set of measurements are representative of the typical

Table 4.2: Weights of components on the helicopter

Component	**Weight (lb)**	**Weight (kg)**
HE 104 DX	0.380	0.173
AR-B1622	0.400	0.182
Xbee Modem	0.220	0.100
Camera	0.420	0.191
Netgear USB Wireless Card	0.043	0.020
Nova Source	0.420	0.191
SM2325-34HS Amplifier	0.388	0.176
Amplifier Heatsink	0.220	0.100
Attenuators (Qty 2)	0.038	0.017
Pelican Case	2.543	1.156
1000 mAH LIPO 14.8V	0.294	0.134
1500 mAH LIPO 14.8V	0.463	0.210
800 mAH LIPO 7.4 V	0.100	0.045
1.5 AH NiCD 4.8 V	0.275	0.125
Yagi Antenna	0.700	0.318
Antenna Bracket	0.350	0.159
Attachment Straps	0.344	0.156
Lower Assembly (total weight)	2.275	1.034
Weight Removed From Lower Assembly(1)	-0.794	-0.361
Weight Removed From Lower Assembly(2)	-0.994	-0.452
Helicopter 12 pounds ready to fly (from brochure)	12.000	5.455
Total	**20.084**	**9.129**

battery payload carried by the helicopter at any given time. These batteries are used to power the RF/computational payload, the RC receiver, gyro, governor, and the camera. The weights of the RF power transmission antenna components are listed next followed by the weights of the payload attachment hardware. In this section there are two negative weights. These negative values correspond to weight that was later removed from the payload attachment in order to improve the endurance of the helicopter. The last item listed is the ready-to-fly weight of the helicopter in the stock condition. Based on all the values, the estimated all up weight of the helicopter should be 9.19 kg (20.22 lb). The actual measured weight of the helicopter with a full load of fuel was 10.16 kg (22.37 lb). The weight discrepancy between these two measurements can be attributed to many factors including the use of a non-stock muffler, the use of the larger 810 mm-high-lift blades, wiring, mounting brackets, varying fuel line lengths, varying amounts of fuel in the lines, connectors, wiring, Velcro straps, zip ties, varying battery sizes, and mounting hardware. The discrepancy between the estimate and the final measured weight is about 10%. In future work this may be a useful measure of how much miscellaneous components needed to support a given piece of hardware will weigh on average across the airframe.

4.7 Mobile Host Wireless Sensor Network Implementation

Figure 4.12 shows an overview of the first implementation of a mobile host wireless sensor network. Typical operation of the sensor network would proceed as follows. In the event that decision makers would like to take measurements from the sensor network on the bridge, the mobile host is dispatch to collect data. The mobile host is piloted using the 72 MHz radio control band, and the operation of the RF/computational payload is achieved using an 802.11g local area network. When

the mobile host arrives at one of the sensor nodes of interest, the command to activate the RF power delivery package is sent over the 802.11g network from the basestation to the mobile host. The Axis 207W wireless webcam broadcasts images to the 802.11g network in order to facilitate the alignment of the receiver and transmitter antennas for RF power delivery. Once the sensor node on the structure has been fully charged up, the sensor node turns on, interrogates its peak displacement sensor, and radios the measurement back to the mobile host using a Zigbee network. The helicopter receives the data over the Zigbee network, stores the data, and performs any relevant structural health monitoring processes on the data. At this time, the basestation can query the mobile host over the 802.11g network requesting the data. When the helicopter receives the request for the data, the helicopter sends the requested information over the 802.11g network. Furthermore, once the data has been received, the basestation can command the mobile host to deactivate its RF power delivery package in order to save energy.

More details on the mobile host wireless sensor network implementation can be found in [57].

4.8 Helicopter Performance

4.8.1 Self-Heating Characteristics of the RF/Computational Package

One of the major concerns regarding the RF/computational payload was the dissipation of heat created by the helicopter, computer, and RF power amplifier. In laboratory experiments, these components would generally be kept cool using a conventional fan, but on the helicopter this capability would not exist. The two main components worthy of attention were the RF power amplifier and the PC104 computer because they generate the most heat. The RF power amplifier was rated

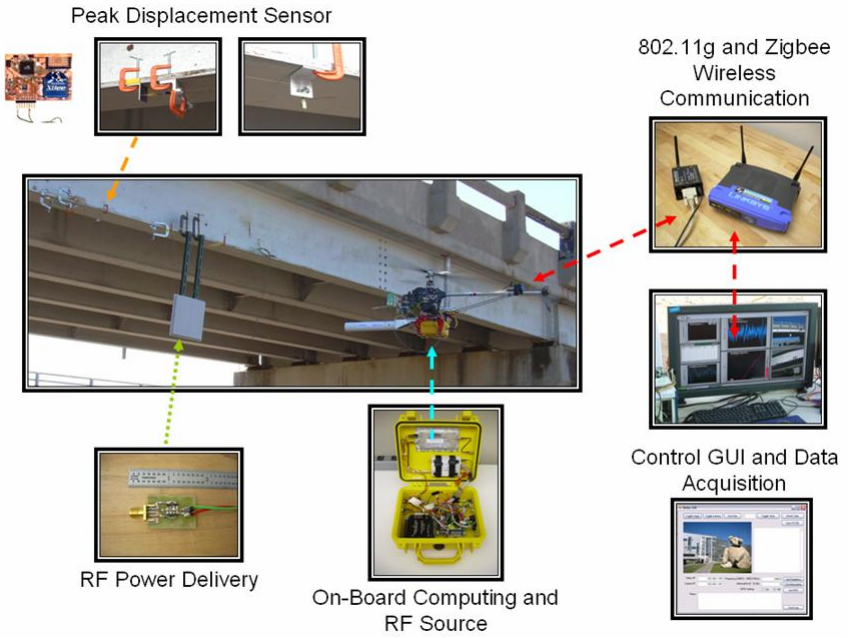

Figure 4.12: Mobile host wireless sensor network overview.

to 55 ^{o}C, the NovaSource was rated to 50^{o}C, the DC-to-DC converter was rated to 71^{o}C, the HE104+DX was rated to 85^{o}C, and the PC104 was rated to 60^{o}C. A proof-test of the payload was conducted prior to the field testing of the mobile host. The goal was to get some information to characterize the mobile host in order to see if additional cooling elements were needed to supplement the passive cooling of the electronics. The desire was to avoid active cooling elements if at all possible. Active cooling elements would add significant weight and power consumption requirements to the mobile host.

The RF/computational payload package was tested as follows. The RF/computational payload was connected to power and the pelican case was placed in the closed position. A thermocouple was placed inside the RF/Computational payload to measure the air temperature inside the box. This test was conducted at the Research Park of Los Alamos where the temperature inside the building is typically maintained at

21^{o}C (70^o F). The computer was then turned on and allowed to boot up. Once the computer booted up, the NovaSource and RF amplifer were turned on and set to transmit. The collection of temperature data was initiated as soon as the RF equipment began transmitting RF power. Temperature data were then collected over the next 13 minute period because it was assumed that no single test of the mobile host prototype would last longer than 10 minutes at most. This determination was based on the RF power delivery time-to-charge results. The resulting air temperature vs. time data can be found in Fig. 4.13.

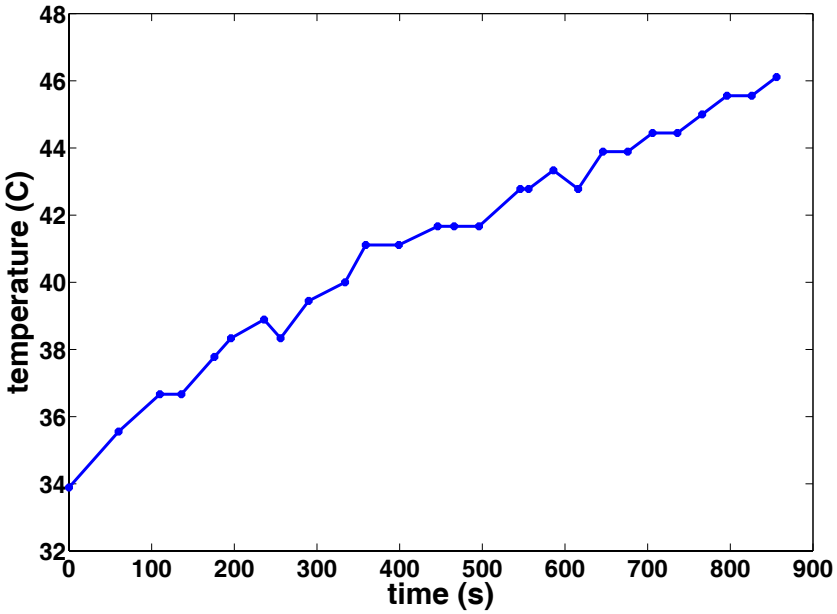

Figure 4.13: Self-heating of helicopter RF/computational payload.

From this plot it can be seen that the air temperature of the RF/computational payload never exceeded 46^{o}C. This value is below the 50^{o}C rating specified for the lowest maximum temperature rating component. In this respect, the RF/computational payload is very close to its maximum upper temperature limit, but because of resource constraints, the package was deemed acceptable for the initial field demon-

stration.

During field testing, the package did perform satisfactorily, but there were occasions that the RF amplifier overheated and became significantly less efficient. It was not unusual for the temperature in the desert to reach 32^{o}C (90^{o}F), which would impede heat dissipation from the RF/computational package. Furthermore, the helicopter engine subjected the RF/computational package to additional heat loads. In order to mitigate these effects, an external fan was placed near the RF/computational package whenever the helicopter was sitting idle on its landing pad for debugging purposes. An image of the helicopter with the fan is shown in Fig. 4.14. The fan provides adequate cooling during helicopter debugging work. Despite the success of the mobile host, future versions of the RF/computational payload should be designed for better heat dissipation performance. Improved heat dissipation performance will be vital for enhancing the reliability of the mobile host.

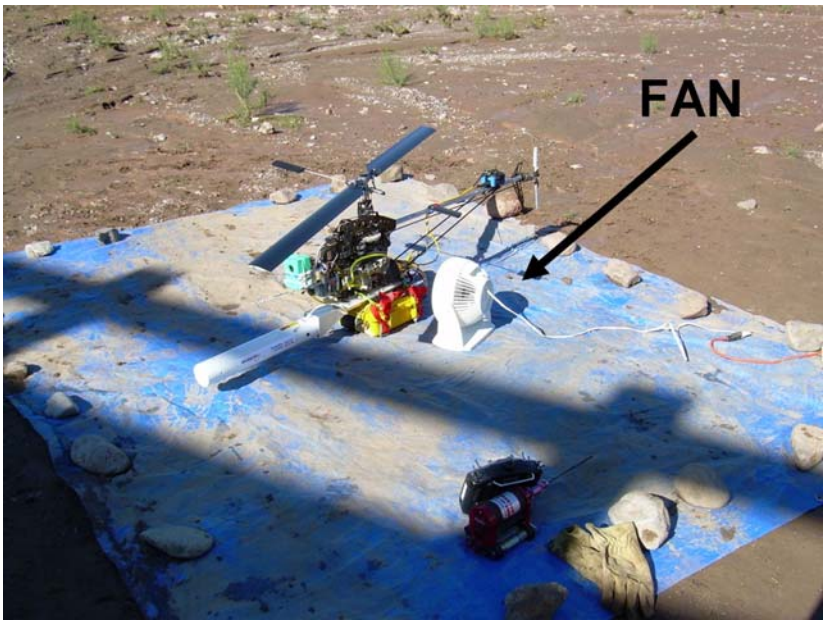

Figure 4.14: Helicopter being cooled by external fan.

4.8.2 Load Carrying Capability of Helicopter

A test of the load bearing capability of the X-Cell Spectra G with the 810 mm high lift blades was conducted on July 31, 2007 in Bernalillo, New Mexico. The altitude in this location is 1635 m. Generally, the air temperature in NM is fairly high (30 ^{o}C) at this time of year, so it is more important to report the density altitude for aircraft performance comparisons. Density altitude is a measure of air density, which is the single most important factor when considering aircraft performance. Air density determines the amount of lift wings can produce, the efficiency of propellers, and the power output of engines based on available oxygen. Density altitude is the altitude in the International Standard Atmosphere (ISA) at which the air density would match the observed air density [59]. The two main factors that affect density altitude are air temperature and humidity. Humidity has a lesser effect on density altitude than temperature, and generally NM is very arid so it is reasonable to use simplified "dry air" formulas that only take into account temperature effects when calculating density altitude. A more detailed description of density altitude can be found in [59].

The formula for density altitude is given in [59] as:

$$Density \text{ Altitude} = 145426 \left[1 - \left(\frac{P_o/P_{sl}}{T_o/T_{sl}} \right)^b \right] \tag{4.1}$$

Here density altitude is given in feet, T_o is the temperature in Kelvin, T_{sl} is the standard sea level temperature in Kelvin (288.15 K), P_o is the pressure in Pascals, P_{sl} is the standard sea level pressure in Pascals (101,325 Pa), and $b = .235$. On the day of the load bearing capability test, the air temperature was $T_o = 34.7^oC$ and the air pressure was $P_o = 83,160\ Pa$. From this formula for the given test conditions, the density altitude is 8740 ft or 2664 meters, which is a typical value for the Bernalillo area in the summer. It is important to note that these values of density altitude are relatively high, especially for a load bearing mission. Note that

the true altitude in Bernalillo, NM is 1635 m, which is significantly lower than the 2664 m the helicopter feels it is operating in. The difference between true altitude and density altitude is caused by the increase in temperature from the ISA value of 4.4°C at Bernalillo's altitude of 1635 m to the measured temperature of 34.7^oC. Added performance could be gained from the helicopter if the load bearing tasks are performed at lower temperature.

Once the density altitude was determined, the next step was to outfit the helicopter for bearing loads. The helicopter undercarriage, Yagi antenna, and an empty pelican case were placed on the helicopter to simulate the weight distribution of the RF/computational payload. The helicopter in its load bearing test configuration can be seen in Fig. 4.15. Bags filled with lead shot were placed inside the empty pelican case to simulate the RF computational payload. Initially, 3.18 kg (7 lb) of lead shot was placed on the helicopter. The helicopter was seen to fly with this payload in a satisfactory manner. The design goal of the helicopter was to carry 4.54 kg (10 lb) of payload in addition to the helicopter airframe. The payload was increased to 5.68 kg (12.25 lb), and the helicopter was flown again. The Spectra G was capable of carrying the extra payload, but the pilot reported that the engine was working very hard to achieve it. It was determined that 5.68 kg (12.25 lb) would be considered the maximum load the helicopter would be able to carry. It was also determined that the payload weight should be maintained below this value.

4.8.3 Fuel Consumption and Time of Flight

The fuel tank on board the helicopter is capable of carrying roughly 270 ml of fuel. The X-Cell Spectra G runs on an 87 octane gasoline-oil mix. The weight of gasoline is roughly 0.72 kg/l (6 lb/gal), so the fuel on board the helicopter weighs roughly 0.2 kg (.426 lb) depending on the temperature. Based on prior experience, the pilot estimated that the X-Cell Spectra G would be able to fly for roughly 30

Figure 4.15: Initial test of helicopter load bearing capability.

minutes on a full tank of fuel in the stock condition. Given that the helicopter weighs 5.45 kg (12 lb) stock, and an additional 4.54 kg (10 lb) of payload would be added to it, a major concern was the amount of time the helicopter would be able to remain in the air. At the time of testing, the helicopter had an all up weight of 10.2 kg (22.37 lb) with a full tank of fuel and all the payload necessary to operate as a mobile host wireless sensor node. The tests at Alamosa Canyon Bridge showed that given these conditions, the helicopter could operate for roughly 7 minutes. After 7 minutes, the fuel tank was either empty or very near to empty. Generally the helicopter would need to finish charging the sensor node in under seven minutes. Past seven minutes, the helicopter would either run out of fuel, or in some cases the engine overheated and the helicopter engine lost all power, most likely caused by vapor lock. It is worth noting that Truth or Consequences, NM has an elevation of 1300 m (4260 ft),

and the temperature of the tests ranged from 31.6^{o}C (88.9^{o}F) to 35 ^{o}C (95^{o}F). The density altitude in Truth or Consequences was lower than that for the Albuqueque load bearing tests, but during the sensor network tests, the helicopter had all the electronics turned on thus generating heat, and the helicopter was run for longer periods of time.

In future work with more elaborate versions of the mobile host wireless sensor network, some changes will need to be made to improve the endurance of the mobile host. First, it will probably be necessary to package the RF/computational payload in a lighter package. Future version of the mobile host will also probably need to use smaller cameras. It may also be beneficial to use a smaller computer if possible. This solution may be difficult to implement if a control system is implemented on the helicopter for maintaining antenna alignment. If these solutions do not improve the performance of the X-Cell Spectra G to a suitable level for a mobile host wireless sensor network, it may be necessary to select a larger helicopter. All the challenges outlined here are predominantly engineering problems, and now that the system has been successfully demonstrated for the first time, it is much easier to begin fine tuning the performance of individual aspects of the sensor network.

4.8.4 Helicopter Pilot

For the first test of the mobile host wireless sensor network, it was decided that there was not adequate time to implement an autopilot system for automatically interrogating the sensor nodes in the network. Instead, a professional radio control helicopter pilot was hired to fly the helicopter as shown in Fig. 4.16. Stan Johnson provided the helicopter flying service for the initial test of the mobile host wireless sensor network.

Utilizing a human pilot had both advantages and disadvantages. On the positive side, the human pilot was very easy to interact with and was very amenable to

changes in the test planning. He was also able to supply a large amount of useful advice based on past experiences.

The disadvantage is that a pilot on the ground does not have a good view of the receiver and transmitter antenna alignment, and how far apart the antennas are, as described in the previous chapter. In addition, it is difficult for a human to maintain the correct alignment for the period of time needed to charge up the node. It is anticipated that the time to charge the node could be greatly reduced if an automatic control system for maintaining the alignment of the antennas could be developed. Such a system could conceivably take image data from the onboard camera and extract useful features from it, such as receiver antenna location. These data could then be fed into a control loop in order to actuate the helicopter servos so the mobile host would maintain proper alignment between the antennas. Furthermore, it is conceivable that automating the mobile host control may make it possible for the mobile host to decrease the distance between the receiver and transmitter antenna during power delivery. Decreasing the distance between the antennas could serve to significantly reduce the amount of time necessary to charge the sensor node.

4.8.5 Summary of Mobile Host

The mobile host development required significant consideration of a variety or requirements including weight, power consumption, heat dissipation and volume. Ultimately an RC helicopter was used as the mobile host platform. It was outfitted with an RF/computational payload responsible for providing wireless power delivery capabilities, wireless network communication, and computational capabilities. Some design considerations and the description of each component were presented in this chapter. Ultimately the mobile host used in this work proved to be adequate for the first demonstration of the mobile host wireless sensor network.

Figure 4.16: Stan Johnson flying the helicopter during initial tests in Albuquerque.

Chapter 5

Conclusions and Future Directions

In this work, the mobile host wireless sensor network has been proposed. A complete version of the mobile host wireless sensor network has been developed, designed, fabricated, and tested. A field demonstration of the mobile host wireless sensor network was successfully completed in August of 2007 at the Alamosa Canyon Bridge, a decommissioned overpass 10 miles north of Truth or Consequences, NM. An extremely low power wireless sensor node was needed in order to make peak displacement measurements, as well as to operate from energy supplied wirelessly from a mobile host. For this purpose, the THINNER sensor node was designed and fabricated. THINNER used recently developed capacitance-to-digital converter technology to interrogate capacitive sensors. A capacitance-based peak displacement sensor with a dynamic range appropriate for the Alamosa Canyon Bridge was developed to operate in conjunction with the THINNER sensor node. A rectenna for converting the microwave energy from the mobile host to DC power was developed and interfaced with the sensor node to power its operation. In order to properly interface the rectenna and the THINNER sensor node, it was necessary to first develop a low-power turn on switch. The turn on switch would prevent energy from reaching THINNER until the voltage on the capacitor supplying the sensor node

was high enough to ensure proper operation of the sensor node. In addition to the sensor node work, a mobile host was developed for delivering power and collecting data from sensor nodes in the network. The mobile host consisted of a commercially available RC helicopter outfitted with a custom designed RF/computational payload. The RF/computational payload provided the helicopter with the means to deliver microwave energy to the sensor nodes in the network. Furthermore, the RF/computational payload also possessed the ability to receive data transmissions from the sensor nodes, and to store the data for future analysis.

The contributions of the dissertation will now be summarized.

5.1 Contributions

- First demonstration of a mobile host wireless sensor network. The mobile-host sensor network is a new paradigm for structural health monitoring. In this dissertation it was used for a structural health monitoring application on the Alamosa Canyon Bridge in Truth or Consequences, NM. During the demonstration an aerial mobile host successfully flew to a peak displacement sensor node. The mobile host then used wireless energy delivery techniques to charge the sensor node from a zero-energy state to a fully charged state. The peak displacement sensor node then collected peak displacement data from the structure, and wirelessly transmitted the measurements back to the mobile host.

- A new capacitance-based sensor node (THINNER) capable of being powered from wirelessly delivered energy was developed. The THINNER sensor node uses a capacitive-to-digital converter to collect data from mechanical-memory sensors capable of storing peak event information in the absence of electrical power. THINNER was specifically designed to be powered from energy delivered to it wirelessly.

- Development of a new capacitance-based peak displacement/strain sensor built to operate with the THINNER sensor node. The peak displacement sensor uses the concept of a mechanical memory to store peak displacement values in the absence of electrical energy. The peak displacement sensor is based on a concentric-cylinder, parallel-plate capacitor design similar to that used by [22].

- Development of a new capacitance-based bolted joint preload sensor built to operate with the THINNER sensor node. The bolted joint preload sensor uses low cost Belleville washers to act as load measurement devices. The response of the washers to bolted joint preload is measured using a concentric-cylinder, parallel-plate, variable capacitor transducer, and a capacitance-to-digital converter.

- A Radio Frequency (RF) to DC converter capable of supplying adequate voltage to the energy storage capacitor for the proper operation of the sensor node was developed and tested. Ultimately a full-wave, voltage quadrupler architecture was chosen as the RF-to-DC converter for the mobile host wireless sensor network demonstration. The selected RF-to-DC converter provided the required voltage and conversion efficiency to allow the aerial mobile host to charge the 0.1 F energy storage capacitor to the required 3.5 V.

- A turn-on switch for ensuring power from the storage capacitor only arrives at the THINNER sensor node when the voltage on the capacitor is adequately high was developed. The turn-on switch is capable of operating solely from the power delivered to the energy storage from the mobile host. The switch does not require any auxiliary power supply to properly operate.

- An RF/computational payload for wireless energy delivery and SHM algorithm implementation capable of being delivered by a commercially available RC helicopter. The RF/computational payload contains the hardware nec-

essary for the mobile host to accomplish its wireless energy delivery role, as well as the mobile host to sensor node communication role. Furthermore, the RF/computational payload also allows for a remote basestation to control its operations through an 802.11g wireless network. The RF/computational payload is also designed to allow the mobile host to collect and store data from multiple sensor nodes so data fusion techniques can be applied for structural health monitoring purposes.

The work presented here will provide a firm foundation for future mobile host wireless sensor network research. Possible enhancements to this work include developing a means to autonomously control the helicopter. This research has shown that significant performance advantages can be obtained, if the precision of the helicopter motion and antenna alignment could be improved. The time required to charge the sensor nodes would be dramatically reduced simply by ensuring the proper alignment and distance between the transmitting and receiving antenna.

It is hoped that this work will aid future researchers in the further development of mobile host wireless sensor networks.

5.2 Future Work

The first version of the mobile host wireless sensor network is a good foundation for a continuing research program in mobile host wireless sensor networks. Future work in this field should focus on three main areas. These areas are to integrate autonomous control into the mobile host in order to improve its ability to maintain proper alignment between the transmit and receive antennas. In addition, effort should be invested in redesigning the RF/computational payload carried by the mobile host in order to reduce its weight and power consumption while maintaining its durability. Lastly, development on the THINNER sensor node and its sensors should continue in order to decrease its power consumption and improve its durability.

First, the mobile host should become more autonomous. The results of the first field demonstration showed that a significant improvement in the efficiency of the RF power delivery scheme could be achieved by maintained the receive and transmit antennas in the proper alignment. The human pilot is not typically able to provide the precise alignment necessary for RF energy delivery. It would be very helpful if an automatic control system could be used to guide the mobile host into the proper location and orientation for optimal wireless power delivery without the intervention of a human pilot. Furthermore, the mobile host could be further configured to take pictures of a suspect structure, and automatically look for evidence of structural degradation such as cracks and corrosion. Enhancing the mobile host with autonomous control would greatly improve its capabilities for collecting structural health monitoring data.

Redesign of the RF/computional payload should be a priority for future versions of the mobile host. The current RF/computational payload is at least twice as heavy as it needs to be. The overwight payload signifigantly shortens the amount of time the mobile host can remain in the air due to heightened fuel consumption. The pelican case currently used to house the RF/computational payload is overweight, and it does not have the best heat dissapation characteristics. Furthermore, many civil structures are located in the vicinity of bodies of water. The RF/computational payload should be waterproof in order to avoid damage in the event it is dropped in water. If the mobile host wireless sensor network is scaled up in the future, it will be necessary to redesign the RF/computational payload.

Lastly, the THINNER sensor node and its sensors would greatly benefit from further development. The power consumption of the THINNER sensor node could be reduced by lowering the duty cycle of the radio. The radio has substantial power requirements even when it is not actively recieving or transmitting data. The radio does not need to be on when the rest of the sensor node is taking measurements, so it may be wise to keep the radio off unless the sensor node is ready to transmitt data.

In addition, the sensors used with the THINNER sensor node are still very much in their infancy. Work on the sensors should be aimed at improving their durability, and enhancing their sensativity. The peak displacement sensor especially needs to be more stable in the face of both mechanical and thermal disturbances. In the case of the bolted joint preload sensor it is espacially important to improve its dynamic range and suitability for inclusion as a civil structure element. Work on improving the durability and measurement range capabilities of the sensors is necessary for making the mobile host wireless sensor network a reality.

In order to scale up the implementation of the mobile host wireless sensor network, it will be important to invest effort in making the mobile host autonomous, redesign the RF/computational payload, and improve the sensors and sensor nodes used in the network for data collection.

Bibliography

[1] "Alkaline manganese dioxide handbook and application manual," Tech. Rep. Alk1.3, Energizer Battery Manufacturing Inc, 2008.

[2] Q. Han, S. Mehrotra, and N. Venkatasubramanian, "Energy efficient data collection in distributed sensor environments," *Distributed Computing Systems, 2004. Proceedings. 24th International Conference on*, pp. 590–597, 2004.

[3] I. Akyildiz, W. Su, Y. Sankarasubramaniam, and E. Cayirci, "Wireless sensor networks: a survey," *Computer Networks*, vol. 38, no. 4, pp. 393–422, 2002.

[4] W. Ye, J. Heidemann, and D. Estrin, "Medium access control with coordinated adaptive sleeping for wireless sensor networks," *IEEE/ACM Transactions on Networking (TON)*, vol. 12, no. 3, pp. 493–506, 2004.

[5] J. Polastre, J. Hill, and D. Culler, "Versatile low power media access for wireless sensor networks," *Proceedings of the 2nd international conference on Embedded networked sensor systems*, pp. 95–107, 2004.

[6] J. Dove, G. Park, and C. Farrar, "Hardware design of hierarchal active-sensing networks for structural health monitoring," *Smart Materials and Structures*, vol. 15, pp. 139–146, January 2006.

[7] L. Tong, Q. Zhao, and S. Adireddy, "Sensor networks with mobile agents," *MILCOM*, vol. 1, pp. 688–693, 2003.

[8] M. L. Sichitiu and V. Ramadurai, "Localization of wireless sensor networks with a mobile beacon," in *IEEE International Conference on Mobile Ad-hoc and Sensor Systems*, pp. 174–183, October 2004.

[9] Y. Tirta, Z. Li, Y.-H. Lu, and S. Bagchi, "Efficient collection of sensor data in remote fields using mobile collectors," in *13th International Conference on*

Computer Communications and Networks, Proceedings., pp. 515–519, October 2004.

[10] P. Corke, S. Hrabart, R. Petersont, D. Rust, S. Saripallit, and G. Sukhatme, "Autonomous deployment and repair of a sensor network using an unmanned aerial vehicle," in *Proceedings of the 2004 IEEE International conference on robotics and automation.*

[11] L. Ma and Y. Chen, "Aerial surveillance system for overhead power line inspection," Tech. Rep. USU-CSOIS-TR-04-08, Center for Self-Organizing and Intelligent Systems (CSOIS), Utah State University, September 2003.

[12] C. Whitworth, A. Duller, D. Jones, and G. Earp, "Aerial video inspection of overhead power lines," *Power Engineering Journal*, vol. 15, pp. 25–32, 2001.

[13] I. T. Golightly, *Visual control of an unmanned aerial vehicle for power line inspection.* PhD thesis, University of Wales, Bangor, May 2006.

[14] B. Esser, N. Pelczarski, and D. Huston, "Wireless inductive robotic inspection of structures," in *Proceedings of the IASTED International Conference Robotics and Applications*, August 2000.

[15] D. Huston, B. Esser, G. Gaida, S. Arms, and C. Townsend, "Wireless inspection of structures aided by robots," in *Proceedings of SPIE Health Monitoring and Management of Civil Infrastructure Systems, Steven B. Chase; A. Emin Aktan; Eds.*, August 2001.

[16] R. Shah, S. Roy, J. Sushant, and W. Brunette, "Data mules: modeling a three-tier architecture for sparse sensor networks,"

[17] A. Kansal, A. Somasundara, D. Jea, M. Srivastava, and D. Estrin

[18] D. Jea, A. Somasundara, and M. Srivastava, *Multiple Controlled Mobile Elements (Data Mules) for Data Collection in Sensor Networks*, pp. 244–257. Springer Berlin / Heidelberg, 2005.

[19] R. Sugihara and R. Gupta, *Improving the Data Latency in Sensor Networks with Controlled Mobility*, pp. 386–399. Springer Berlin / Heidelberg, 2008.

[20] C. R. Farrar, T. A. Duffey, S. W. Doebling, and D. A. Nix, "A stastistical pattern recognition paradigm for vibration-based structural health monitoring," *Structural Health Monitoring 2000*, 1999.

[21] H. Sohn., C. Farrar, F. M. Hemez, D. D. Shunk, S. W. Stinemates, B. R. Nadler, and J. J. Czarnecki, "A review of structural health monitoring literature from 1996-2001," Tech. Rep. LA-13976-MS, Los Alamos National Labs, 2004.

[22] T. S. Mita, A., "A smart sensor using a mechanical memory for structural health monitoring of a damage- controlled building," *Smart Materials and Structures*, 2003.

[23] J. A. Carlson, J. M. English, and D. J. Coe, "A fexible, self-healing sensor skin," *Smart Materials and Structures*, vol. 15, pp. 129–135, September 2006.

[24] M. M. Andringa, *Unpowered Wireless Sensors for Structural Health Monitoring.* PhD thesis, University of Texas at Austin, December 2006.

[25] K. J. Loh, J. P. Lynch, and N. A. Kotov, "Passive wireless strain and pH sensing using carbon nanotube-gold nanocomposite thin films," in *Sensors and Smart Structures Technologies for Civil, Mechanical, and Aerospace Systems, Proc. of SPIE Vol. 6529*, 2007.

[26] Y. Jia, K. Sun, F. J. Agosto, and M. T. Q. nones, "Design and characterization of a passive wireless strain sensor," *Measurement Science and Technology*, vol. 17, p. 2869Ű2876, September 2006.

[27] Z. L. Sameer R. Sonkusale, "A wireless data and power telemetry system using novel BPSK demodulator for non-destructive evaluation of structures," in *IEEE Sensors Conference*, 2007.

[28] D. Thompson, D. Card, and G. Bridges, "The interrogation limits for passive wireless sensors," in *Structural Health Monitoring 2007, Quantification, Validation and Implementation*, 2007.

[29] V. K. Varadan and V. V. Varadan, "Microsensors, microelectromechanical systems (mems), and electronics for smart structures and systems," *Smart Materials and Structures*, vol. 9, pp. 953–972, 2000.

[30] H. Subramanianyx, V. K. Varadanyk, V. V. Varadanyk, and M. J. Vellekoopz, "Design and fabrication of wireless remotely readable MEMs based microaccelerometers," *Smart Materials and Structures*, vol. 6, pp. 730–738, October 1997.

[31] X. Zhao, T. Qian, G. Mei, C. Kwan, R. Zane, T. P. Christi Walsh and, and Z. Popovic, "Active health monitoring of an aircraft wing with an embedded piezoelectric sensor/actuator network: Ii.wireless approaches," *Smart Materials and Structures*, vol. 16, pp. 1218–1225, June 2007.

[32] WenH.Ko, D. J. Young, J. Guo, M. Suster, H.-I. Kuo, and N. Chaimanonart, "A high-performance MEMs capacitive strain sensing system," *Journal of Microelectromechanical Systems*, vol. 15, pp. 1069–1077, March 2006.

[33] A. Devices, "Ad7745 datasheet," tech. rep., Analog Devices, 2005.

[34] Atmel, "ATmega128L datasheet," tech. rep., Atmel Corporation, 2007.

[35] "Powerstor supercapacitors p series," Tech. Rep. Data Sheet 4306, Cooper Bussmann, 2007.

[36] W. Brown, "The history of power transmission by radio waves," *IEEE Transactions on Microwave Theory and Techniques*, 1984.

[37] Voltage Multipliers Inc, *Voltage Multiplier Design Guide: Multipliers Ű Analysis and Design.*

[38] J. Almen, "The uniform section disk spring," *American Society of Mechanical Engineers*, 1936.

[39] W. Young, *Roark's Formulas for Stress and Strain.* McGraw-Hill, 1989.

[40] B. Thompson, "The application of capacitors for structural load and displacement sensors," tech. rep., University of California San Diego, Aug 2007.

[41] J. PARADISO and T. STARNER, "Energy scavenging for mobile and wireless electronics," *IEEE pervasive computing*, vol. 4, no. 1, pp. 18–27, 2005.

[42] C. P. Townsend, S. W. Arms, and M. J. Hamel, "Remotely powered multichannel microprocessor-based telemetry systems for smart implantable devices and smart structures," in *Proceedings of SPIE*, vol. 3673, pp. 150–156, 1999.

[43] N. Chaimanonart, W. H. Ko, and D. J. Young, "Remote RF powering system for MEMS strain sensors," in *Proceedings of IEEE Sensors 2004*, pp. 1522–1525, 2004.

[44] M. Ryan, "An universal, inductively coupled battery charger for robot power supplies," in *Proceedings of the 2006 Australasian Conference on Robotics and Automation*, 2006.

[45] B. H. Chavanne, "Small UAVs may recharge on power lines," *Aviation Week's DTI*, 2007.

[46] K. M. Z. Shams and M. Ali, "Wireless power transmission to a buried sensor in concrete," *IEEE Sensors Journal*, vol. 7, pp. 1573–1577, December 2007.

[47] I. D. Avramov, "The RF-powered surface wave sensor oscillatorŮa successful alternative to passive wireless sensing," *IEEE transactions on ultrasonics, ferroelectrics, and frequency control*, vol. 51, pp. 1148–1156, September 2004.

[48] "Pittsburgh zoon and aquarium: Making wireless sensor networks truly wireless using RF power," tech. rep., Powercast, 2006. Ligonier, Pennsylvania.

[49] D. Pozar, *Microwave Engineering Third Edition*. John Wiley and Sons, 2005.

[50] "Multipath and diversity," Tech. Rep. 27147, Cisco Systems Technical Note, 2006. San Jose, California.

[51] D. Mascarenas, "Development of an impedance method-based wireless sensor node for monitoring of bolted joint preload," Master's thesis, University of California San Diego, 2006.

[52] L. R. Newcome, *Unmanned Aviation: A Brief History of Unmanned Aerial Vehicles*. American Institute of Aeronautics and Astronautics, 2004.

[53] Wikipedia, "RQ-4 global hawk," August 2003.

[54] "Global hawk becomes first UAV to receive national certificate of authorization to fly in national airspace." Northrup Grummen Press Release, August 2003.

[55] 9th Reconnaissance Wing Public Affairs, "Beale airmen, ISR assets support california wildfires," October 2007.

[56] F. Granelli, "2.4 GHz for the common pilot." www.masportaviator.com, July 2007.

[57] K. Lin, "Olympus manual," tech. rep., University of California San Diego, 2007.

[58] "AUVSI/ONR engineering primer document for the autonomous underwater vehicle (AUV) team competition," tech. rep., Association for Unmanned Vehicle Systems International (AUVSI), US Navy Office of Naval Research, 2007.

[59] Wikipedia, "Density altitude." www.wikipedia.com, May 2008.